Departament d'Enginyeria Electrònica
UNIVERSITAT POLITÈCNICA DE CATALUNYA

Studies on Organic Solar Cells based on Small-Molecules: Tetraphenyldibenzoperiflanthene and fullerene C_{70}

Thesis presented to obtain the qualification of Doctor from the Universitat Politècnica de Catalunya

Sergi Galindo Lorente

Director: *Dr. Joaquim Puigdollers González*

June 2015

UNIVERSITAT POLITÈCNICA DE CATALUNYA
BARCELONATECH
Escola de Doctorat

Curs acadèmic: 2014-2015

Acta de qualificació de tesi doctoral

Nom i cognoms
Sergi Galindo Lorente

Programa de doctorat
Doctorat d'Enginyeria Electrònica

Unitat estructural responsable del programa
Departament d'Enginyeria Electrònica

Resolució del Tribunal

Reunit el Tribunal designat a l'efecte, el doctorand / la doctoranda exposa el tema de la seva tesi doctoral titulada Studies on Organic Solar Cells based on Small-Molecules: Tetraphenyldibenzoperiflanthene and fullerene C_{70} _____.

Acabada la lectura i després de donar resposta a les qüestions formulades pels membres titulars del tribunal, aquest atorga la qualificació:

☐ NO APTE ☐ APROVAT ☐ NOTABLE ☐ EXCEL·LENT

(Nom, cognoms i signatura)	(Nom, cognoms i signatura)	
President/a	Secretari/ària	
(Nom, cognoms i signatura)	(Nom, cognoms i signatura)	(Nom, cognoms i signatura)
Vocal	Vocal	Vocal

_____, _____ d'/de _____ de _____

El resultat de l'escrutini dels vots emesos pels membres titulars del tribunal, efectuat per l'Escola de Doctorat, a instància de la Comissió de Doctorat de la UPC, atorga la MENCIÓ CUM LAUDE:

☐ SÍ ☐ NO

(Nom, cognoms i signatura)	(Nom, cognoms i signatura)
President de la Comissió Permanent de l'Escola de Doctorat	Secretari de la Comissió Permanent de l'Escola de Doctorat

Barcelona, _____ d'/de _____ de _____

“Serem allò que vulguem ser”

Miquel Martí i Pol

A Estefanía

A la meva família i amics

A la iaia Carmen

Agraïments

És un plaer per mi expressar el meu agraïment a les moltes persones que han fet possible la realització d'aquesta tesi. Em sento molt afortunat de la gran quantitat de persones que m'han fet costat durant aquesta etapa.

En primer lloc, vull agrair al meu director de tesi Dr. Joaquim Puigdollers. Es diu que un professor es fa responsable d'ensenyar-te; d'altra banda un mestre ensenya un camí per aprendre i desenvolupar un coneixement sobre allò que desconeixes. Les lliçons de mestre que m'has donat són, sens dubte, el més valuós d'haver fet la tesi. Gràcies també per introduir-me en el món de la investigació. També per la teva paciència i motivació.

Al Prof. Ramón Alcubilla, responsable de la sala blanca i director del Centre de Nanoenginyeria (CRnE) de la Universitat Politècnica de Catalunya (UPC), pels teus consells i pel teu suport en tot moment.

Al Dr. Cristóbal Voz per la teva paciència i les teves explicacions, sobretot sobre les diferents recombinacions i models de les cèl·lules solars.

A Albert Marsal, per l'ajuda incondicional en tot moment. Les teves idees per solucionar problemes tècnics i la teva col·laboració en la fabricació i mesura dels transistors orgànics han estat vitals per aquesta tesi.

A Mehrad Ahmadpour per la teva intensa participació en la fabricació de moltes cèl·lules solars. Les teves ganes il·lusió, junt amb la resta d'estudiants del grup de cèl·lules solars orgàniques: Guillermo Gerling, Siti Winny, Mulugeta Ayele, Som Mahato.

A tota la resta de membres del grup de Micro i Nano Tecnologies (MNT) de la UPC, particularment als meus companys i amics Dr. Alfredo Boronat, Arnau Coll, Dr. David Hernández, Gema López...

Als tècnics del CRnE de la UPC: Dr. Trifon Trifonov i Dr. Montse Domínguez; així com als tècnics de la sala blanca de la UPC: Miguel García i Xavier Fermín per la seva col·laboració en tot moment perquè tot funcioni correctament.

Al Grup d'Energia Solar del Departament de Física Aplicada i Òptica de la Universitat de Barcelona, particularment a Dr. José Miguel Asensi, Dr. Joan Bertomeu, Dr. Aldrin Antony, Dr. Paz Carreras i Dr. Rubén Roldán.

Al Prof. M.K. Jayaraj i a Vikas L S i a la resta del grup Nanophotonic & Optoelectronic Devices Laboratory del Department of Physics de la Cochin University of Science and Technology (CUSAT) per la vostra col·laboració i la seva bona acollida durant la meva estada a la Índia.

A les Dr. Stephanie Cheylan i Dr. Mónica della Pirriera per la vostra bona acollida i els seus consells durant els meus primers dies al laboratori.

Al Dr. César Moreno per les teves profitoses discussions científiques.

Al Dr. Stamatis Georgakopoulos per les teves explicacions dels transistors i per llegir-te bona part de la tesi. A Francesc Bejarano per la seva lectura crítica sobre els conceptes de química orgànica. A la resta del grup NANOMOL del Institut de Ciència de Materials de Barcelona, pel vostre suport durant l'escriptura de la tesi.

A Dr. Marta Mas pel teu suport i paciència mentre he estat escrivint la tesi.

A la tota la meva família, als meus pares, Màxim i Carme, a la meva germana Marina i el meu germà Màxim, a la meva tieta Marga pel vostre suport incondicional. Gràcies Màxim per la teva motivació científica i l'ajuda en l'edició de la tesi.

A Estefanía. M'has acompanyat tota la tesi. Ningú millor que tu sap el que ha costat. Ningú ho ha patit tant. Gràcies.

Moltes gràcies a tots!

Resum

En aquesta tesi s'investiguen cèl·lules solars orgàniques basades en semiconductors de petita molècula. En particular, les cèl·lules solars orgàniques d'aquesta tesi han emprat tetraphenyldibenzoperiflanthene com material donador i ful·lerè C_{70} com material acceptador.

En la primera part d'aquesta tesi, ens centrem en la influència de la densitat d'estats de la capa donadora en els paràmetres característics de les cèl·lules solars. Més endavant, es presenten cèl·lules solars orgàniques amb una estructura p-i-n, on la capa intrínseca s'obté per l'evaporació conjunta del donador i l'acceptador. S'analitza la influència del gruix de la capa intrínseca de la cèl·lula solar p-i-n en la característica de la cèl·lula solar.

En la segona part, es presenta un circuit equivalent per a les cèl·lules solars orgàniques. S'afegeix un nou terme en el model estàndard que representa les pèrdues de recombinació a la capa activa del dispositiu. L'anàlisi de les característiques de corrent – tensió mesurades a diferents intensitats de llum permeten l'estimació del terme de recombinació. El model separa clarament les qüestions tecnològiques (resistències en sèrie i en paral·lel) dels efectes relacionats amb la física del dispositiu (pèrdues de recombinació). També permet l'obtenció d'un producte de la mobilitat - temps de vida efectiu a la capa activa del dispositiu a ser determinat, la caracterització del seu estat de degradació.

Abstract

This work deals with the research on organic solar cells based on small-molecules semiconductors. In particular, organic solar cells of this thesis have been used tetraphenyldibenzoperiflanthene as donor material and fullerene C_{70} as acceptor material.

In the first part of this thesis, we focus on the influence of the density of states of the donor layer on the characteristic parameters of solar cells. Further, organic solar cells with p-i-n structure are presented, where the intrinsic layer is obtained by coevaporation of donor and acceptor. The influence of the thickness of the intrinsic layer on the p-i-n solar cell characteristic is analysed.

In the second part, an equivalent circuit for organic solar cells is presented. A new term is added to the standard model representing recombination losses in the active layer of the device. The analysis of the characteristics of current - voltage measured at different illumination intensities allows the estimation of the term recombination. The model clearly separates technological issues (series and parallel resistance) from effects related to the physics of the device (recombination losses). It also allows obtaining an effective mobility-lifetime product in the active layer of the device to be determined, characterising its state of degradation.

Table of contents

List of figures

List of abbreviations

AFM	Atomic Force Microscopy
AM	Air Mass
a-Si:H	Hydrogenated amorphous silicon
BCP	Bathocuproine
Bphen	Bathophenanthroline
c	speed of light
CdTe	Cadmium Telluride
CIGS	Copper Indium Gallium Selenide
c-Si	crystalline silicon
CT	Charge Transfer
CV	Cyclic Voltammetry
CZTS	Copper Zinc Tin Sulphide
DOS	Density-Of-States
DSSC	Dye-Sensitized Solar Cells
E_{EX}	binding exciton
Eg	energy band gap
E_P	energy of a photon
EQE	External Quantum Efficiency
ETL	Electron Transport Layer
FET	Field Effect Transistor
FF	Fill Factor
FIB	Focused Ion Beam
h	Planck's constant
HIT	Heterojunction with Intrinsic Thin layer
HOMO	Highest Occupied Molecular Orbital
HTL	Hole Transport Layer
IP	Ionization Potential
IPES	Inverse Photoemission Spectroscopy
IQE	Internal Quantum Efficiency
I_{SD}	current between source and drain
ITO	Indium Tin Oxide
J	current density

J_0	reverse bias saturation current density
J_{PH}	photocurrent generated per unit area
J_{SC}	Short circuit current density
k_B	Boltzmann constant
L_D	exciton diffusion length
LUMO	Lowest Unoccupied Molecular Orbital
MoO_3	Molybdenum Oxide
MTR	Multiple Trapping and Release model
N	diode ideality factor
OD	Optical Density
OLED	Organic Light Emitting Diode
OSC	Organic Solar Cell
OTFT	Organic Thin Film Transistor
P_0	incident illumination power
Q	elementary charge
QD	Quantum Dot
RF–ID	Radio Frequency - Identification Tag
R_P	parallel resistance
R_S	series resistance
SCLC	Space Charge Limited Current
SEM	Scanning Electron Microscope
SR	spectral response
T	Transmission
TEM	Transmission Electron Microscopy
TMO	Transition Metal Oxide
TOF	Time of flight
UPS	Ultraviolet Photoelectron Spectroscopy
V	applied voltage
V_G	gate voltage
VIM	Variable Illumination Measurement
V_{OC}	open circuit voltage
V_{SD}	Source-drain voltage
V_T	threshold voltage
η	power conversion efficiency
η_A	photon absorption efficiency
η_{CC}	carrier collection efficiency
η_{CT}	charge transfer efficiency
η_{ED}	exciton diffusion efficiency
$\mu\tau$	mobility-lifetime
τ_0	lifetime of the exciton

1. Introduction

1.1 Motivation

Organic electronics is a division of materials science which deals with electrically-conductive semiconductors based on polymers and small-molecules. It is called organic electronics because these polymers and small-molecules are carbon-based. Organic electronics devices have attracted much attention during last decades due to their potential advantages. Devices using organic semiconductors should be cheaper and easier to manufacture than the corresponding ones based on inorganic semiconductors. Among them, organic light emitting diodes (OLEDs) [1–2], organic thin film transistors (OTFTs) [3–6] and organic solar cells (OSCs) [7–9] are rapidly developing towards commercial applications.

OLEDs are used to create digital displays and lighting applications, in devices such as mobile phones and portable digital media players, car radios and digital cameras among others. OTFTs have already been demonstrated in applications like sensors [10–11], memory devices [12–13], flexible displays [14–16] and radio frequency identification tags (RF–IDs) [17–18]. Another application of organic semiconductors is in the field of photovoltaic solar cells, emerging as alternative of traditional photovoltaic technologies. This thesis is focused on the interesting field of solar cells based on organic semiconductors.

Today, the photovoltaic market is dominated by solar cells based on crystalline silicon. Photovoltaics modules based on crystalline silicon present efficiencies on the order of 15–20%; nevertheless it is the price what has pulling up this technology on top. Photovoltaic modules based on crystalline silicon costs about 0.5–0.7 €/watt peak, making this technology competitive with other renewable sources.

However, research laboratories are looking for new technologies that could lower down these prices. The most promising technological alternatives are: thin films for photoactive layers and solar concentrators. In addition, they are looking for products that could overcome some of the

limitations of crystalline silicon in terms of flexibility and weigh. In this sense, during the last decade, many efforts have been focused on the fabrication of solar cells based on organic semiconductors. Organic semiconductors can be processed at near ambient temperature over large area, opening the possibility to fabricate large area devices on flexible substrates.

Light's ability to generate electric current was first observed in 1839 by A. E. Becquerel when he discovered the photoelectrochemical process [19]. Thenceforth, different technologies have emerged in photovoltaic solar cells. Figure 1.1 shows the evolution of the best power conversion efficiency for each solar cell technology during last decades.

The best efficiency reported for a monocrystalline silicon solar cell is 25% [20–21] getting quite close to the "practical" limit of around 26% [22]. Although efficiencies of solar cells based on monocrystalline silicon are very high, it is very important to keep an eye on solar cells based on multicrystalline silicon, since today 5 out of 10 sold solar cells are manufactured using this material. Multicrystalline silicon is cheaper than monocrystalline silicon, but unfortunately has also a lower optoelectronic quality due to a higher amount of crystal defects and metal impurities. Currently, the record efficiency in multicrystalline silicon solar cell is 20.4% [23].

Thin film solar cell is the alternative technology to the predominant crystalline silicon and its market-share has been increasing in recent years to about 9% of worldwide photovoltaic production in 2013 [24]. Thin-film technologies reduce the amount of active material in a cell, having a film thickness from a few nanometres to tens of micrometers. Thin-film solar cells are usually categorised by the photovoltaic material which they are made of. Cadmium Telluride (CdTe), Copper Indium Gallium Selenide (CIGS) and hydrogenated amorphous silicon (a-Si:H) are thin-film materials with long research tradition, and modules based on these materials are well established. Currently, the module market prices of these technologies are quite similar and slightly lower than c-Si solar modules, 0.46–0.63 €/watt peak. OSC, Dye-Sensitized Solar Cells (DSSC) (this type of solar cell was invented by Michael Grätzel and Brian O'Regan [25] and are also known as the Grätzel solar cell), Quantum Dot (QD) solar cells, Copper Zinc Tin Sulphide (CZTS) solar cells have also emerged in the frame of thin film technology.

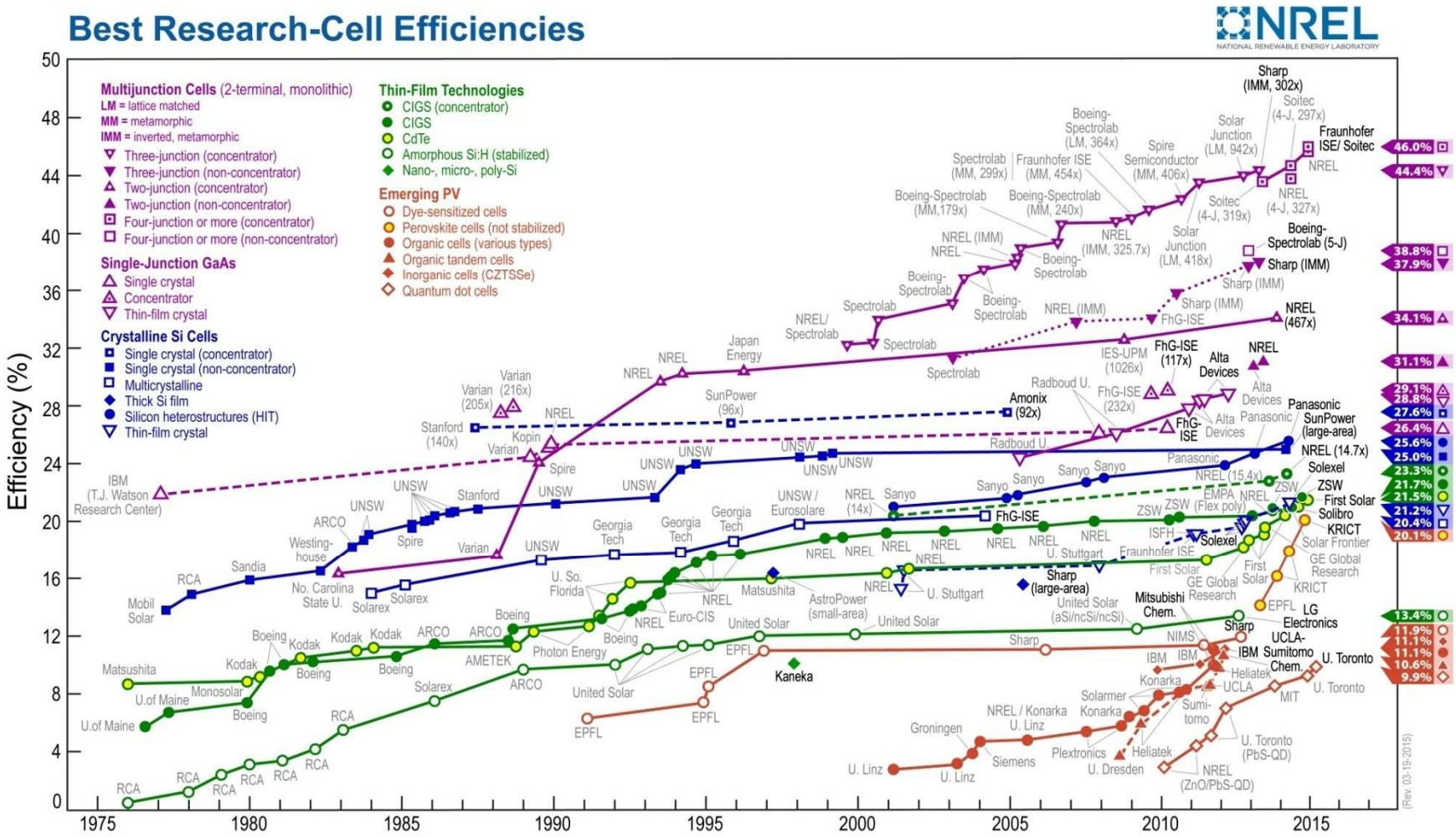

Figure 1.1 - Evolution of record cell efficiencies of different solar cell technologies. This graph is provided by the NREL (http://www.nrel.gov/ncpv/images/efficiency_chart.jpg 2-04-2015)

The last group of solar cells (OSC, DSSC, QD, and CZTS solar cells) belongs to what has been called third generation solar cells. The physics behind their working principles are not well established and some technological issues, mainly regarding its time stability, have limited its influence to the research labs. Although some companies, such as DyeSol or Heliatek, start to produce some of these solar cells (DSSC, OSC), their higher prices and poor stability, compared to the crystalline silicon counterparts, has limited its wide spreading [26–27].

In 2014, researchers at the Zentrum für Sonnenenergie und Wasserstoff Forschung (ZSW) in Stuttgart achieved a certified 21.7% conversion rate in a CIGS thin-film cell [28]. On the other hand, the best CdTe solar cell efficiency has reached 21.5% by First Solar [29].

Recently, a new actor has made act of presence in the competitive world of solar cells technologies: perovskites-based solar cells. A perovskite solar cell is a type of solar cell which includes a perovskite structured compound, most commonly a hybrid organic-inorganic lead or tin halide-based material, as the light-harvesting active layer. The properties that make this type of solar cell very attractive are: controllable energy bandgap by the halide content [30–31] and long diffusion length, for both holes and electrons, of over one micrometre [32]. Solar cell efficiencies of devices using these materials have increased from 3.8% in 2009 [33] to 20.1% achieved by the Korean Research Institute of Chemical Technology (KRICT) in 2014 [34], making this the fastest advancing solar technology to date.

Figure 1.2 compare the evolution during last three decades of record efficiencies for various promising third generation solar cells with the standard a-Si:H solar cells. Perovskites solar cells efficiencies are also included. DSSC and a-Si:H solar cells (pink and blue curves) do not shown significant improvement in power conversion efficiency during last two decades. Actually, the best efficiency is 12.3% for DSSC obtained in laboratory by École Polytechnique Fédérale de Lausanne (EPFL) [35] and 13.4% for a-Si:H solar cells reached by LG Electronics [23]. On the other hand, the record power conversion efficiency of OSCs (red curve, for small area; and green curve for larger than 1 cm^2) have shown exponential increase, mainly since 2005. However, this tendency seems to have stopped in 2012, when was reported the highest power conversion efficiency of OSC with 12%, achieved by Heliatek Company and using triple tandem solar cell geometry [36]. It is worth to mention that most of the research labs working on dye and organic solar cells have shifted its activities to perovskites technology. This is especially true for dye solar cells, since technology processes are quite similar for both technologies.

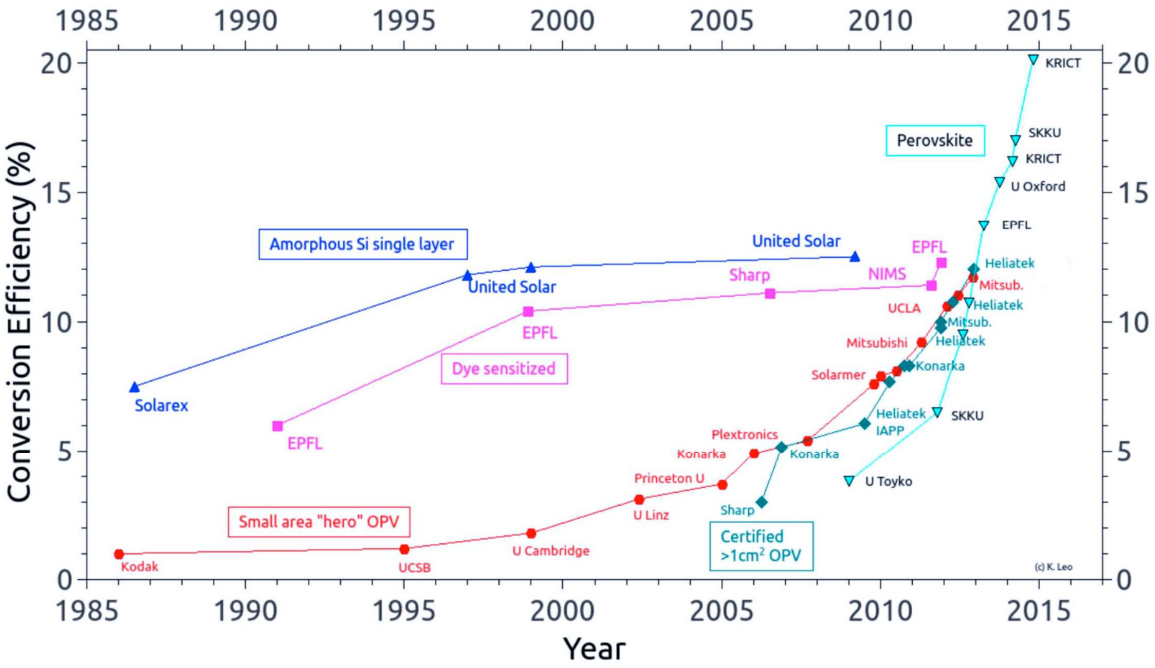

Figure 1.2 - Evolution of efficiencies from emerging solar cells (source: http://www.orgworld.de)

Traditionally, the study of semiconducting organic materials focused on small organic molecules in the crystalline state, such as: anthracene, naphthalene or copper phthalocyanine [37–39]. Research activities were concentrated on phenomena associated with charge transport in individual molecules; in general they showed poor semiconducting electrical characteristics, and during many years few papers arise on this topic. However, this situation start to change when in 1977, Alan J. Heeger, Alan MacDiarmid and Hideki Shirakawa reported high electrical conductivity in oxidized iodine-doped polyacetylene. They claimed that polyacetylene halides could be the forerunners of a new class of organic polymers with electrical properties which may be systematically and controllably varied over a wide range by chemical doping [40]. For this research, they were awarded with the Nobel Prize in Chemistry in 2000 “for the discovery and development of conductive polymers”. The breakthrough of the thin film organic solar cell was made in 1986 by Ching Tang, when reported a power conversion efficiency of 1% [41]. Tang’s cell comprises a bilayer structure of a donor and acceptor materials (copper phthalocyanine and perylene tetracarboxylic derivative) and demonstrated that the properties in the interface region are primarily responsible for the photogeneration of charges. The efficiencies of the reported organic solar cells did not exceed 1% for many years. In 1992 Hiramoto *et al*. published the bulk heterojunction solar cell by mixing donor and acceptor materials in a blend layer [42]. The use of bulk heterojunction in active layer allowed a higher exciton dissociation and as a consequence

higher power conversion efficiency. Further improvements in solar cell performance were achieved by the introduction of organic doped materials [43] and the use of p-i-n concept [44].

The huge diversity of organic molecules (and polymers) and the possibility of tailoring the material properties using chemistry processes allow the synthesis of new semiconductor compounds with specific properties, such as the optical gap or the photoluminescence.

Methods from organic chemistry allow the fabrication of customised solar cells, as well as multi-colour and semi-transparent solar cells [45–46]. The low material consumption during the fabrication process and the light weight devices foreseen expect low costs for production of OSCs. The possibility to deposit on plastic substrates, replacing the conventionally used rigid glass substrates, and on large area attracts the attention of the photovoltaic industry. However, the current challenges on the way to cost effective mass production are the low solar cell efficiencies as well as the short lifetimes.

1.2 Objective of this Thesis

The objective of this thesis was the fabrication of solar cells based on organic small-molecule semiconductors deposited in a high vacuum system. The structural and optoelectronic properties of the deposited thin-films were correlated with the optoelectronic performance of the fabricated solar cells.

All the solar cells were fabricated on glass substrates with a pre-patterned indium tin oxide (ITO) layer. The device structure was: glass / ITO / small-molecule / metal, where small-molecule corresponds to the active layer. The fabrication was carried out in the Centre for Research in NanoEngineering (CRnE) of the Universitat Politècnica de Catalunya (UPC).

The research in Micro and Nano Technologies (MNT) group is focused on understanding how advanced electronic devices work and how they performance can be improved. Group facilities include a Clean Room with main silicon processing equipment. The group have a strong experience in photovoltaics solar cells, reaching high power conversion efficiency (22%) in crystalline silicon (c-Si) solar cell and (18%) in Heterojunction with Intrinsic Thin layer (HIT) silicon solar cell.

Ten years ago, the MNT group started a new research line focused on the fabrication of organic devices based on small-molecules organic semiconductors. The research started with the

fabrication of OTFTs using a basic evaporator with two sources for organic materials. Later on, MNT group acquired a glovebox to fabricate organic solar cells. The glovebox is equipped with two evaporator systems: one dedicated to the deposit organic molecules (home-made) and the other for metals. At the beginning of my thesis, my work was focused on the preparation and calibration of the organic evaporator. The fabrication of organic solar cells complement the other photovoltaic technologies carried out in the group.

In the scope of this thesis, the materials used are commercial; however it was also explored the feasibility of new organic compounds provided by chemistry groups in the frame of collaborative projects.

On the other hand, OTFTs were also fabricated to determine the electrical properties of organic molecules. The electrical measurements of OTFT allow the determination of the electrical field-effect mobility and density-of-states (DOS) of organic semiconductor.

In order to understand the electrical behaviour of small-molecule organic solar cells, such as recombination losses or influence of the electrical field effect, additional optoelectronic characterisation of the solar cells was performed. Variable Illumination Measurements (VIM) was be useful to study the recombination process and get an analytical model.

1.3 Structure of this Thesis

The thesis is organised as follows. The Chapter 1 includes the motivation, the objective and the structure of this thesis. In Chapter 2 some insights about the properties of organic semiconductors are reviewed. In Chapter 3 describes the principles of organic solar cells. The experimental materials and methods, especially fabrication tools and characterisation of OSCs are explained in Chapter 4. In Chapter 5 the influence of the DOS on the open circuit voltage in the organic solar cells is discussed. The influence of carrier bimolecular recombination is also studied. On the other hand, in Chapter 6 are studied the monomolecular recombination losses in the active layer using an analytical model.

The Appendix I contains additional information (not included in the respective chapters for clarity reasons), such as the fabrication of OTFTs and the determination of carrier mobility and density of states of localised states.

References

[1] C. W. Tang, S. A. VanSlyke, "Organic electroluminescent diodes", *Appl. Phys. Lett.* 51 (**1987**) 913.

[2] J. H. Burroughes, D. D. C. Bradley, A. R. Brown, R. N. Marks, K. Mackay, R. H. Friend, P. L. Burns, A. B. Holmes. "Light-emitting diodes based on conjugated polymers", *Nature* 347 (**1990**) 539.

[3] Y. Yamashita, "Organic semiconductors for organic field-effect transistors", *Sci. Technol. Adv. Mater*. 10 (**2009**) 024313.

[4] C. D. Dimitrakopoulos, P. R. L. Malenfant, "Organic Thin Film Transistors for Large Area Electronics", *Adv. Mater*. 14 (**2002**) 99.

[5] H. Klauk, "Organic thin-film transistors", *Chem. Soc. Rev.* 39 (**2010**) 2643.

[6] C. Reese, M. Roberts, M. Ling, Z. Bao, "Organic thin film transistors", *Mater. Today* 7 (**2004**) 20.

[7] P. Peumans, S. Uchida, S. R. Forrest, "Efficient bulk heterojunction photovoltaic cells using small-molecular-weight organic thin films" *Nature* 425 (**2003**) 158.

[8] F. C. Krebs, "Fabrication and processing of polymer solar cells: A review of printing and coating techniques", *Sol. Energy Mater. Sol. Cells* 93 (**2009**) 394.

[9] H. Hoppe, N. S. Sariciftci, "Organic solar cells: An overview", *J. Mater. Res.* 19 (**2004**) 1924.

[10] Z.-T. Zhu, J. T. Mason, R. Dieckmann, G. G. Malliaras, "Humidity sensors based on pentacene thin-film transistors", *Appl. Phys. Lett.* 81 (**2002**) 4643.

[11] B. K. Crone, A. Dodabalapur, R. Sarpeshkar, A. Gelperin, H. E. Katz, Z. Bao, "Organic oscillator and adaptive amplifier circuits for chemical vapor sensing", *J. Appl. Phys.* 91 (**2002**) 10140.

[12] S. J. Kim, J. S. Lee, "Flexible organic transistor memory devices", *Nano Lett.* 10 (**2010**) 2884.

[13] M. Chang, P. Lee, S. P. McAlister, A. Chin, "A flexible organic pentacene nonvolatile memory based on high-k dielectric layers" *Appl. Phys. Lett.* 93 (**2008**) 233302.

[14] G. H. Gelinck, H. Edzer A. Huitema, E. van Veenendaal, E. Cantatore, L. Schrijnemakers, J. B. P. H. van der Putten, T. C. T. Geuns, M. Beenhakkers, J. B. Giesbers, B. Huisman, E. J. Meijer, E. M. Benito, F. J. Touwslager, A. W. Marsman, B. J. E. van Rens, D. M. de Leeuw, "Flexible active-matrix displays and shift registers based on solution-processed organic transistors", *Nat. Mater.* 3 (**2004**) 106.

[15] L. S. Zhou, S. Park, B. Bai, J. Sun, S. C. Wu, N. J. Thomas, N. Shelby, F. Diane, Y. Hong, "Pentacene TFT driven AM OLED displays" *IEEE Electr. Device L.* 26 (**2005**) 640.

[16] M. Mizukami, N. Hirohata, T. Iseki, K. Ohtawara, T. Tada, S. Yagyu, T. Abe, T. Suzuki, Y. Fujisaki, Y. Inoue, S. Tokito, T. Kurita, "Flexible AM OLED panel driven by bottom-contact OTFTs", *IEEE Electr. Device L.* 27 (**2006**) 249.

[17] W. Clemens, I. Fix, J. Ficker, A. Knobloch, A. Ullmann, "From polymer transistors toward printed electronics", *J. Mater. Res.* 19 (**2004**) 1963.

[18] P. F. Baude, D. A. Ender, M. A. Haase, T. W. Kelley, D. V. Muyres, S. D. Theiss, "Pentacene-based radio-frequency identification circuitry", *Appl. Phys. Lett.* 82 (**2003**) 3964.

[19] E. Becquerel, "Mémoire sur les effets électriques produits sous l'influence des rayons solaires", *C. R. Acad. Sci.* 9 (**1839**) 561.

[20] M. A. Green, "The path to 25% silicon solar cell efficiency: History of silicon cell evolution", *Prog. Photovolt: Res. Appl.* 17 (**2009**) 183.

[21] J. Zhao, A. Wang, M. A. Green, "24.5% Efficiency silicon PERT cells on MCZ substrates and 24.7% efficiency PERL cells on FZ substrates", *Prog. Photovolt: Res. Appl.* 7 (**1999**) 471.

[22] R. M. Swanson, "Approaching the 29% limit efficiency of silicon solar cells", *Proceedings of the 31st IEEE Photovoltaic Specialists Conference*, Orlando, USA (**2005**) 889.

[23] M. A. Green, K. Emery, Y. Hishikawa, W. Warta, E. D. Dunlop, "Solar cell efficiency tables (version 42)", *Prog. Photovolt: Res. Appl.* 21 (**2013**) 827.

[24] Photovoltaics Report, Fraunhofer ISE, July 28 (**2014**) 18.

[25] B. O'Regan, M. Grätzel, "A low-cost, high-efficiency solar cell based on dye-sensitized colloidal TiO_2 films", *Nature* 353 (**1991**) 737.

[26] http://www.heliatek.com/newscenter/latest_news/heliatek-liefert-heliafilm-fuer-asiens-groesste-biopv-installation-in-singapur/?lang=en (02/05/2015).

[27] http://www.dyesol.com/partners/manufacturing-partners (02/05/2015).

[28] http://www.pv-tech.org/news/zsw_sets_21.7_cigs_cell_record (05/04/2015).

[29] http://investor.firstsolar.com/releasedetail.cfm?releaseid=864426 (05/04/2015).

[30] E. G. Eperon, S. D. Stranks, C. Menelaou, M. B. Johnston, L. M. Herz, H. J. Snaith, "Formamidinium lead trihalide: A broadly tunable perovskite for efficient planar heterojunction solar cells", *Energy Environ. Sci.* 7 (**2014**) 982.

[31] J. H. Noh, S. H. Im, J. H. Heo, T. N. Mandal, S. I. Seok, "Chemical management for colorful, efficient, and stable inorganic-organic hybrid nanostructured solar cells", *Nano Lett.* 13 (**2013**) 1764.

[32] S. D. Stranks, G. E. Eperon, G. Grancini, C. Menelaou, M. J. P. Alcocer, T. Leijtens, L. M. Herz, A. Petrozza, H. J. Snaith, "Electron-hole diffusion lengths exceeding 1 micrometer in an organometal trihalide perovskite absorber", *Science* 342 (**2013**) 341.

[33] A. Kojima, K. Teshima, Y. Shirai, T. Miyasaka, "Organometal halide perovskites as visible-light sensitizers for photovoltaic cells", *J. Am. Chem. Soc.* 131 (**2009**) 6050.

[34] http://www.photon.info/photon_news_detail_en.photon?id=90531 (05/04/2015).

[35] A. Yella, H. Lee, H. N. Tsao, C. Yi, A. K. Chandiran, M..K. Nazeeruddin, E. Wei-Guang Diau, C. Yeh, S. M Zakeeruddin, M. Grätzel, "Porphyrin-Sensitized Solar Cells with Cobalt (II/III)-Based Redox Electrolyte Exceed 12 Percent Efficiency", *Science* 334 (**2011**) 629.

[36] "Heliatek consolidates its technology leadership by establishing a new world record for organic solar technology with a cell efficiency of 12%" (http://www.heliatek.com/wp-content/uploads/2013/01/130116_PR_Heliatek_achieves_record_cell_effiency_for_OPV.pdf) (22-02-2013).

[37] F. R. Lipsett, "On the production of single crystals of naphthalene and anthracene", *Can. J. Phys.* 35 (**1957**) 284.

[38] T. Kajiwara, H. Inokuchi, S. Minomura, "Charge mobility of organic semiconductors under high pressure anthracene", *Bull. Chem. Soc. Jpn.* 40 (**1967**) 1055.

[39] G. H. Heilmeier, G. Warfield, S. E. Harrison, "Applicability of the band model to metal-free phthalocyanine single crystals", *Phys. Rev. Letters* 8 (**1962**) 309.

[40] H. Shirakawa, E. J. Louis, A. G. MacDiarmid, C. K. Chiang, A. J. Heeger, "Synthesis of electrically conducting organic polymers: Halogen derivatives of polyacetylene, (CH) x" *J.C.S. Chem. Comm.* 16 (**1977**) 578.

[41] C. W. Tang, "Two layer organic photovoltaic cell", *Appl. Phys. Lett.* 48 (**1986**) 183.

[42] M. Hiramoto, H. Fujiwara, M. Yokoyama, "p-i-n like behavior in three-layered organic solar cells having a co-deposited interlayer of pigments", *J. Appl. Phys.* 72 (**1992**) 3781.

[43] M. Pfeiffer, T. Fritz, J. Blochwitz, A. Nollau, B. Plönnigs, A. Beyer, K. Leo, "Controlled doping of molecular organic layers: Physics and device prospects", *Advances in Solid State Physics* 39 (**1999**) 77.

[44] B. Maennig, J. Drechsel, D. Gebeyehu, P. Simon, F. Kozlowski, A. Werner, F. Li, S. Grundmann, S. Sonntag, M. Koch, K. Leo, M. Pfeiffer, H. Hoppe, D. Meissner, N. Sariciftci, I. Riedel, V. Dyakonov, J. Parisi, "Organic p-i-n solar cells", *Applied Physics A: Materials Science & Processing* 79 (**2004**) 1.

[45] L. Wen, Q. Chen, F. Sun, S. Song, L. Jin, Y, Yu, "Theoretical design of multi-colored semi-transparent organic solar cells with both efficient color filtering and light harvesting", *Sci. Rep.* 4 (**2014**) 7036.

[46] R. R. Lunt, V. Bulovic, "Transparent, near-infrared organic photovoltaic solar cells for window and energy-scavenging applications", *Appl. Phys. Lett.* 98 (**2011**) 113305.

2. Organic Semiconductors

In this chapter the basic chemical and physical properties of organic semiconductors are introduced, as they are required for understanding the results presented in this thesis. First, the formation of molecular orbitals theory is discussed. Later, electrical and optical properties of organic semiconductors materials are described, as well as charge transport mechanism in organic materials.

2.1 Introduction

Organic semiconductors are promising materials for organic electronics due to their favourable properties, allowing them to be utilised in high throughput and low-cost fabrication methods.

Organic semiconductors are carbon-based compounds, usually also composed of other element atoms such as oxygen, nitrogen or sulphur, with semiconducting properties. The commonly used organic semiconductors can be categorised as oligomers (small-molecules) or conjugated polymers. Small-molecules have low molecular weight; in contrast, polymers, at least in principle, consist of a nearly unlimited number of repeatable monomers and have long molecular chains. Figure 2.1 and Figure 2.2 depicts the most used as absorbers in organic photovoltaics.

An important difference between small-molecules and polymers lies in the way how they are processed to form thin-films. Whereas small-molecules are usually deposited via thermal evaporation or sublimation under ultra-high vacuum, conjugated polymer are generally deposited using solution-processed methods, such as spin-coating, ink-jet printing or doctor blade techniques.

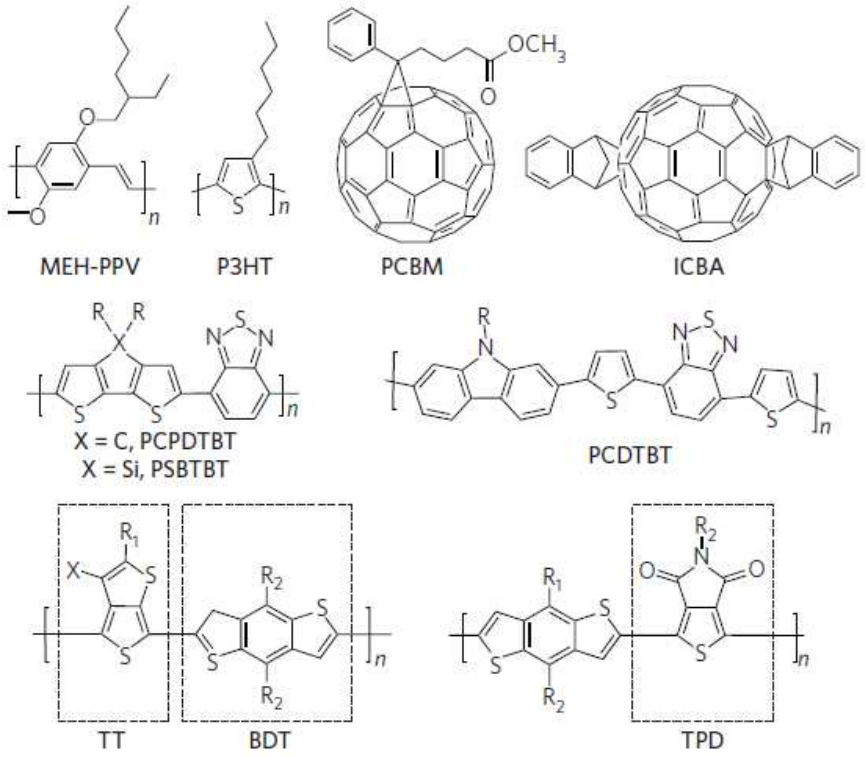

Figure 2.1 - Chemical structures of polymers most used in organic solar cells.

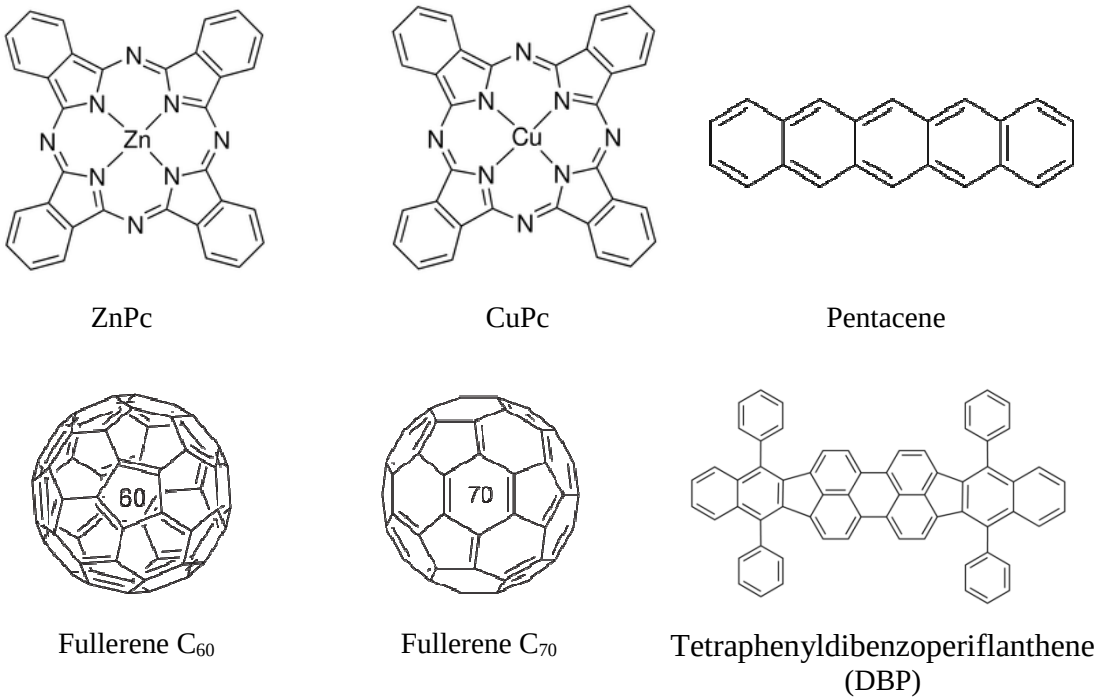

Figure 2.2 - Chemical structures of small-molecules most used in organic solar cells.

Small-molecules are very attractive for application in solar cells because they have several advantages versus polymers such as:

- *Short synthesis*: less than five steps are usually needed to synthesize the compound. Its well-defined chemical structures make them synthetically well reproducible.
- *Higher purity*: small-molecule materials have well-defined molecular weights, allowing for straightforward separation of the host from the impurities. They are easily purified by re-crystallization and/or sublimation.
- Better *control on the structure and morphology* of the deposited film; depending on the growth parameters (substrate temperature, pressure inside the deposition chamber and deposition rate) the deposited film can be poly-crystalline or amorphous in nature.
- *Solvents (potentially toxic) are not needed.*
- *Multilayer devices:* The preparation of well-defined multilayer structures, such as tandem solar cells, is comparatively easy because of the control of the layer thickness on the nanometre scale.

2.2 Molecular Orbital Theory

There are a large number of binding configurations of carbon (several millions of compounds were reported). A carbon atom has six electrons and its ground state configuration is $1s^2 2s^2 2p^2$, where *s* orbitals are fully occupied and two of three p_x, p_y, p_z orbitals are occupied by one electron. When carbon atom makes a bond with another atom, hybridization occurs between *s* and *p* orbitals. The hybridization sp^3 occurs when a carbon atom connects via four single bonds to other atoms by σ-bonds, such saturated compounds are good electrical insulators (Figure 2.3). Examples of this binding configuration are alkanes, or saturated polymers such us polyethylene $\left(\text{- } CH_2 - CH_2 \text{ -}\right)_n$, polystyrene or polypropylene.

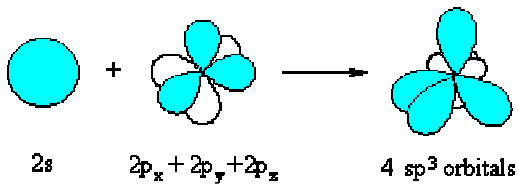

Figure 2.3 - Hybridization sp^3.

On the other hand, molecules containing double or triple bonds are more complex and interesting from the point of view of the optical and electrical properties, for instance ethylene, $H_2C=CH_2$. In this case carbon atoms exhibit a sp^2 hybridization which means that one *s* orbital and two *p* orbitals are combined. Figure 2.4 depicts sp^2 hybridization.

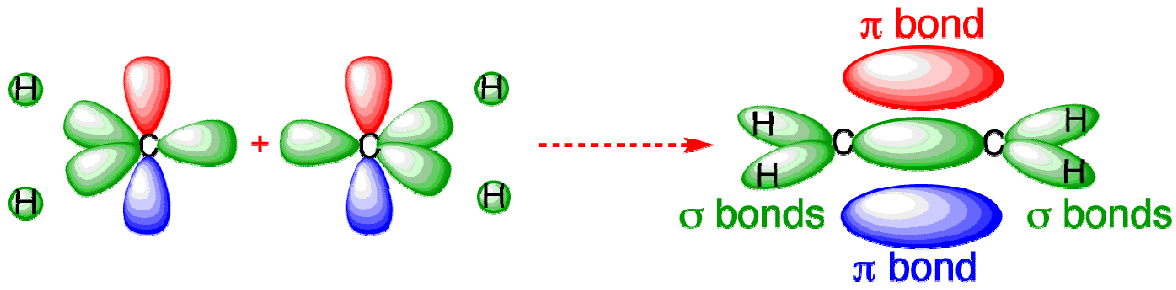

Figure 2.4 - sp^2-hybridization of the valence electrons of two carbon atoms lead to molecular π- and σ-bondings.

In each carbon atom, three sp^2 hybrid orbitals are arranged in a trigonal planar geometry (120º between them), while the non-hybridized $2p_z$ remain perpendicular to this plane. The combination of one sp^2 orbital from each carbon atom gives two orbitals in the final molecule known as σ and σ*. The side-by-side overlapping of both $2p_z$ orbitals also results in two orbitals in the final molecule: π and π*. These orbitals are ordered from lower energy to higher energy as follows: σ, π, π*, σ*. The orbitals π and σ are filled with electrons and constitute the double bond (stronger σ bond and weaker π bond). The energetically highest occupied molecular orbital is called HOMO. On the other hand, the energetically lowest unoccupied molecular orbital is called LUMO. Comparing to inorganic semiconductors, it should be noted that HOMO is the analogue of valence band and LUMO is the analogue of conduction band. In the case of ethylene molecule, the π orbital is the HOMO meanwhile the π* is the LUMO (Figure 2.5).

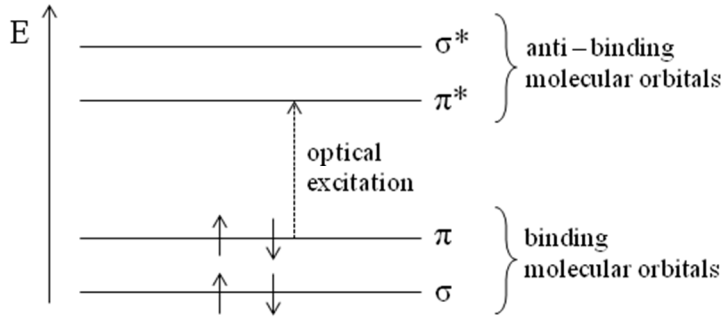

Figure 2.5 - Energetic diagram of molecular orbitals of an ethylene molecule

The HOMO–LUMO is the lowest electronic transition. The difference between the π-π* molecular orbital is called energy band gap (*Eg*) and confers the optoelectronical properties of a semiconductor.

If the molecule presents an alternation of simple and double bonds over a planar segment the system is said to be π-conjugated. This system can be presented in many forms, as well as small-molecules, conjugated polymers or molecular crystals. For each double bond a new pair of π, π* orbitals appear in the energetic diagram of orbitals of the final molecule, and the gap between occupied and empty states in these π systems becomes smaller. In this kind of molecules, the molecular orbitals, from lower to higher energy, are: σ,…, σ_n, π, …, π_n, π_n^*, …, σ_n^*.

If carbon atoms form larger molecules, typically with benzene rings as the basic unit, the HOMO–LUMO gap becomes so small that the HOMO electrons can overcome this energetic barrier in such way that they do not belong to a single bond or atom, but rather to a group of atoms. The π-bonds become delocalised and form a π-system which often has the extensions of the molecule. Figure 2.6 depicts π-electrons moving along the conjugated chain as a flip-flop between single and double bonds.

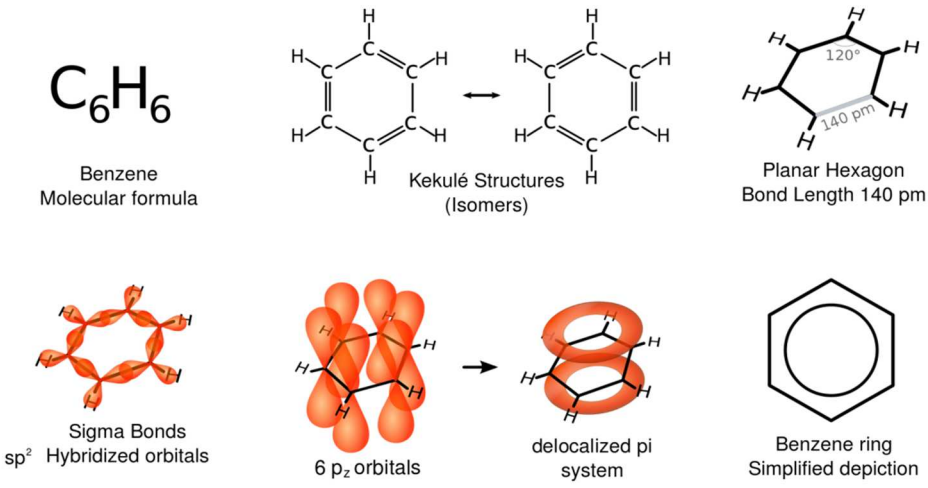

Figure 2.6 - Scheme of electron delocalization in a benzene ring.

The ionization potential (IP) is the minimum amount of energy required to extract an electron from the molecule. On the other hand, the electron affinity (EA) is defined as the amount of energy released when an electron is added to a molecule. In this work, we set HOMO equal to the IP and the LUMO to the EA.

Due to a small molecular interaction (overlapping of the π-orbitals) in the organic solid, the charge carrier transport level for holes (HOMO) is only weakly broadened. The LUMO corresponds to the electron transport level in organic solids.

The value of the HOMO level is often determined by means of cyclic voltammetry and photoemission yield spectroscopy techniques, while the value of the LUMO level is usually measured by cyclic voltammetry (CV) or calculated by adding up the measured HOMO level and the measured optical bandgap. CV allows the estimation of the energetic levels from liquid solutions; in contrast, the technique used to measure the HOMO level in thin films is ultraviolet photoelectron spectroscopy (UPS) (or inverse photoemission spectroscopy (IPES) in the case of the LUMO level).

2.3 Optical properties

Optical density (OD) is the amount of attenuation (or gradual intensity loss) that occurs when light passes through an optical component. Optical attenuation may result from not only absorption of light but also from scattering of light. Higher OD values indicate a higher level of blocking. The OD can be calculated from optical transmission (T) measurements (Eq. 2.1):

$$OD = -\log_{10}(T) \tag{2.1}$$

The optical density of a material relates to the sluggish tendency of the atoms of a material to maintain the absorbed energy of an electromagnetic wave in the form of vibrating electrons before reemitting it as a new electromagnetic disturbance. When the material is more optically dense a wave will move slowly through the material. The OD depends on the material and its thickness.

On the other hand, the optical absorption coefficient (α) determines how far into a material light of a particular wavelength can penetrate before it is absorbed. The absorption coefficient only depends on the material and on the wavelength of light which is being absorbed. In a material with a low absorption coefficient, light is only poorly absorbed, and if the material is thin enough, it will appear transparent to that wavelength. Inorganic semiconductor materials have a sharp edge in their absorption coefficient, since light which has energy below the band gap does not have sufficient energy to excite an electron into the conduction band from the valence band. Consequently this light is not absorbed. The absorption coefficient for hydrogenated amorphous

silicon (a-Si:H), crystalline silicon (c-Si) and pentacene semiconductors materials is shown below (Figure 2.7).

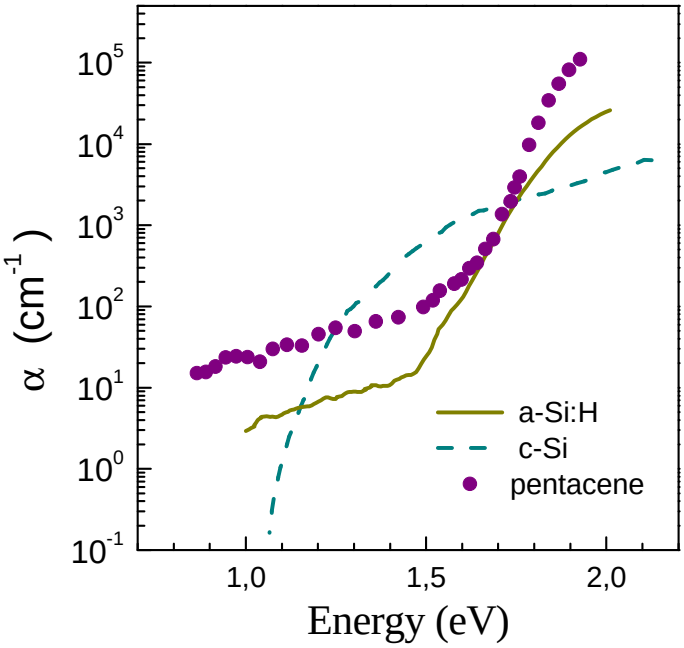

Figure 2.7 – Optical absorption coefficients for different thin film semiconductors.

The Figure 2.7 shows that, even for those photons which have energy above the band gap, the absorption coefficient is not constant, but still depends strongly on wavelength. The probability of absorbing a photon depends on the likelihood of having a photon and an electron interact in such a way as to move from one energy band to another. For photons which have energy very close to that of the band gap, the absorption is relatively low since only those electrons directly at the valence band edge can interact with the photon to cause absorption. As the photon energy increases, not just the electrons already having energy close to that of the band gap can interact with the photon. Therefore, a larger number of electrons can interact with the photon and result in the photon being absorbed.

The absorption coefficient, α, is related to the extinction coefficient, k, by the following formula:

$$\alpha = \frac{4\,\pi\,k}{\lambda} \tag{2.2}$$

where λ is the wavelength. If λ is in nm, it is necessary to multiply by 10^7 to get the absorption coefficient in units of cm^{-1}.

Organic semiconductors are characterised by high absorption coefficients which make it possible to manufacture thin film devices. The use of such thin layers reduces the amount of active material required and also makes light-weight. In addition, this allows the production of flexible devices, and even the realization of semitransparent solar cells which can be integrated into windows and glass facades.

2.4 Charge Carrier Transport

Due to the weak electronic coupling in organic semiconductors, the charge carriers can be effectively localised on a single molecule. Disordered molecular solids exhibit generally an inhomogeneous energy distribution of their localised transport states. Therefore, the charge carrier transport between adjacent molecules is thermally activated and the mobility increases with increasing temperature [1]. This kind of thermally activated charge carrier transport is known as hopping transport. The mobility due to thermally assisted hopping is many orders of magnitude lower than that due to band transport. The charge transport mechanism via a localised hopping mechanism is characterized by a radical ion that polarizes the surrounding neutral molecules. The rate of this hopping process may be expressed with Marcus theory [2–3]. Sometimes the ensemble of localised states within a certain energy range is called band. It is stated here, that the term band in this context has nothing to do with energy bands in an ideal crystal.

In contrast, band-like conduction can occur in organic semiconductors if its structure is well organised like in the case of organic crystals. Similar to inorganic semiconductors, the conductivity in very pure and highly ordered organic solids is limited by scattering processes with phonons [4]. In contrast to the hopping transport, the conductivity is increasing with decreasing temperature due to a reduction of the respective scattering probability.

It can be summarized, that in well-organized organic crystals the charge transport is based on polaron bands, while the hopping transport prevails in polycrystalline and amorphous materials. Next, the most used charge transport models in organic semiconductors are briefly exposed. However, it is important to note that a full comprehensive theory to describe the charge transport in organic semiconductors is still lacking.

Hopping Mechanism

A theory involving electron transfer based on oxidation – reduction reactions assuming very little spatial overlap of the electronic orbitals of two reacting molecules was introduced by Marcus in 1956 [5]. The charge transport can be described as involving a self-exchange electron (hole) transfer from a charged molecule to a next neutral one by hopping of charges. According to this theory, two major parameters determine self-exchange rates [2] [6]:

i. the electronic coupling between adjacent molecules, which needs to be maximized.

ii. the reorganization energy, which needs to be small for efficient charge transport.

Here the reorganization energy corresponds basically to the sum of geometry relaxation energies switching from the neutral state to the charged state and vice versa. All this elucidates the strong importance of intermolecular interactions on the efficiency of charge carrier hopping and their related mobility since they are directly related.

Multiple Trapping and Release Model

Introduced originally to description of the low mobility of hydrogenated amorphous silicon devices [7], in the Multiple Trapping and Release (MTR) model the charge carriers are assumed to travel in narrow, delocalised bands and interact with a high concentration of localised trap levels. Further adapted by Horowitz et al. [8–9] the localised trap levels are believed to arise from defects and impurities in both the molecular and crystal structure. In the decentralised band the charge carriers have a band mobility μ_0, but interact further by trapping and detrapping with localised states. The trapping and release mechanisms determines the overall mobility and the thermally activated behaviour. The trap distribution (Density of States (DOS) within the gap) is believed to be exponentially shaped. Also, the often observed gate voltage, i.e. electric field, dependence of the charge carrier mobility can be described with this model.

2.4.1 Determination of the charge carrier mobility

The charge carrier mobility characterises how quickly a charge can move through a metal or semiconductor. The term carrier mobility refers in general to both electron and hole mobility in semiconductors. The charge carrier mobility of an organic material can be determined from different approaches. The charge carrier mobilities of organic materials greatly vary depending on the kind of charge carriers, namely, whether they are holes or electrons, molecular structures, and materials morphologies. Due to the fact that the mobility depends on several parameters, the

measuring conditions have a strong impact on the results. In some cases device stacks have to be made which differ compared to a typical solar cell stack. The morphology which could depend on the layer device stack influences on the mobility. Common methods are now considered, with focus on the field effect transistor which is used in this work.

Time of flight method

Time of flight (TOF) is one of the most established experimental techniques for mobility measurements in organic disordered systems. This method is a rather simple and direct approach, shown by Warta and Karl [10] for naphthaline and Kitamura et al. [11] for the molecule CuPc. The TOF method is based on the measurement of the carrier transit time (τ), namely, the time required for a charge carriers photo-generated near one of the electrodes by a short intense light pulse to drift across the layer with a well-known thickness to the other electrode under an applied electric field. Samples used for the measurement are consisting of organic layer sandwiched between the two electrodes, where one of which is transparent for light pulse.

In the case of measuring a hole drift mobility, the transparent electrode is held at a positive potential with respect to the ground, while the other one is grounded through a resistance which has a much smaller resistance than the sample. This leads to an applied potential V in the material. Hole charges are generated by photo-excitation of the film through irradiation with a short pulse laser (the wavelength of which depends on the absorption band of materials). One of the advantages of using TOF technique is that the hole and electron mobility can be studied separately.

For the mobility calculation the thickness *d*, the applied voltage V, and the transit time τ_d between the optical excitation and the arrival of the charges at the electrode have to be known (Eq. 2.3):

$$\mu = \frac{d^2}{\tau_d V} \tag{2.3}$$

Space charge limited current

The theory of space charge limited current (SCLC) between plane parallel electrodes was first given by Mott and Gurney (1940) [12]. Later, in 1969, it was also applied in organic semiconductors [13].

The current flow is limited either by barriers at the electrodes (injection and extraction) or through transport in the organic layer. To get SCLC ohmic contacts are required. Then, the current flow is limited by the charge carrier mobility. An additional requirement is that only one kind of charge carriers is injected and the other one is blocked. This can be realized by choosing a suitable stack design (e.g. electron- or hole only devices [14–15]).

The carrier drift mobility measured by SCLC method is based on the analysis of current density (J) – applied voltage (V) characteristics in dark. Generally, the J–V characteristics are linear at low drive voltages, showing ohmic behaviour. At high applied voltages, the J–V characteristics become space-charge limited because of the injection of charge carriers from one electrode. When the contact between the electrode and the organic layer is ohmic, the current is transport limited instead of injection limited. In the case of SCLC, the current-voltage characteristic does not satisfy the ohmic law any longer and shows a superlinear behaviour of V^2 and is described in the absence of any trapping effects. The space-charge-limited current J is given by Eq. 2.4, which is known as the Mott-Gurney law:

$$J = \frac{9}{8}\,\mu\,\epsilon\,\epsilon_0\,\frac{V^2}{L^3} \tag{2.4}$$

where ϵ is the dielectric constant, V the applied voltage, and L the thickness of the semiconductor material.

The interpretation of J–V curves becomes more complex in the presence of traps. They first exhibit a linear regime, where transport is injection-limited, followed by a sudden increase for an intermediate range of applied biases; finally, the V^2 dependence of the trap-free SCLC regime is reached. The extent of the intermediate region is governed by the spatial and energetic distribution of trap states.

Organic Field Effect Transistor (OFET)

An OFET is a three terminal device in which an organic semiconductor is placed on a dielectric and connected to the source and drain electrodes. The OFET electrical characterisation is a common method used to determine the charge carrier mobility of organic materials [16–17], which can measure the average charge carrier drift velocity per unit electric field. It is a measure of how easily charge carriers can move in the device. This method has been used in MNT group since ten years ago, further details about the calculation of charge carrier mobility from OFET characterisation can be found in Appendix I.

Expressions derived for inorganic-based transistors in the linear and saturated regimes prove to be readily applicable to organic transistors (OFETs) [18]. These expressions read in the linear regime (Eq. 2.5):

$$I_{SD} = \frac{W}{L} \mu C (V_G - V_T) V_{SD} \tag{2.5}$$

and in the saturated regime (Eq. 2.6):

$$I_{SD} = \frac{W}{2L} \mu C (V_G - V_T)^2 \tag{2.6}$$

Where, I_{SD} and V_{SD} are the current and voltage bias between source and drain, respectively, V_G denotes the gate voltage, V_T is the threshold voltage at which the current starts to rise, C is the capacitance of the gate dielectric, and W and L are the width and length of the conducting channel. From these expressions carrier mobility can be estimated.

Transport is affected by structural defects within the organic layer at the interface, the surface topology and polarity of the dielectric, and/or the presence of traps at the interface (that depends on the chemical structure of the gate dielectric surface). Also, contact resistance at the source and drain metal/organic interfaces plays an important role. The contact resistance becomes gradually more important when the length of the channel is reduced and the transistor operates at low fields. Its effect can be omitted via four-probe measurements [19–20].

The charge mobilities extracted in the saturated regime are generally higher than those in the linear regime due to different electric-field distributions. The mobility can sometimes be found to be gate-voltage dependent [21]. This observation is often related to the presence of traps due to structural defects and/or impurities (that the charges injected first have to fill prior to establishment of a current) and/or to dependence of the mobility on charge carrier density (which is modulated by V_G) [22].

Comparisons of mobilities measured by different methods

One of the important differences between the different mobility measurement methods is the geometry of the sample in which the charge mobility is characterised. The thickness of samples for the measurement is different depending upon the method. In TOF and SCLC, the sample is sandwiched between two electrodes and the conduction of the charges is perpendicular to the substrate plane. By contrast, in a FET the charge mobility is characterised within the plane of the

substrate. The analysis of SCLC curves for specifically designed single carrier devices or time-of-flight experiments are some alternatives. However, these methods very often lead to incorrect results as analytical expressions are not valid in most of the cases involving organic semiconductors [23].

Nonetheless, it is important to note that this geometrical difference is irrelevant when one study the charge transport properties in an amorphous material but becomes fundamental when the material present some molecular organisation such as liquid crystal materials or crystalline materials.

References

[1] P. M. Borsenberger, L. Pautmeier, H. Bässler, "Charge transport in disordered molecular solids" *J. Chem. Phys.* 94 (**1991**) 5447.

[2] V. Coropceanu, J. Cornil, D. A. da Silva, Y. Olivier, R. Silbey, J. L. Bredas, "Charge transport in organic semiconductors", *Chem. Rev.* 107 (**2007**) 926.

[3] J. Nelson, J. J. Kwiatkowski, J. Kirkpatrick , J. M. Frost, "Modeling charge transport in organic photovoltaic materials", *Acc. Chem. Res.* 42, (**2009**) 1768.

[4] W. Warta, R. Stehle, N. Karl, "Ultrapure, High Mobility Organic Photoconductors", *Appl. Phys. A* 36 (**1985**) 163.

[5] R. A. Marcus. "On the Theory of Oxidation-Reduction Reactions Involving Electron Transfer", *J. Chem. Phys.*, 24 (**1956**) 966.

[6] J.-L. Bredas, D. Beljonne, V. Coropceanu, J. Cornil, "Charge-Transfer and Energy-Transfer Processes in π-Conjugated Oligomers and Polymers: A Molecular Picture". *Chem. Rev.*, 104 (**2004**) 4971.

[7] P. G. Le Comber, W. E. Spear, "Electronic Transport in Amorphous Silicon Films", *Phys. Rev. Lett.*, 25 (**1970)** 509.

[8] G. Horowitz, R. Hajlaoui, P. Delannoy. "Temperature Dependence of the Field - Effect Mobility of Sexithiophene. Determination of the Density of Traps". *J. Phys. III France*, 5 (**1995**) 355.

[9] G. Horowitz, M. E. Hajlaoui, R. Hajlaoui. "Temperature and gate voltage dependence of hole mobility in polycrystalline oligothiophene thin film transistors", *J. Appl. Phys.*, 87 (**2000**) 4456.

[10] W. Warta, N. Karl, "Hot holes in naphthalene: High, electric-field-dependent mobilities", *Phys. Rev. B*, 32 (**1985**) 1172.

[11] M. Kitamura, T. Imada, S. Kako, Y. Arakawa, "Time-of-Flight Measurement of Lateral Carrier Mobility in Organic Thin Films", *Jpn. J. Appl. Phys.* 43 (**2004**) 2326.

[12] N. F. Mott, R. W. Gurney, "Electronic Processes in Ionic Crystals", *Oxford University Press*, New York City, **1940**.

[13] M. A. Lampert, "Simplified Theory of Space-Charge-Limited Currents in an Insulator with Traps", *Phys. Rev.* 103 (**1956**) 1648.

[14] H. Antoniadis, J. N. Miller, D. B. Roitman, I. H. Cambell, "Effects of hole carrier injection and transport in organic light-emitting diodes", *IEEE Trans. Electron Devices* 44 (**1997**) 1289.

[15] P. M. Blom, M. J. M. d. Jong, C. T. Liedenbaum, "Device physics of polymer light-emitting diodes", *Polym. Adv. Technol.* 9 (**1998**) 390.

[16] H. Katz, "Organic molecular solids as thin film transistor semiconductors", *J. Mater. Chem.* 7 (**1997**) 369.

[17] C. D. Dimitrakopoulos, D. J. Mascaro, "Organic thin-film transistors: a review of recent advances", *IBM J. Res. Dev.* 45 (**2001**) 11.

[18] G. Horowitz "Organic field-effect transistors", *Adv. Mater.* 10 (**1998**) 365.

[19] P.V. Pesavento, R. J. Chesterfield, C. R. Newman, C. D. Frisbie, "Gated four-probe measurements on pentacene thin-film transistors: contact resistance as a function of gate voltage and temperature", *J. Appl. Phys.* 96 (**2004**) 7312.

[20] C. Goldmann, S. Haas, C. Krellner, K.P. Pernstich, D.J. Gundlach, B. Batlogg, "Hole mobility in organic single crystals measured by a "flip-crystal" field-effect technique", *J. Appl. Phys.* 96 (**2004**) 2080.

[21] C.D. Dimitrakopoulos, S. Purushothaman, J. Kymissis, A. Callegari, J.M. Shaw, "Low-voltage organic transistors on plastic comprising high-dielectric constant gate insulators", *Science* 283 (**1999**) 822.

[22] C. Tanase, E.J. Meijer, P.W.M. Blom, D.M. de Leeuw, "Unification of the hole transport in polymeric field-effect transistors and light-emitting diodes", *Phys. Rev. Lett.* 91 (**2003**) 216601.

[23] T. Kirchartz, "Influence of diffusion on space-charge-limited current measurements in organic semiconductors", *Beilstein J. Nanotechnol.* 4 (**2013**) 180.

3. Organic Solar Cells

A brief introduction to organic solar cells is given in this chapter. Firstly, an equivalent electrical circuit, useful to characterise any type of solar cell, is presented. Following, the working principle of the organic solar cells is introduced with special attention to its peculiarities, such as the creation and dissociation of excitons, the origin of the open circuit voltage as well as the recombination processes. Finally, the most used architectures in organic solar cells are detailed.

3.1 Solar Cells Characterisation

A solar cell is a device that converts directly the light into electricity. The standard parameters used to characterise the performance of a solar cell are described briefly in this section. These parameters will be useful to compare the electrical performance of different solar cells. Moreover, its analysis allows a deep understanding of the physics governing its electrical behaviour.

3.1.1 Current - Voltage characteristics

When a solar cell is measured in dark, the current density *vs.* voltage (*J*–*V*) characteristic shows the typical diode characteristic. Under illumination, the dark *J*–*V* curve is shifted towards negative currents because of the generated photocurrent (Figure 3.1). Photocurrent density is defined as the photocurrent generated per unit area (J_{PH}). The electrical power generated by a solar cell can be identified by the area enclosed in the fourth quadrant of the *J*–*V* curve under illumination. Short circuit current density (J_{SC}), open circuit voltage (V_{OC}) and fill factor (*FF*) values are the main parameters that characterise a solar cell. These three parameters determine the power conversion efficiency of a solar cell (η).

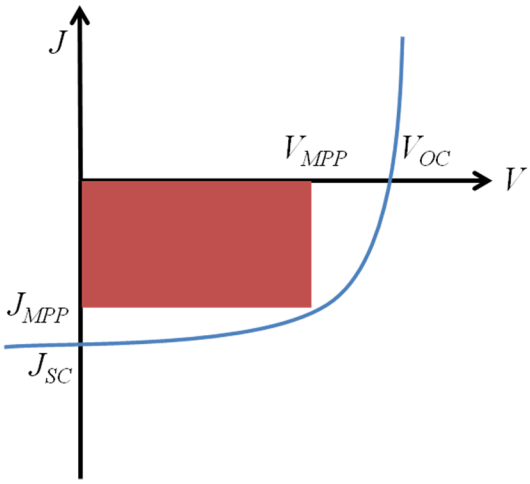

Figure 3.1 - *J–V* curve of a PV cell under illumination (blue line) conditions. The open circuit voltage (V_{OC}) and the short-circuit current (J_{SC}) are shown. The maximum power output is given by the red square (current density in maximum power point (J_{MPP}) and voltage in maximum power point V_{MPP}).

Open Circuit Voltage

The voltage between the two terminals of a solar cell under illumination at which no current flows through the device is called the open circuit voltage (V_{OC}). V_{OC} is the maximum voltage that the photovoltaic cell can provide to the external circuit. Likewise, V_{OC} can also be thought of as the point at carrier generation and recombination exactly balance each other and no net current exists at any point inside the device.

Short Circuit Current Density

When there is not voltage applied only short-circuit current density J_{SC} flows through the solar cell terminals. J_{SC} is the maximal current density the photovoltaic cells can provide to the external circuit. In ideal solar cell (without parasitic resistances), the J_{SC} will be the same as the J_{PH}. Thus, for monochromatic exposure the spectral dependence of the charge carrier generation can be measured.

Fill Factor

Fill factor is one of the key parameter to evaluate the performance of a solar cell. The maximum power point (*MPP*) of a solar cell can be measured in the fourth quadrant of the *J–V* curve (Figure 3.1). The fill factor of a device is defined as the ratio between the maximum power delivered to an external circuit and the product of V_{OC} and J_{SC} (Eq. 3.1). Graphically, the FF is a measure of the "squareness" of the solar cell and is also the area of the largest rectangle which will fit in the *J–V* curve.

$$FF = \frac{MPP}{J_{SC}V_{OC}} = \frac{J_{MPP}V_{MPP}}{J_{SC}V_{OC}} \tag{3.1}$$

Because of the diode behaviour and the presence of resistances and recombination losses, $|J_{MPP}|$ and V_{MPP} are always lower than $|J_{SC}|$ and V_{OC}, respectively.

Power Conversion Efficiency

Power conversion efficiency (η) is defined as the percentage of incident illumination power P_o that is converted into electrical output power and is calculated from the maximum power at the MPP over the incident light power P_0 [1].

$$\eta = \frac{J_{MPP}V_{MPP}}{P_0} = \frac{FFJ_{SC}V_{OC}}{P_0} \tag{3.2}$$

To certify reliable comparison of different solar cells standard test conditions are used. Thereby, incident solar power density (*Po*) standards have been defined. National American Society for Testing Materials (ASTM) standard E948 and International Electrotechnical Commission (IEC) standard 60904-1 specifies a set of common test conditions and methods to measure the electrical performance of photovoltaic cells. They are named the Standard Testing Conditions (STC) and are defined as follows:

1. Temperature of the device under test (DUT) is to be 25˚ ± 1˚C;
2. Spectral distribution of the light is to be AM1.5 ± 25%;
3. Irradiance measured at the plane of the solar cell is to be 1 sun ± 2%

The spectrum standard is the AM1.5 which can be approached by commercial solar simulators (Figure 3.2). AM is the air mass coefficient defined by direct optical path length through the Earth's atmosphere, expressed as a ratio relative to the path length at the zenith. AM1.5 atmosphere thickness corresponds to a solar zenith angle of z = 48.19°. Therefore, AM1.5 is useful to represent the overall yearly average for mid-latitudes.

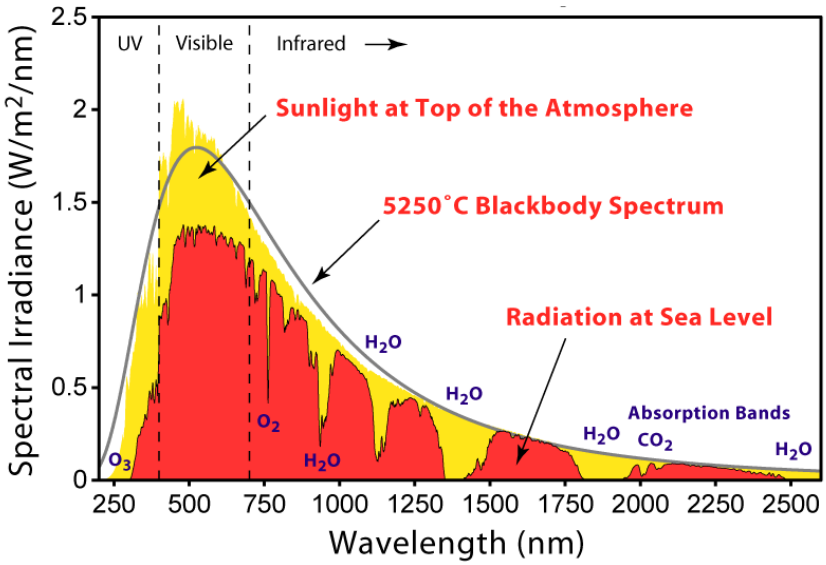

Figure 3.2 - Spectral irradiance of the AM1.5 (red area) solar spectrum up to 2600nm.

3.1.2 Equivalent circuit for solar cell

The current – voltage characteristic of an ideal solar cell can be defined as the sum of the Shockley equation (Eq. 3.3) that describes the electrical behaviour of the diode in dark conditions [1] with an added term, J_{PH}, corresponding to the photocurrent provided by the diode under illumination conditions (Eq. 3.4):

$$J(V) = J_0\left(e^{\frac{eV}{nk_BT}} - 1\right) \tag{3.3}$$

$$J(V) = -J_{PH} \tag{3.4}$$

where J is the current density, J_0 reverse bias saturation current density, n is the diode ideality factor, k_B is the Boltzmann constant, and T is the absolute temperature.

Assuming a generation rate of charge carriers independent of the applied voltage V and adding up Eq. 3.3 and Eq. 3.4, current density of a solar cell can be expressed as:

$$J(V) = J_0\left(e^{\frac{eV}{nk_BT}} - 1\right) - J_{ph} \tag{3.5}$$

Eq. 3.5 defines the characteristic of an ideal solar cell. Eq. 3.5 leads to the equivalent electrical circuit depicted in Figure 3.3.

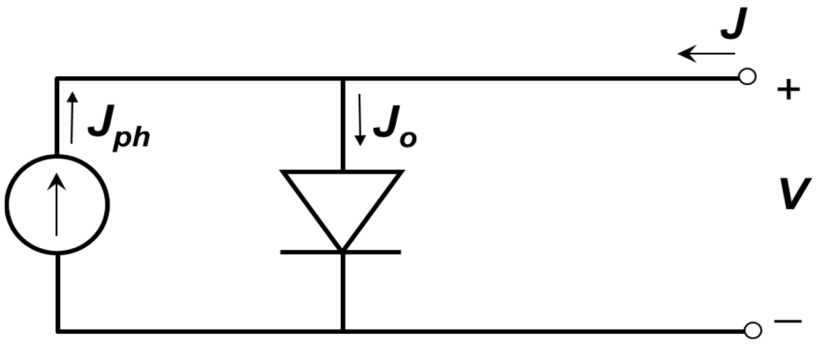

Figure 3.3 - Ideal solar cell consisting of a current source and an ideal diode in parallel.

As mentioned above, the Shockley equation (Eq. 3.5) can only be used for describing the electrical behaviour of ideal solar cells. In real devices, additional parallel resistance (R_P) and series resistance (R_S) must be taken into account.

- *Parallel resistance (R_P)*: also known as shunt resistor R_{SH}. It is due to shunt currents through shorts or pin-holes in the device.
- *Series resistance (R_S)*: represents Ohmic losses in the front and rear electrodes mainly due to the contact resistances.

Considering the effects of R_P and R_S the equivalent electrical circuit becomes (Figure 3.4):

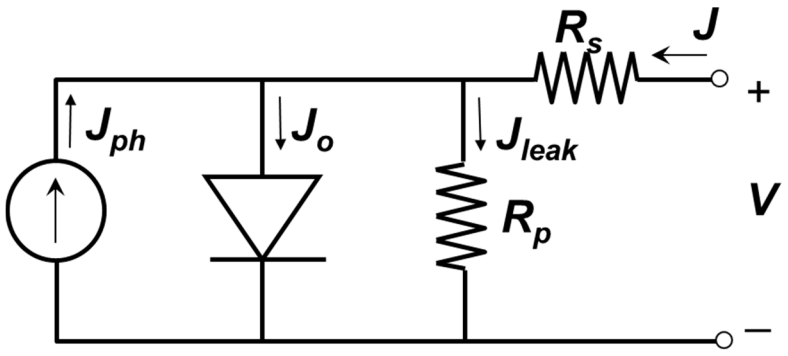

Figure 3.4 - Equivalent circuit of a solar cell including an additional shunt resistor R_P as well as a series resistor R_S.

Solving the equivalent circuit, the electrical characteristics of a non-ideal solar cell can be described by the following equation [1–3]:

$$J(V) = J_0\left(e^{\frac{e(V-R_sJ)}{nk_BT}} - 1\right) - J_{ph} + \frac{V - R_sJ}{R_p} \tag{3.6}$$

3.1.3 Spectral Response of solar cell

The spectral response *SR* (λ) is an important way to characterise the optical response of the solar cell and, in general, is a powerful tool to optimise their performance. The spectral response represents the current per irradiated light power in A/W for a certain wavelength. *SR* (λ) can be expressed as the J_{PH} per incident power (Eq. 3.7):

$$SR(\lambda) = \frac{J_{ph}(\lambda)}{P(\lambda)} \tag{3.7}$$

Furthermore, the External Quantum Efficiency (*EQE*) of a device determines the conversion efficiency of an absorbed photon into a free charge carrier (extracted electron-hole pair) and depends on wavelength (Eq. 3.8).

$$EQE \equiv \frac{N \text{ of electrons of external circuit}}{N \text{ of incident photons}} \tag{3.8}$$

The *EQE* can be derived from the spectral response considering that the energy of a photon $E_P = hc / \lambda$ with *h* being Planck's constant, *c* the speed of light and *q* the elementary charge using the following (Eq. 3.9):

$$EQE\ (\lambda) = SR(\lambda)\frac{hc}{q\lambda} \tag{3.9}$$

The short-circuit current density expected under a light source can be estimated from the *EQE* and the spectral irradiance of the light source by integrating the product of the *EQE* and the photon flux density (Eq. 3.10):

$$J_{SC} = \int_0^\infty qEQE\ (\lambda)\frac{\lambda}{hc}E_\lambda^{AM\,1.5}d\lambda \tag{3.10}$$

where $E_\lambda^{AM1.5}$ is the spectral irradiance of the AM1.5 spectrum.

The *EQE* can be converted into the internal quantum efficiency (*IQE*) if only the fraction of the actually absorbed photons is considered (Eq. 3.11):

$$IQE\ (\lambda) = \frac{EQE\ (\lambda)}{1 - R(\lambda) - T(\lambda)} \tag{3.11}$$

where *R(λ)* is the reflected light and *T(λ)* is the transmitted light.

3.2 Working principle of Photovoltaic Solar Cells

In this section, the physics behind the working principles of organic solar cells will be briefly described. To understand the physics behaviour of organic solar cell requires a deep knowledge of the working principle of a photovoltaic solar cell. We review in the following the fundamental principles for photovoltaic effect. A general approach is introduced to describe solar cells in terms applicable to all possible device structures including p-n homo- and heterojunction cells (i.e., Si, CIGS, CdTe), bulk heterojunction devices (i.e., organic solar cells), or nanostructured photoelectrochemical cells (i.e., DSCs)[4–5].

1. Any photovoltaic device requires a light absorber that converts electrons from thermal equilibrium into an excited state upon absorption of photons (Figure 3.5). Upon photon absorption, an electron is excited into an electronic state at higher energy, leaving a positive charge behind at low energy.

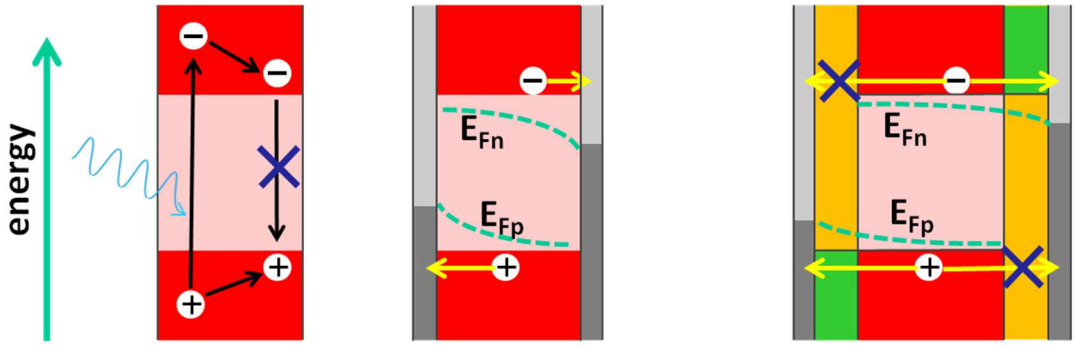

Figure 3.5 - Ideal structure of a photovoltaic device. The currents are driven by the gradient of electrochemical potential. On the left hand side the holes are blocked, while on the right and side electrons are blocked before reaching the contacts. Figure adapted from [6].

2. Either this excited state is metastable by itself or the electron is transferred into a metastable, high-energy state while the remaining positive charge gets into a metastable low-energy state.

3. A transport mechanism is necessary to bring electrons to a high electron energy contact or (negative potential), while the remaining positive charge needs a driving force to achieve the low energy contact [4]. Currents of electrons and holes respectively are driven by gradients of their electrochemical potential.

4. The contacts have to show some selectivity for charge collection such that positive charges cannot recombine with electrons from the high-energy contact, while electrons from the high energy-state should not reach the low-energy contact.

The selectivity of the contacts can be achieved using different approaches. The simple way is to add a thin layer with a strong selectivity character (for holes or electrons). These layers are usually called Hole (or Electron) Transport Layer (HTL, ETL). A HTL should be inserted between the donor and the anode electrode, whereas the ETL should be placed between acceptor and cathode electrode.

Examples of materials used as HTL in organic devices (including OLEDs and TFTs) are:

- Transition Metal Oxides (TMOs): molybdenum oxide (MoO_x) [7], vanadium pentaoxide (V_2O_5) [8], tungsten trioxide (WO_3) [9–10], rhenium dioxide (ReO_2) [11], nickel oxide (NiO) [12].

- *Solution processed organic materials*: poly(3,4-ethylenedioxythiophene) polystyrene sulfonate (PEDOT-PSS) [13], triindoles, triazatruxene (TAT), and N-trimethyltriindole (TMTI) [14].

- *Carbon-based nanostructures:* Carbon nanotubes (CNT) [15] and Graphene oxide (GO) [16–18].

As ETL the following compounds have been reported to have good selectivity for electrons:

- Lithium fluoride (LiF) [19], calcium (Ca) [20], bathocuproine (BCP) [21], bathophenanthroline (BPhen) [22], 1,3,5-tris(2-N-phenylbenzimidazolyl) benzene (TPBi) [23], zinc oxide (ZnO) [24], titanium oxide (TiOx) [25], caesium carbonate (Cs_2CO_3) [26].

The concept of the selectivity contacts was first introduced some years ago by some authors (see for example: Peter Würfel [5] and Juan Bisquert [27]). Although for many years this approach was used to describe the electrical behaviour of organic and dye sensitized solar cells, its simplicity and powerfulness it has caused that more and more authors use it as the theoretical framework for explaining the photovoltaic working principle of other types of solar cells; as well as crystalline silicon solar cells [28–29].

This definition is useful to describe any kind of photovoltaic solar cell, and can be easily applied to cells with an intrinsic absorber sandwiched between an n- and p- doped layers (n-i-p or p-i-n). Electrons are excited into some electronic state in the conduction band (CB), directly followed by phonon emission such that electrons decay to the bottom of the CB, which is the metastable high-energy state. The electric field across the intrinsic layer provides a driving force for electron

and hole transport toward the respective contact, while a doped n- and p-type layer close to the high- and low-energy contact provides the required transport selectivity due to a valence band (VB) offset that creates a barrier for hole transport toward the cathode, and a anode offset between the absorber and the p-type layers blocks electrons from recombining at the anode [30].

Organic solar cells operate very similar to p-i-n cells with the difference that the metastable high-energy state corresponds to the LUMO level of the acceptor while the HOMO level of the donor defines the low-energy state. Photovoltaic action in p-n homojunction silicon solar cells is often entirely attributed to the built-in electric field that provides a driving force for holes and electrons toward the cathode and anode, respectively. However, selective charge collection at the cathode is at least as important to achieve high conversion efficiencies.

While the above principles are basic requirements for PV action, they do not say much about the efficiency of the process. For the development of efficient single-junction solar cells, additional criteria have to be fulfilled:

- The energy bandgap of the absorber (E_G) should be in the range between 0.9 and 1.7 eV (absorption onset between 1380 and 730 nm), for which the detailed balance limit predicts a theoretical efficiency limit above 30%. This bandgap estimation take into account that photons with sub-band-gap energy are not absorbed ($h\nu < E_G$) while only a fraction of the photon energy (E_G / $h\nu$) above the band gap is converted into electric power while the fraction ($h\nu - E_G$) / $h\nu$ is mostly converted into heat.

- The inverse absorption coefficient α^{-1} should be shorter than the minority carrier diffusion length L_D. This criteria is a rather rough statement saying that within a minority carrier diffusion length, most of the photons should be absorbed in order to provide diffusion as a transport mechanism to reach the respective contact. This statement is useful for the development of new absorber materials because α^{-1} as well as L_D are material properties and can be characterised without the need to produce the whole device. However, this criteria neglects additional parameters that can cause a gradient of the minority carrier quasi-Fermi level [1] (which is the driving force minority carrier), such as the electric fields, gradients of the electron affinity, and band gap or band

[1] Quasi Fermi level is a term that describes the population of charges separately in the conduction band or valence band, when their populations are displaced from equilibrium. This displacement could be caused by the application of an external voltage, or by exposure to light.

discontinuities. In contrast to the diffusion length, these parameters are defined by the device structure and can only be characterised in a complete solar cell.

- During the transport from the absorber to the high- and low-energy contact, the loss of energy due to discontinuities of the valence or the conduction band has to be minimised. As the previous point, this parameter is defined by device structure, which provides a general guideline for the band structure of a solar cell.

3.3 Working principle of Organic Solar Cells

At this point, it is worthwhile to note that, in contrast to inorganic semiconductors, the term *donor* and the term *acceptor* are used in relation to organic solar cells. Thus, a donor can describe a molecule (material) which transfers an electron to another molecule. Therefore, an acceptor can describe a molecule (material) which receives an electron from another molecule.

Another important difference of organic versus inorganic semiconductors is the existence of the exciton. The exciton is an electron-hole pair, where electron and hole are bound by Coulomb force (Eq 3.12).

$$F_C = \frac{1}{4\pi\varepsilon\varepsilon_0}\frac{q^2}{r^2} \tag{3.12}$$

where r is the distance between the two charges q, ε_0 is the vacuum permittivity and ε the permittivity of the organic medium.

In organic semiconductors the formed excitons are Frenkel type, whereas in inorganic semiconductors (like crystalline silicon) they usually are Wannier Mott-type. The latter are often thermally dissociated at room temperature, which is not the case in a Frenkel exciton where the binding energy is ten times greater. Due to the high dielectric constant the Wannier Mott exciton has a radius larger than the lattice spacing; in contrast, Frenkel excitons tend to be small, of the same order as the size of the unit cell because of the low dielectric constant values found in organic semiconductors. This aspect is of essential importance to describe the operation of organic solar cells, as discussed below.

Due to the low dielectric constant permittivity in organic materials (~3) photoexcitation leads to a strongly bound exciton, which needs (in the case of solar cells) to be dissociated into free electrons and holes (carriers) [31]. The dissociation takes place at the donor/acceptor (D/A)

interface. Once the exciton is dissociated, electron and hole, diffuse up to the corresponding electrodes, where they are collected and giving rise to an electric current.

Exciton dissociation is energetically favourable when the energy of binding exciton (E_{EX}) is larger than the difference between ionization potential of the donor (IP_D) and the electron affinity of the acceptor (EA_A) [32–33].

$$E_B^{exc} > IP_D - EA_A \tag{3.13}$$

If the difference is not sufficient the exciton will recombine (geminate recombination) without contributing to the photocurrent. Exciton dissociation can also occur at the organic semiconductor/metal interfaces or in presence of impurities (e.g. oxygen) [34].

Organic solar cells are generally fabricated in thin film form of donor (*D*) and acceptor (*A*) materials, with suitable energy levels matching, between two electrodes. One electrode must be transparent to allow the incident light reaching the photoactive materials.

The conversion of the photon energy into free charge carriers in an organic solar cell could be explained in the follow simplified steps (Figure 3.6):

1. *Light absorption* of the photon in one of the respective absorber layers (shown here for a donor layer and *exciton creation*.
2. *Exciton diffusion* to the donor/acceptor interface.
3. *Charge transfer state*: exciton gets separated due to a favourable energy offset overcoming the exciton binding energy [35–36].
4. *Charge transport:* free charge carriers are generated and transported through the respective layer.
5. *Collection of the charges* at the electrodes.

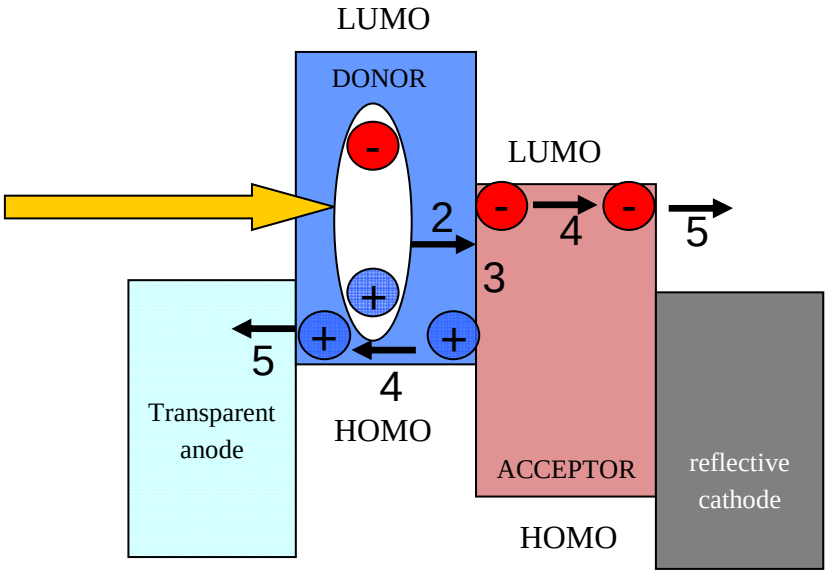

Figure 3.6 - Diagram showing the photogeneration in organic solar cell: from photon absorption to free carriers.

Light absorption

The first step in the photovoltaic process consists in the absorption of the light. In most organic solar cell only a small percentage of the incident light is absorbed. Principal reasons are:

- *Thickness of photoactive materials*: the organic layer is too thin. Low charge carrier mobilities and the low exciton diffusion lengths require layer thickness between 20 and 100 nm. Fortunately, the high optical absorption coefficients (e.g. > 10^5 cm^{-1}) of organic semiconductors allow that organic solar cells could work with a layer thickness of a few tens of nanometres.

- *Semiconductor bandgap too high* with typically values about 2 eV. Besides the high absorption coefficient, only a small portion of the incident light is absorbed because of higher bandgap values.

When the electron is excited by the light absorption an exciton is created. For most organic semiconductors permittivity values (ε) lies between 1 and 6 [37] which is quite low compared to the permittivity of inorganic semiconductors (as for instance silicon) which exhibits ε = 12. Excitons in inorganic semiconductors are usually of Wannier-Mott type. Their radius is in most cases larger than the lattice spacing and the charges are quasi-free. In contrast, the attractive force between electrons and holes in organic solids, where the exciton is initially localised in one molecule, is much higher and the binding energy is comparably strong. Such strongly bound excitons are called Frenkel excitons [38].

Exciton diffusion

After the generation of excitons, they diffuse through the donor or acceptor phase and dissociate into free charges at the D/A interface or recombine wasting the photons. Ideally, all photoexcited excitons should reach the D/A interface, but due to the small exciton diffusion length some excitons recombine before to reach the D/A interface. The exciton diffusion length (L_D) can be estimated by (Eq. 3.14):

$$L_D = \sqrt{\tau_0 D} \tag{3.14}$$

where τ_0 is the lifetime of the exciton and D is the diffusion coefficient. In literature, exciton diffusion lengths can vary from 1 nm to more than 50 nm, depending on the material [39–41].

Due to their electrical neutrality, exciton movement is not affected by electric field, and consequently, they diffuse through the organic semiconductor isotropically. This diffusion is usually described as a Förster-type incoherent energy transfer process [42] and typically acts to lower the energy of the exciton. The diffusion process can result in trapping of the exciton in states originating from aggregates or defects. These states give rise to the tail of the density of states [43].

Only the excitons which are able to reach the D/A interface can contribute to the photocurrent. Exciton diffusion lengths have strong influence on the device design, because of the trade-off between light absorption and recombination. As consequence, the active layer thickness must be tuned to absorb light and to allow the exciton to reach the D/A interface.

Charge transfer state

At the D/A interface, strongly bound excitons might dissociate, contributing to charge carrier generation. The dissociation of the exciton happens via an intermediate state, a so-called charge transfer (CT) state. The electrons will be transferred to the electronegative acceptor, provided that the exciton binding energy (E_B^{exc}) is overcome by this charge transfer process. This requirement is often satisfied by an energetic offset between the donor and acceptor LUMOs. If the electron is transferred from the LUMO of the donor to the LUMO of the neighbouring acceptor the charge transfer (CT) exciton is formed, where the resulting electron-hole pairs still experience Coulombic attraction because donor and acceptor phases are physically close to each other at the interfaces. Then, in this intermediate state the two charges are located on separate neighbouring molecules [44–45] (Figure 3.7). The binding energy of the CT state (E_B^{CT}) was

reported to be in the range of 0.1–0.5 eV [46–48], which is significantly larger than the thermal energy at room temperature (~25 meV).

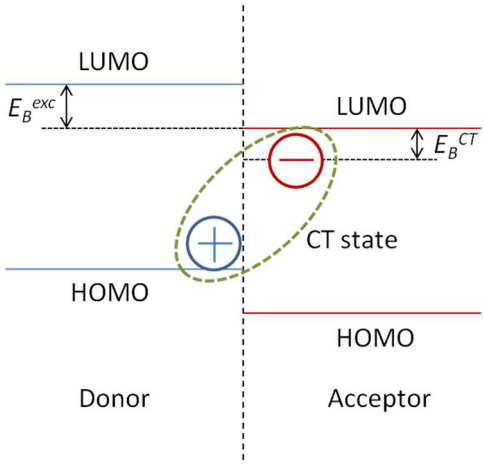

Figure 3.7 - Scheme of the creation of exciton and charge-transfer states. The energy of this state depends upon the Coulomb attraction of the electron and hole and therefore their separation as illustrated by the dotted ellipsoid. For simplicity, the binding energies are shown relative to the LUMOs.

Charge Transport

Once the charge carriers are separated, the electrons are in the acceptor phase whereas hole remains in the donor phase. Free charges must be transported from the D/A interface through the organic materials towards the respective electrodes to produce photocurrent. The charge transport in organic materials can be described by a hopping mechanism [49], instead of band transport. In the case of solar cells, the driving force is mainly the gradient of electrons and holes concentration. Thus, the free charges (electrons and holes) diffuse to corresponding electrode. Currents of electrons and holes are driven by gradients of their electrochemical potential. The only possible loss mechanism in the charge transport is recombination between electrons and holes during the journey to the electrodes (bimolecular recombination). Nevertheless, this process is known to be very efficient and fast. A common measure for charge transport efficiency is the mobility-lifetime ($\mu\tau$) product, which expresses the average distance a charge carrier travels at a fixed electric field before it recombines. Further analysis and experiments have been done about $\mu\tau$ product in Chapter 6.

Collection the charges

An efficient collection of charges at their respective electrodes requires that the charge must overcome the potential barrier of organic/metal interface [50]. This can be realised by using doped layers to create selective contacts. The semipermeable contacts let the collection of one

kind of charge carriers through and block the other one. There is only a direct loss path if contacts are not selective and a charge carrier reaches the "wrong" contact, where it recombines.

External Quantum Efficiency

Each of these steps of conversion of photon energy into free charge carriers occurs with a certain efficiency η. The *EQE* of organic solar cells can be expressed multiplying these efficiencies (Eq. 3.15):

$$EQE = \eta_A \, \eta_{ED} \, \eta_{CT} \, \eta_{CC} \tag{3.15}$$

where η_A is related to the photon absorption efficiency, η_{ED} to the exciton diffusion efficiency, η_{CT} to the charge transfer efficiency, and η_{CC} to the carrier collection efficiency. The η_{ED} restricts the *EQE*, because of the exciton diffusion length has values in the range of nanometres. The distance an exciton is able to travel during its lifetime has strong influence on the design and optimisation of materials and devices (i.e. the thicknesses of active layers).

From the spectra of the *EQE*, photocurrent contribution of a limited wavelength region can be studied. Hence, the contribution of each material to the photocurrent can be obtained, since the different photoactive materials absorb in different spectral regions.

3.3.1 Carrier Recombination

Recombination processes are mechanisms losses that decrease the power conversion efficiency of the solar cells. There are two types of recombination in organic solar cells: geminate and nongeminate recombination.

- *Geminate recombination* takes place when a coulombically bound electron–hole pair (exciton) generated from the absorption of a single photon recombines before the electron and hole are separated into free charge carriers. The probability of geminate recombination is independent of carrier density and geminate losses happen within nanoseconds of absorption [51–52].

- *Nongeminate recombination* is the recombination of free charge carriers and encompasses both trap-assisted (Shockley-Read-Hall) and bimolecular mechanisms (Langevin). Nongeminate recombination losses are carrier density dependent and typically occur after micro to milliseconds when illumination conditions are comparable 1 sun [53–54].

Geminate recombination

Onsager was the first to described quantitatively geminate recombination [55]. His model calculates the probability that a coulombically bound electron-hole pair will escape its Coulomb attraction and generate free charges. The competition between dissociation of CT state and its recombination to the ground state depends upon the magnitude of the coulombic attraction felt by this CT state (Figure 3.8). In particular, Onsager proposed a definition for a Coulomb capture radius (alternatively called the Onsager radius), r_c, define the distance at which the Coulomb attraction energy equals the thermal energy k_BT. If the thermalisation length a is greater than the Coulomb capture radius r_c, the charge carriers are considered to be fully dissociated. If, however, the thermalisation length is smaller than r_c, then the dissociation of the CT state into free charges occurs with a certain escape probability, while geminate recombination occurs with a complementary probability.

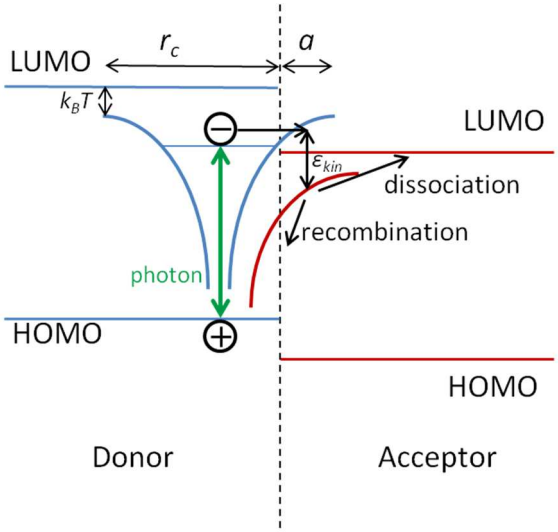

Figure 3.8 - Electron thermalisation length (a) versus coulomb capture radius (r_C).

Nongeminate recombination

Direct nongeminate recombination refers to the recombination of a free electron with a free hole in the semiconductor. Most often, nongeminate recombination takes place via defect states in the gap (Shokley-Read-Hall), where a free electron (or hole) is captured by a trapped hole (or electron). Nongeminate recombination is usually referred in the literature as bimolecular recombination, in the sense that the electron and hole that recombina come from different dissociated excitons.

3.3.2 Parameters characteristics of Organic Solar Cells

In the next paragraphs the V_{OC}, J_{SC}, parasitic resistances (R_P, R_S) and FF will be analysed in detail for the case of organic solar cells.

Open Circuit Voltage

The V_{OC} is related to the splitting of the quasi-Fermi levels of hole and electron in the active layer under steady-state illumination at the anode and cathode (Figure 3.9) [56]. Under this condition, carrier generation and recombination exactly balance each other and no net current exists at any point inside the device.

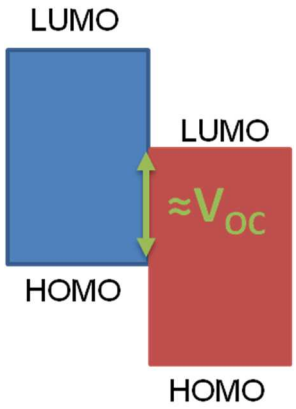

Figure 3.9 - The open circuit voltage in organic solar cells is related to the difference between HOMO level of the donor and LUMO level of the acceptor.

Many reports have shown that in organic solar cells, V_{OC} is linearly correlated to the difference between the HOMO level of the donor and the LUMO level of the acceptor (Eq. 16) [57–58], and it does not depend on the work functions of the electrodes [59].

$$V_{OC} = (1/q)\,(|E_{\mathrm{HOMO,D}}| - |E_{\mathrm{LUMO,A}}| - \Delta) \tag{3.16}$$

where q is the elementary charge, $E_{\mathrm{HOMO,D}}$ is the HOMO level energy of the donor and $E_{\mathrm{LUMO,A}}$ is the LUMO level energy of the acceptor. One the most cited work was done by Brabec et al. in 2001 [57]. They synthesized a series of fullerene derivatives with different LUMO levels and blended them with a common donor poly(2-methoxy-5-(30,70-dimethyloctyloxy)- 1,4-phenylenevinylene) (MDMO-PPV). In their experiments, V_{OC} was always linearly dependent on the LUMO level of the acceptor. While the work function of the cathode varied in the wide range of 2.87 eV (Ca) to 4.28 eV (Au), the variation of V_{OC} was comparatively very small (<0.2 V). In 2006, Scharber [58] carefully studied a series of organic solar cell devices (26 polymer donor

materials with different HOMO levels blended with a common acceptor), and proposed an empirical value of 0.3 for V_{OC} losses. It should be noted that the V_{OC} loss of 0.3 eV is obtained from experimental data, and it is not based on theoretical background. A similar relation was reported by Veldman et al. [60] based on a detailed analysis of the charge transfer emission in polymer/fullerene blends. A number of studies suggested that the physical reasons of this 0.3V loss factor limiting the maximum achievable V_{OC} in organic solar cells could be related to the effect of disorder [61–62]. Durrant and co-workers [63–64] analyse the impact of charge carrier recombination and the donor acceptor microstructure on the V_{OC} of bulk polymer solar cells. They developed a comprehensive model describing the V_{OC} of bulk heterojunction solar cells device based on transient optoelectronic analyses. They found for different polymer-fullerene solar cells V_{OC} losses in the range of 0.225–0.435V.

Although the origin of the losses has been discussed widely no clean conclusions have been established. Anyhow, there is a consensus the major losses resulting in a decreased V_{OC} are related to the disorder in organic semiconductors [65] and non-geminate recombination [66].

Materials for organic solar cells are soft materials. During the film preparation, interactions between molecules, kinks in the polymer chains, and the degrees of crystallinity of organic semiconductors can all introduce disorder into the system. Furthermore, the regioregularity, molecular weight, and purity variation are all important causes of disorder. The control of film deposition is an important subject in the field of organic solar cells. Thus, disorder should also be taken into consideration when discussing origin of V_{OC} in organic solar cell.

As consequence of disorder and defects localised states appear within the bandgap of the semiconductor. Similar to the well-studied inorganic hydrogenated amorphous silicon (a-Si:H) semiconductor, disorder induces band tails states and deep traps in the electronic structure. The distribution in the gap states downshifts the electron quasi-Fermi level and upshifts the hole quasi-Fermi level, which obviously reduces V_{OC}. For the same reason, disorder in organic materials plays a role in bringing the electron quasi-Fermi level down away from the LUMO level of the acceptor, and lifting up the hole quasi-Fermi level away from the HOMO level of the donor, and consequently reduce the V_{OC}. The distribution of density of states (DOS) in the tail can be approximated as a Gaussian or exponential type.

Nongeminate recombination in organic solar cells annihilates carriers and hence causes energy loss, reducing V_{OC} as a result. At V_{OC} photo-generated carriers remain and accumulate inside the device, thereby bimolecular mechanism governs the recombination.

The influence of the DOS on the V_{OC} in small-molecule organic solar cells is discussed in section 3 of Chapter 5.

Short Circuit Current

The J_{SC} in organic solar cell is ideally proportional to the absorbed photons and dependent on the free charges carriers to reach the electrodes. The number of photons absorbed depends on the absorption coefficient of the material and the device architecture, as well as the thickness of the active layer or reflecting back electrodes [1].

The major loss of J_{SC} is leaded by monomolecular recombination, where carriers recombine through a trap or a recombination centre.

Parasitic Resistances

- *Parallel resistance (Rp)*: In organic solar cells, *Rp* is mainly attributed to recombination of charge carriers near the donor-acceptor interface.
- *Series resistance (Rs)*: In organic solar cells, *Rs* considers conductivity i.e. mobility of the specific charge carrier in the respective transport medium. For example, mobility of holes in a p-type material. The mobility can be affected by space charges and traps. *Rs* is also increased with a longer travelling distance of the charges in i.e. thicker transport layers.

Fill Factor

The value of *FF* depends mainly on parasitic resistances. Typical values for *FF* are 0.65 to 0.85 for good organic solar cells.

3.4 Device architecture

In the following a brief summary, including the strengths and weak points, of the four most used architectures of organic solar cells is given:

Single layer cell. Single layer structures consist of only one semiconductor material between two electrodes (Figure 3.10). Single layer cells and are often referred to as Schottky type devices or Schottky diodes since charge separation occurs at the rectifying (Schottky) junction with one electrode. The other electrode interface is supposed to be of ohmic contact [67–70]. The

structure is simple but the absorption is usually low using a single type of molecule. Since both positive and negative charges travel through the same material, recombination losses are generally high.

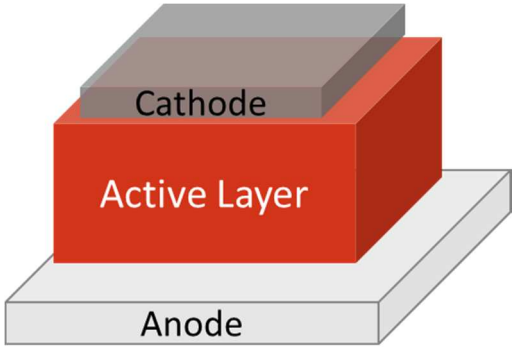

Figure 3.10 - Diagram of single layer organic solar cell.

Bilayer cell. This kind of solar cell contain two layers sandwiched with the conductive electrodes (Figure 3.11).This structure benefits from the separated charge transport layers that ensure connectivity with the correct electrode and give the separated charge carriers only little chance to recombine with its counterpart. The principal drawback is the small interface area that allows only excitons to reach it and get dissociated.

This architecture has an important limitation which relates to the exciton diffusion length in the organic materials. The exciton diffusion length is dependent on the exciton lifetime and is in the range of 10–40 nm.

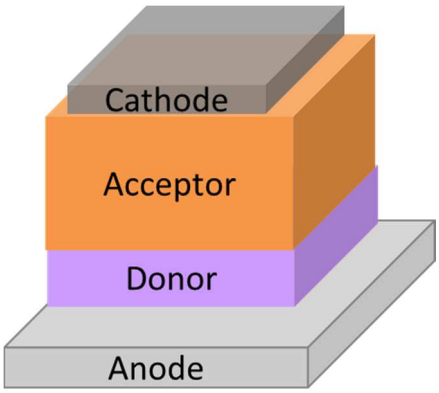

Figure 3.11 - Diagram of bilayer organic solar cell.

Bulk Heterojunction cell. A mixture of donor and acceptor materials is sandwiched between anode and cathode (Figure 3.12). The strong point of this type is the large interface area, allowing high molecular mixing and, thereforen, most excitons can reach the D/A interface. This

accounts for the intrinsically low exciton diffusion lengths and allows for more generated excitons to be separated into free charge carriers. However, the charges have to be transported to the electrodes via closed and short percolation pathways. Otherwise transport losses by trapping or recombination may occur. Hence, the connectivity with the correct electrode is the big weak point of this structure. As a result, the photocurrent is usually higher in bulk heterojunction than in at heterojunction solar cells [71–72].

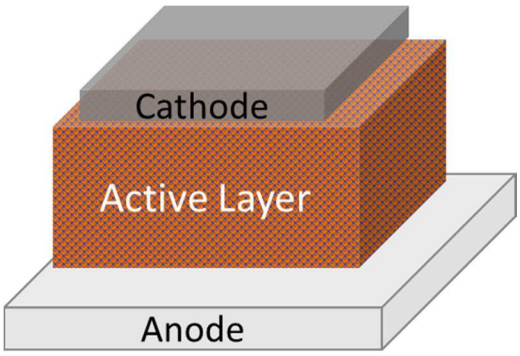

Figure 3.12 - Diagram of Bulk Heterojunction organic solar cell.

p-i-n cell. This type represents the successful attempt to unify the advantages of the two structures described previously. The photoactive donor/acceptor heterojunction (intrinsic layer) is sandwiched between semipermeable layers, which act as selective membranes, facilitating charge transport to the respective contacts (Figure 3.13).

The semipermeable layers can be formed either by using doped wide-gap materials or charge (hole and electron) transport layers. In this thesis, transparent materials with wide band gap are used as semipermeable layers. Charge separation occurs in the intrinsic layer and charge transport can only occur via the corresponding transport layer. In Chapter 5, we study the influence of the thickness of the intrinsic layer on the performance of the solar cells.

Additionally, the electron transport layer also protects the active layer against damage due to the metal deposition [73]. BCP (2,9-dimethyl-4,7-diphenyl-1,10-phenanthroline) and BPhen (bathophenanthroline; 4,7-diphenyl-1,10-phenanthroline) are typical molecules used for electron transport layers. On the other hand, Transition Metal Oxides (TMOs) and PEDOT:PSS can be used as a hole transport layers. In this thesis, Molybdenum Oxide (MoO_3) and BCP are the materials employed as hole and electron transport layers respectively.

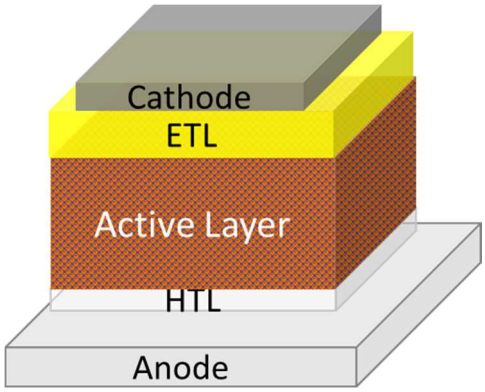

Figure 3.13 - Diagram of p-i-n organic solar cell

Tandem Cells. Organic tandem solar cells were first introduced by Hiramoto et al. in 1990 [74]. Tandem solar cells with organic semiconductors are solar cells with multiple D/A heterojunctions made of different semiconductor materials. Ideally, each D/A heterojunction will produce electric current in response to different wavelengths of light; thereby a broader harvesting of the solar spectrum is achieved [75]. Thermal evaporation processing allows an easy stacking of organic layers to form multiple heterojunctions.

The tandem solar cells concept is particularly interesting in the case of small-molecule solar cells with p-i-n structure. The single p-i-n devices feature good device performance with high *FF* and high Internal Quantum Efficiency (*IQE*). Nevertheless, to achieve high power conversion efficiencies both *IQE* and the total absorption need to be high. The single p-i-n cells suffer from too low absorption in two aspects. Firstly, the absorption spectra of the photoactive layers do not cover the complete range of the sun spectrum. In addition, the photoactive layers have to be thin enough to avoid recombination losses and space charge limitation of the current flow. Therefore, they are optically thin even at the absorption maxima.

An approach to overcome these problems is to stack several junctions with either identical or complementary absorption spectra on top of each other. The V_{OC} is then given by the sum of the open circuit voltages of the individual cells. The flow of photocurrent in stacked junction cells requires easy recombination of charge carriers with low energetic losses at the interface between the individual cells. For that reason, each D/A heterojunction is separated by a thin layer as recombination zone, shown in Figure 3.14 [76].

Today, this architecture combined with p-i-n subcells has achieved the world record efficiency in organic solar cells.

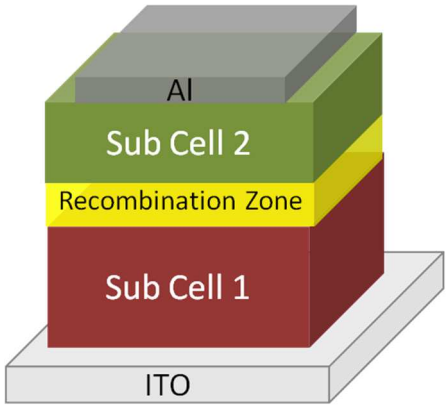

Figure 3.14 - Diagram of tandem organic solar cell.

References

[1] H. Hoppe, N. S. Sariciftci, "Organic solar cells: an overview", *J. Mater. Res.* 19, (**2004**) 1924.

[2] N. W. Ashcroft, N. D. Mermin, "Solid state physics", Saunders College Publishing, Fort Worth, **1976**.

[3] A. W. Hains, Z. Liang, M. A. Woodhouse, B. A. Gregg, "Molecular semiconductors in organic photovoltaic cells", *Chem. Rev.* 110 (**2010**) 6689.

[4] M. A. Green, "Photovoltaic Principles", *Physica E* 14 (**2002**) 11.

[5] P. Würfel, "Physics of Solar Cells – From Principles to New Concepts", Wiley-VCH: New York, **2005**.

[6] S. Rühleet, A. Y. Anderson, H-N. Barad, B. Kupfer, Y. Bouhadana, E. Rosh-Hodesh, A. Zaban, "All-Oxide Photovoltaics", *J. Phys. Chem. Lett.* 3 (**2012**) 3755.

[7] D. W. Zhao, P. Liu, X. W. Sun, S. T. Tan, L. Ke, A. K. K. Kyaw, "An inverted organic solar cell with an ultrathin Ca electron-transporting layer and MoO_3 hole-transporting layer", *Appl. Phys. Lett*. 95 (**2009**) 153304.

[8] J Meyer, K Zilberberg, T Riedl, A Kahn, "Electronic structure of Vanadium pentoxide: An efficient hole injector for organic electronic materials", *J. Appl. Phys.* 110 (**2011**) 033710.

[9] S. Han, W. S. Shin, M. Seo, D. Gupta, S. J. Moon, S. Yoo, "Improving performance of organic solar cells using amorphous tungsten oxides as an interfacial buffer layer on transparent anodes", *Org. Electron.* 10 (**2009**) 791

[10] C. Tao, S. Ruan, G. Xie, X. Kong, L. Shen, F. Meng, C. Liu, X. Zhang, W. Dong, W. Chen, "Role of tungsten oxide in inverted polymer solar cells" *Appl. Phys. Lett*. 94 (**2009**) 043311.

[11] Z. Tan, L. Li, F. Wang, Q. Xu, S. Li, G. Sun, X. Tu, X. Hou, J. Hou, Y. Li, "Solution-Processed Rhenium Oxide: A Versatile Anode Buffer Layer for High Performance Polymer Solar Cells with Enhanced Light Harvest", *Adv. Energy Mater.* 4 (**2014**) 1300884.

[12] M. D. Irwin, D. B. Buchholz, A. W. Hains, R. P. H. Chang, T. J. Marks, "p-Type semiconducting nickel oxide as an efficiency-enhancing anode interfacial layer in polymer bulk-heterojunction solar cells" *Proc. Natl. Acad. Sci. USA* 105 (**2007**) 2783.

[13] J. Ouyang, C.-W. Chu, F.-C. Chen, Q. Xu, Y. Yang, "High-Conductivity Poly(3,4-ethylenedioxythiophene):Poly(styrene sulfonate) Film and Its Application in Polymer Optoelectronic Devices", *Adv. Funct. Mater.* 15 (**2005**) 203.

[14] S. W. Shelton, T. L. Chen, D. E. Barclay, B. Ma, "Solution-Processable Triindoles as Hole Selective Materials in Organic Solar Cells", *ACS Appl. Mater. Interfaces* 4 (**2012**) 2534.

[15] E. Kymakis, M. M. Stylianakis, G. D. Spyropoulos, E. Stratakis, E. Koudoumas, C. Fotakis, "Spin coated carbon nanotubes as the hole transport layer in organic photovoltaics" *Sol. Energ. Mat. Sol. Cells* 96 (**2012**) 298.

[16] S. -S. Li, K. -H. Tu, C. -C. Lin, C. -W. Chen, M. Chhowalla, "Solution-Processable Graphene Oxide as an Efficient Hole Transport Layer in Polymer Solar Cells", *ACS Nano* 4 (**2010**) 3169.

[17] J.-M. Yun, J.-S. Yeo, J. Kim, H.-G. Jeong, D.-Y. Kim, Y.-J. Noh, S.-S. Kim, B.-C. Ku, S.-I. Na, "Solution-Processable Reduced Graphene Oxide as a Novel Alternative to PEDOT: PSS Hole Transport Layers for Highly Efficient and Stable Polymer Solar Cells", *Adv. Mater.* 23 (**2011**) 4923.

[18] F. Bonaccorso, Z. Sun, T. Hasan, A. C. Ferrari, "Graphene photonics and optoelectronics", *Nature Photon.* 4 (**2010**) 611.

[19] K. Kawano, C. Adachi, "Reduced initial degradation of bulk heterojunction organic solar cells by incorporation of stacked fullerene and lithium fluoride interlayers", *Appl. Phys. Lett.* 96 (**2010**) 053307.

[20] B. Paci, A. Generosi, V. Rossi Albertini, P. Perfetti, R. de Bettignies, C. Sentein, "Time-resolved morphological study of organic thin film solar cells based on calcium/aluminium cathode material", *Chem. Phys. Lett.* 461 (**2008**) 77.

[21] J. Huang, J. Yu, H. Lin, Y. Jiang, "Detailed analysis of bathocuproine layer for organic solar cells based on copper phthalocyanine and C_{60}" *J. Appl. Phys.* 105 (**2009**) 073105.

[22] N -N. Wang, J. -S. Yu, H. Lin, Y. -D. Jiang "Organic Photovoltaic Cells with Improved Performance Using Bathophenanthroline as a Buffer Layer" *Chin. J. Chem. Phys.* 23 (**2010**) 84.

[23] J. Yu, N. Wang, Y. Zang, Y. Jiang, "Organic photovoltaic cells based on TPBi as a cathode buffer layer", *Sol. Energ. Mat. Sol. Cells* 95 (**2011**) 664.

[24] Y. Sun, J. H. Seo, C. J. Takacs, J. Seifter, A. J. Heeger, "Inverted Polymer Solar Cells Integrated with a Low-Temperature-Annealed Sol-Gel-Derived ZnO Film as an Electron Transport Layer" *Adv. Mater.* 23 (**2011**) 1679.

[25] C. Waldauf, M. Morana, P. Denk, P. Schilinsky, K. Coakley, S. A. Choulis, C. J. Brabec, "Highly efficient inverted organic photovoltaics using solution based titanium oxide as electron selective contact", *Appl. Phys. Lett.* 89 (**2006**) 233517.

[26] F. C. Chen, J. L. Wu, S. S. Yang, K. H. Hsieh, W. C. Chen, "Cesium carbonate as a functional interlayer for polymer photovoltaic devices" *J. Appl. Phys.*103 (**2008**) 103721.

[27] J. Bisquert, "Nanostructured Energy Devices: Equilibrium Concepts and Kinetics" CRC Press, 2014.

[28] A. Cuevas, D. Yan, "Misconceptions and misnomers in solar cells", *IEEE J. Photovoltaics*, 3 (**2013**) 916.

[29] U. Würfel, A. Cuevas, P. Würfel, "Charge Carrier Separation in Solar Cells", *IEEE J. Photovoltaics* 5 (**2015**) 461.

[30] W. Jaegermann, A. Klein, T. Mayer, "Interface Engineering of Inorganic Thin-Film Solar Cells - Materials-Science Challenges for Advanced Physical Concepts. *Adv. Mater.* 21 (**2009**) 4196.

[31] G. P. Nicholson, A. F. Castro, "Organic photovoltaics: principles and techniques for nanometre scale characterization", *Nanotechnology* 21 (**2010**) 492001.

[32] N. S. Sariciftci, L. Smilowitz, A. J. Heeger, F. Wudl, "Semiconducting polymers (as donors) and buckminsterfullerene (as acceptor): photoinduced electron transfer and heterojunction devices", *Synt. Met.* 59 (**1993**) 333.

[33] J. J. M. Halls, J. Cornil, D. A. dos Santos, R. Sibley, D. H. Wang, A. B. Holmes, J. L. Bredas, R. H. Friend, "Charge-and energy-transfer processes at polymer/polymer interfaces: A joint experimental and theoretical study" *Phys. Rev. B* 60 (**1999**) 5721.

[34] J.-M. Nunzi, "Organic photovoltaic materials and devices", *C. R. Physique* 3 (**2002**) 523.

[35] J. J. M. Halls, K. Pichler, R.H. Friend, S.C. Moratti, A.B. Holmes, "Exciton diffusion and dissociation in a poly(p-phenylenevinylene)/C60 heterojunction photovoltaic cell", *Appl. Phys. Lett.* 68 (**1996**) 3120.

[36] J.J.M. Halls, R. H. Friend, "The photovoltaic effect in a poly(p-phenylenevinylene)/perylene heterojunction", *Synth. Met.* 85 (**1997**) 1307.

[37] O. D. Gordan, M. Friedrich, D. R. T. Zahn, "The anisotropic dielectric function for copper phthalocyanine thin films", *Org. Electron.* 5 (**2004**) 291.

[38] J. Frenkel, "Some remarks on the theory of the photoelectric effect", *Phys. Rev.* 38 (**1931**) 309.

[39] S. Yoo, B. Domercq, B. Kippelen, "Efficient thin-film organic solar cells based on pentacene/C_{60} heterojunctions", *Appl. Phys. Lett.* 85 (**2004**) 5427.

[40] D. E. Markov, E. Amsterdam, P. W. M. Blom, A. B. Sieval, J. C. Hummelen, "Accurate measurement of the exciton diffusion length in a conjugated polymer using a heterostructure with a side-chain cross-linked fullerene layer", *J. Phys. Chem. A* 109 (**2005**) 5266.

[41] Y. Terao, H. Sasabe, C. Adachi, "Correlation of hole mobility, exciton diffusion length, and solar cell characteristics in phthalocyanine/fullerene organic solar cells", *Appl. Phys. Lett.* 90 (**2007**) 103515.

[42] T. Förster, "Energiewanderung und Fluoreszenz", *Naturwissenschaften* 33 (**1946**) 66.

[43] P. Peumans, A. Yakimov, S. R. Forrest, "Small molecular weight organic thin-film photodetectors and solar cells" *J. Appl. Phys.* 93 (**2003**) 3693.

[44] A. Petersen, A. Ojala, T. Kirchartz, T. A. Wagner, F. Wurthner, U. Rau, "Field-dependent exciton dissociation in organic heterojunction solar cells" *Phys. Rev. B* 85 (**2012**) 245208.

[45] B. A. Gregg, J. van de Lagemaat, "Solar cells: Folding photons" *Nature Photon.* 6 (**2012**) 278.

[46] X.-Y. Zhu, Q. Yang, M. Muntwiler, "Charge-transfer excitons at organic semiconductor surfaces and interfaces", *Acc. Chem. Res.* 42 (**2009**) 1779.

[47] T. Drori, C.-X. Sheng, A. Ndobe, S. Singh, J. Holt, Z. V. Vardeny, "Below-gap excitation of π-conjugated polymer-fullerene blends: Implications for bulk organic heterojunction solar cells", *Phys. Rev. Lett.* 101 (**2008**) 037401.

[48] M. Hallermann, S. Haneder, E. Da Como, "Charge-transfer states in conjugated polymer/fullerene blends: Below-gap weakly bound excitons for polymer photovoltaics", *Appl. Phys. Lett.* 93 (**2008**) 053307.

[49] H. Bässler, "Charge Transport in Disordered Organic Photoconductors a Monte Carlo Simulation Study", *Phys. Stat. Sol. (b)* 175 (**1993**) 15.

[50] L- M. Chen, Z. Xu, Z. Hong, Y. Yang, "Interface investigation and engineering – achieving high performance polymer photovoltaic devices", *J. Mater. Chem.* 20 (**2010**) 2575.

[51] D. Credgington, F. C. Jamieson, B. Walker, T. -Q. Nguyen, J. R. Durran, "Quantification of geminate and non-geminate recombination losses of a solution-processed diketopyrrolopyrrole-based bulk heterojunction solar cell", *Adv. Mater.* 24 (**2012**) 2135.

[52] J. Kniepert, M. Schubert, J. C. Blakesley, D. Neher, "Photogeneration and recombination in P3HT/PCBM solar cells probed by time-delayed collection field experiments", *J. Phys. Chem. Lett.* 2 (**2011**) 700.

[53] C. G. Shuttle, B. O'Regan, A. M. Ballantyne, J. Nelson, D. D. C. Bradley, J. R. Durrant, "Bimolecular recombination losses in polythiophene:fullerene solar cells" *Phys. Rev. B* 78 (**2008**) 113201.

[54] S. R. Cowan, W. L. Leong, N. Banerji, G. Dennler, A. J. Hegger, "Identifying a threshold impurity level for organic solar cells: enhanced first-order recombination via well-defined $PC_{84}BM$ traps in organic bulk heterojunction solar cells", *Adv. Funct. Mater*. 21 (**2011**) 3083.

[55] L. Onsager, "Initial Recombination of Ions", *Phys. Rev*., 54 (**1938**) 554.

[56] J. Bisquert, D. Cahen, G. Hodes, S. Rühle, A. Zaban, "Physical chemical principles of photovoltaic conversion with nanoparticulate, mesoporous dye-sensitized solar cells", *J. Phys. Chem. B* 108 (**2004**) 8106.

[57] C. J. Brabec, A. Cravino, D. Meissner, N. S. Sariciftci, T. Fromherz, M. T. Rispens, L. Sanchez, J. C. Hummelen, "Origin of the open circuit voltage of plastic solar cells", *Adv. Funct. Mater.* 11 (**2001**) 374.

[58] M. C. Scharber, D. Mühlbacher, M. Koppe, P. Denk, C. Waldauf, A. J. Heeger, C. J. Brabec, "Design rules for donors in bulk-heterojunction solar cells-towards 10% energy-conversion efficiency", *Adv. Mater.* 18 (**2006**) 789.

[59] C. Uhrich, D. Wynands, S. Olthof, M. K. Riede, K. Leo, S. Sonntag, B. Maennig, M. Pfeiffer, "Origin of open circuit voltage in planar and bulk heterojunction organic thin-film photovoltaics depending on doped transport layers", *J. Appl. Phys.* 104 (**2008**) 043107.

[60] A. Veldman, S.C.J. Meskers, R.A.J. Janssen, "The energy of charge-transfer states in electron donor-acceptor blends: insight into the energy losses in organic solar cells" *Adv. Funct. Mater.* 19 (**2009**)1939.

[61] P.K. Nayak, G. Garcia-Belmonte, A. Kahn, J. Bisquert, D. Cahen, "Photovoltaic efficiency limits and material disorder", *Energy Environ. Sci*. 5 (**2012**) 6022.

[62] A. Manor, E.A. Katz, "Open-circuit voltage of organic photovoltaics: Implications of the generalized Einstein relation for disordered semiconductors", *Sol. Energ. Mat. Sol. Cells* 97 (**2012**) 132.

[63] D. Credgington, J. R. Durrant, "Insights from Transient Optoelectronic Analyses on the Open-Circuit Voltage of Organic Solar Cells" *J Phys. Chem. Lett.* 3 (**2012**) 1465.

[64] C. G. Shuttle, B. O'Regan, A. M. Ballantyne, J. Nelson, D. D. C. Bradley, J. de Mello, J. R. Durrant, "Experimental determination of the rate law for charge carrier decay in a polythiophene:fullerene solar cell" *Appl. Phys. Lett.* 92 (**2008**) 1.

[65] G. García-Belmonte, J. Bisquert, "Open-circuit voltage limit caused by recombination through tail states in bulk heterojunction polymer-fullerene solar cells" *Appl. Phys. Lett.* 96 (**2010**) 113301.

[66] D. Credgington, R. Hamilton, P. Atienzar, J. Nelson, J. R. Durrant, "Non-Geminate Recombination as the Primary Determinant of Open-Circuit Voltage in Polythiophene:Fullerene Blend Solar Cells: an Analysis of the Influence of Device Processing Conditions" *Adv. Funct. Mater.* 21 (**2011**) 2744.

[67] C. W. Tang, A. C. Albrecht, "Photovoltaic effects of metal–chlorophyll-a–metal sandwich cells", *J. Chem. Phys.* 62 (**1975**) 2139.

[68] Y. Y. Merritt, H. J. Hovel, "Organic solar cells of hydroxy squarylium", *Appl. Phys. Lett.* 29 (**1976**) 414.

[69] F. J. Karnpas, M. Gouterman, "Merocyanine organic solar cells", *J. Phys. Chem.* 81 (**1977**) 690.

[70] D. L. Morel. A. K. Ghosh. T. Feng. E. L. Stogryn. P. E. Purwin, R. F. Shaw, C. Fishman, "High-efficiency organic solar cells", *Appl. Phys. Lett.* 32 (**1978**) 495.

[71] A. W. Hains, Z. Liang, M. A. Woodhouse, B. A. Gregg, "Molecular semiconductors in organic photovoltaic cells", *Chem. Rev*. 110 (**2010**) 6689.

[72] F. Padinger, R. Rittberger, N. Sariciftci, "Effects of Postproduction Treatment on Plastic Solar Cells", *Adv. Funct. Mater.* 13 (**2003**) 85.

[73] P. Peumans, A. Yakimov, S. Forrest, "Small molecular weight organic thin-film photodetectors and solar cells", *J. Appl. Phys.* 93 (**2003**) 3693.

[74] M. Hiramoto, M. Suezaki, M. Yokoyama, "Effect of thin gold interstitial-layer on the photovoltaic properties of tandem organic solar cell", *Chem. Lett.* 19 (**1990**) 327.

[75] M. Riede, C. Uhrich, J. Widmer, R. Timmreck, D. Wynands, G. Schwartz, W.-M. Gnehr, D. Hildebrandt, A. Weiss, J. Hwang, S. Sundarraj, P. Erk, M. Pfeiffer, K. Leo, "Efficient organic tandem solar cells based on small molecules", *Adv. Funct. Mater.* 21 (**2011**) 3019.

[76] J. Xue, B. Rand, S. Uchida, S. Forrest, "A hybrid planar-mixed molecular heterojunction photovoltaic cell", *Adv. Mater.* 17 (**2005**) 66.

4. Materials and Experimental Methods

This Chapter presents the materials used in this thesis to fabricate the solar cells. Additionally, the thin film deposition techniques and the experimental set-up used for solar cell deposition and characterisation are explained in detail.

4.1 Materials

The chemical structure and the main optoelectronic properties of the organic semiconductors used in this work are presented in this section.

Tetraphenyldibenzoperiflanthene

Tetraphenyldibenzoperiflanthene (DBP) is a p-type semiconductor (donor electron material). DBP molecule has a symmetrical structure (Figure 4.1). DBP molecule is only composed of carbon and hydrogen atoms.

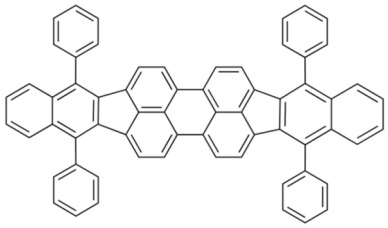

Figure 4.1 - Structure of Tetraphenyldibenzoperiflanthene (DBP)

Numerous donor materials have been developed in last decades. DBP is a promising electron donor material for photovoltaic applications and has been used in many laboratories around the world since 2009 [1–6].

The principal advantages of DBP in application to solar cells are the high optical absorption and the high HOMO level. High optical absorption values allow a reduction in the thickness of the active layer, which is a favourable condition for the exciton to reach the donor – acceptor (D/A) interface. The HOMO energy level of DBP is estimated to be around -5.5eV [1], which makes

DBP suitable for employment with fullerene acceptors. The high HOMO energy leads to a high open circuit voltage (V_{OC}) because the difference between the HOMO energy of the donor and the lowest unoccupied molecular orbital (LUMO) energy of the acceptor is proportional to V_{OC} [7].

Fullerene C_{70}

A fullerene is any molecule composed of only carbon atoms in the form of a hollow sphere, ellipsoid, tube, and many other shapes. C_{70} is the fullerene molecule consisting of 70 carbon atoms. It is a cage-like structure which resembles a rugby ball, made of 25 hexagons and 12 pentagons, with a carbon atom at the vertices of each polygon and a bond along each polygon edge (Figure 4.2).

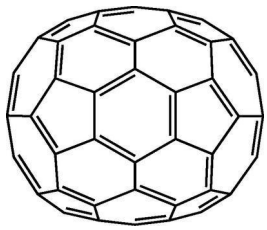

Figure 4.2 - Structure of fullerene C_{70}

C_{70} was discovered in 1985 by Robert Curl, Harold Kroto and Richard Smalley [8]. They found C_n clusters (for even n with n > 20) using laser evaporation of graphite of which the most common were C_{60} and C_{70}. They were awarded the 1996 Nobel Prize in Chemistry for their discovery of fullerenes.

C_{70} is used as electron acceptor and electron transporting molecule. The energy levels of C_{70} are -6.1eV for the IP and -4.0eV for EA. C_{70} can forms brownish crystals with a bandgap of 1.77 eV [9].

Molybdenum oxide MoO_3

Molybdenum oxide is a transition metal oxide (TMO). Previous works presented transition metal oxides such as V_2O_5, WO_3, and MoO_3 as conducting p-type materials, with the electron affinity and ionization energy of MoO_3 in the order of 2.3 and 5.3–5.4 eV, respectively [10–11]. However, it has been recently demonstrated with direct and inverse photoemission spectroscopy measurements that MoO_3 exhibits a high electron affinity (EA) of 6.7 eV and may consequently be used as p-type dopant for materials with deep HOMO levels. MoO_3 as well as other similar transition metal oxides are n-type materials exhibiting very deep lying electronic states and more

commonly used as hole transport layer [12–15]. In Figure 4.3, a schematic energy-level diagram of several TMOs and organic semiconductors. The lower shaded regions represent the valence bands and the upper shaded regions represent the conduction bands. The dashed lines indicate the position of the Fermi level for each oxide. Oxides with their Fermi levels close to the valence band are p-type semiconductors, and oxides with their Fermi levels close to the conduction band are n-type semiconductors [16].

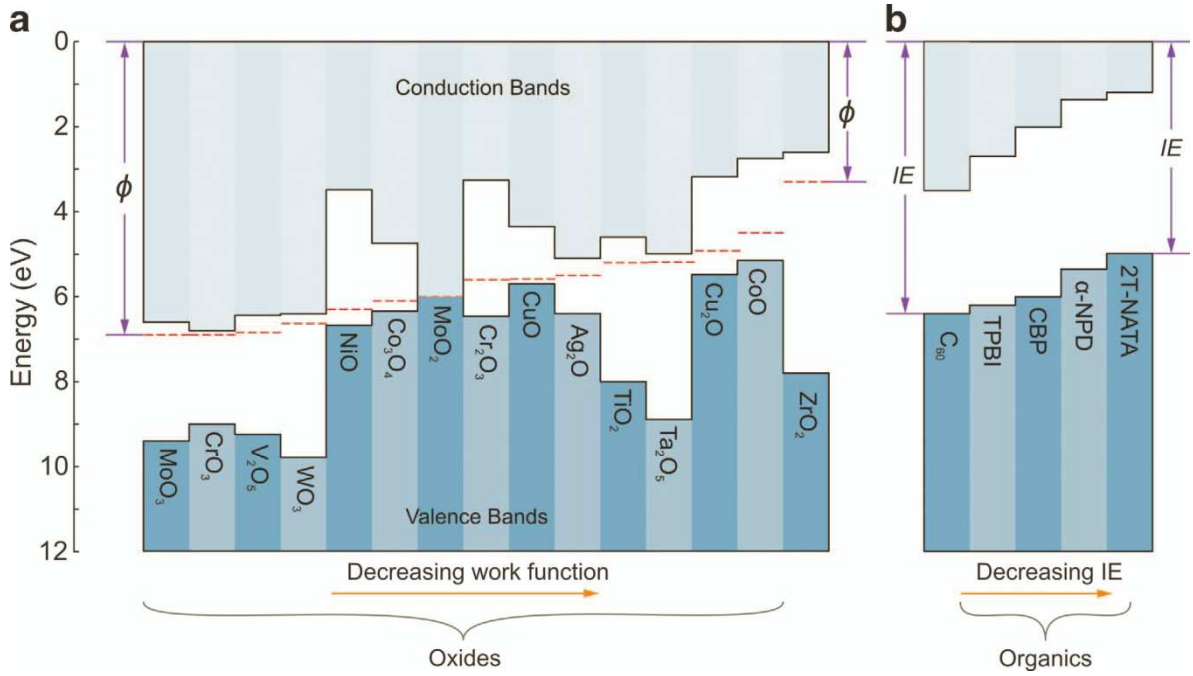

Figure 4.3 - Schematic energy-level diagrams of (a) several transition metal oxides and (b) several organic semiconductors. Figure obtained from [16].

MoO_3 is one of the most commonly used transition metal oxide in organic electronics applications, because it is evaporated at relatively low temperature (~ 400 °C). Hence, it can be easily deposited in vacuum from a crucible. In contrast, the evaporation temperatures of V_2O_5 and WO_3 are significantly higher.

MoO_3 layer has been used in OLEDs to improve hole injection from the anode to the organic emitters. Moreover, it has been reported that devices containing MoO_3 are more stable in the air than those fabricated using alternative hole transport layer (like PEDOT:PSS) [17]. Metal oxides interlayer has also been used in organic photovoltaic cells. Enhancement in power conversion efficiencies was observed. In particular, the use of MoO_3 interlayer between the ITO anode and the donor layer in small-molecule solar cells enhance the fill factor due to the reduction in series resistance, which improves the power conversion efficiency [14].

Bathocuproine BCP

Bathocuproine, 2,9-dimethy-4,7-diphenyl -1,10-phenathroline (Figure 4.4), also called BCP, is a well known material used as electron transport layer in applications such as organic light-emitting diodes [18] and organic solar cells [19–21]. The appearance of BCP is white or yellow crystalline powder. BCP is soluble in organic solvents such as nitrobenzene and insoluble in water.

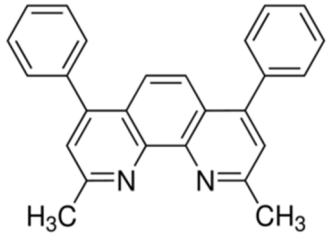

Figure 4.4 - Chemical structure of bathocuproine (BCP).

BCP is a wide-gap electron transport material. The role of BCP layer inserted between active layer and aluminium contact in organic solar cells was investigated by Vogel et al. [20]. In that work, BCP dramatically improves electron transport out of the C_{60} film into the aluminium electrode. Consequently, BCP buffer layer reduces geminate recombination of excitons at the C60–Al interface. For that reason, the BCP layer is used to make a selective cathode. In addition, it prevents damage to the active organic layer by the metal deposition. The optimal BCP thickness for application in organic solar cells is between 8 and 10 nm [21].

4.2 Experimental Methods

The fabrication process of organic solar cells is detailed in this section. Substrate preparation, organic and metal depositions are described. At the end of the chapter, specifications of electrical set up used for devices characterisation are exposed.

The fabrication and characterisation of the devices of this thesis has been carried out the Centre for Research in Nanoengineering (CRnE) and in the clean room facilities of the Departament d'Enginyeria Electrònica (DEE) from Universitat Politècnica de Catalunya. MNT group has a long experience on the fabrication of solar cells based on inorganic semiconductors (silicon). Clean room facilities (located in the basement of the DEE, Campus Nord) used for fabrication and characterisation of solar cells are detailed below.

Facilities at the Clean Room of the DEE

There are several deposition systems in the clean room of UPC: one evaporation system based on electron beam and Joule effect, another evaporation system based on magnetron sputtering and a Plasma Enhanced Chemical Vapour Deposition (PECVD) system devoted to the deposition of hydrogenated amorphous silicon and alloys. In addition, thermal ovens are utilised to perform annealing, doping diffusion processes and to growth silicon dioxide on crystalline silicon wafers. Moreover, two photolithographic systems with resolution around one micrometre are used. In order to measure the film thickness there are a profilometer and an ellipsometer. The last is used to measure the thickness and index of refraction for thin dielectric films.

At the moment, MNT the research activities based on inorganic solar cells include: crystalline silicon solar cells with interdigitated back contact electrodes (maximum efficiency 22%), Heterojunction with Intrinsic Thin-Film (HIT solar cells, with 18% efficiency). Besides, MNT group is also fabricating porous silicon for thermo-photovoltaic applications.

As it mentioned in the Chapter 1, the MNT group from DEE proposed to fabricate organic solar cells about ten years ago. In 2002, the MNT group started a new research line focused on the fabrication of organic devices based on small-molecules semiconductors. The objective was to widen up the technology know-how of the group. For this purpose, the group acquired a new deposition systems based on two Joule-effect evaporators (Oerlikon). The MNT group acquired the organic evaporator UNIVEX 300 from Leybold Systems (Figure 4.5). The group began the research in organic electronics with manufacturing organic field effect transistors (OFETs) to study the electronic properties of organic semiconductors. Metal contacts were deposited using the evaporator from Edwards. The need to avoid oxygen incorporation during the device fabrication pushed the group to be equipped with a new evaporation system integrated in a glovebox.

Figure 4.5 - Organic Evaporator UNIVEX 300 (left); Inside view of the chamber with two crucibles for p- and n-type respectively (right). In operation since 2006.

The glovebox MB200B from the company MBraun allows to fabricate the whole devices in an inert atmosphere (Figure 4.6). The glovebox is equipped with two evaporation systems: one is devoted to the deposition of organic semiconductors and the other one is used evaporate metals to deposit the electrodes. Thus, the complete device can be fabricated in inert atmosphere. Hence, the semiconductor materials properties are not affected due to contact with oxygen or moisture.

At the beginning of this thesis, my work was focused to tune-up the equipment to fabricate organic solar cells. The organic evaporator was designed by the MNT group. The parts composing this evaporator were purchased to different companies. Vacuum chamber was designed in collaboration with the Spanish company Trinos Vacuum (http://www.vacuum-projects.net/). The adaptation of a vacuum deposition system to the glove box cannot be done in a straightforward way. The system is equipped with five organic sources provided by Creaphys (http://www.creaphys.com/). This system enables to coevaporate up to five different organic molecules (two of them simultaneously) (Figure 4.7). This allows fabrication of intrinsic layers (mixture of donor and acceptor molecules) or doping organic semiconductors. The temperature at the crucible is controlled by two PID controllers. Substrate temperature is also controlled by heater (Figure 4.8).

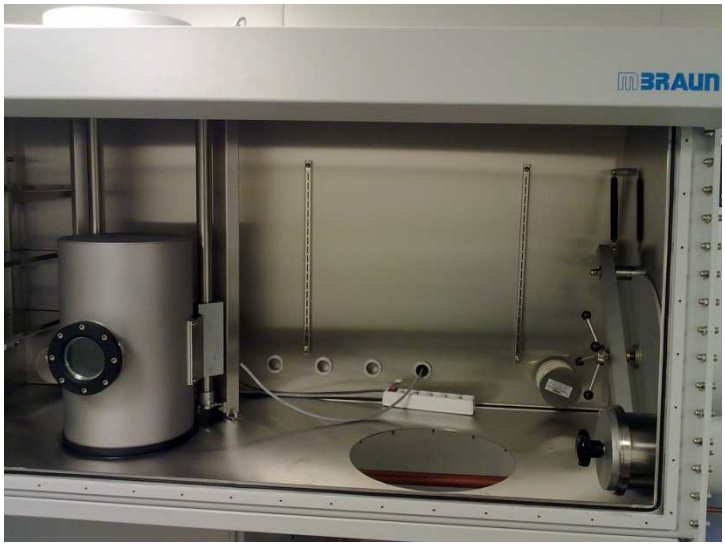

Figure 4.6 - Glovebox MB200B from MBraun with metal evaporator in 2010, before the installation of organic evaporator.

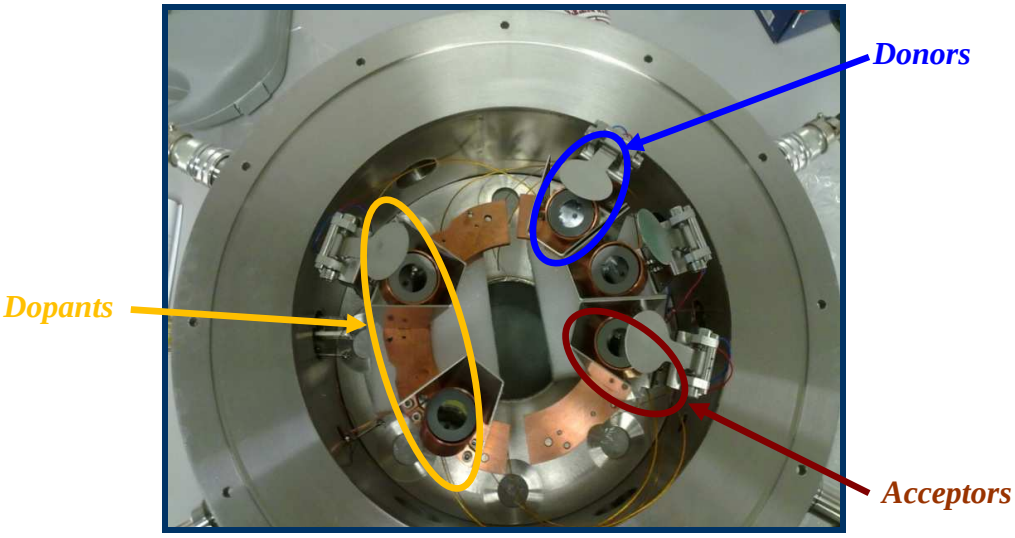

Figure 4.7 - Top view of organic evaporation sources. Each organic source is equipped with a shutter (controlled externally). Moreover an additional shutter is located behind the holder substrate.

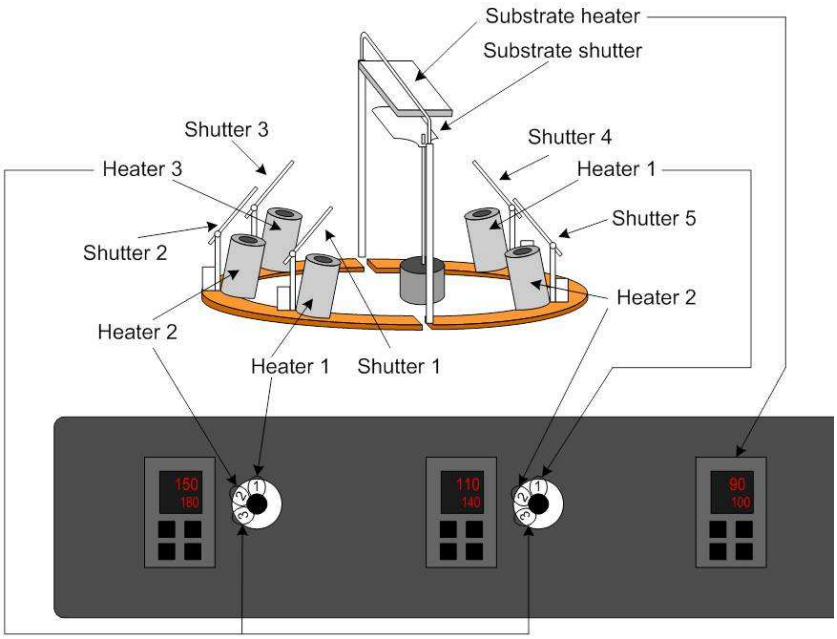

Figure 4.8 - Schematic of organic chamber with the connections between the three temperature controllers with five evaporation sources and substrate holder.

The metal evaporator uses Joule-effect to evaporate thin films onto a given substrate. It can deposit materials with a specified thickness of up to 1500 nanometers. Deposition rate is controlled by the use of a quartz crystal monitor. It was programmed to evaporate with a suitable rate in order to not damage the organic layers. Finally, the glovebox was ready to fabricate organic solar cells in 2012 (Figure 4.9).

Figure 4.9 - Glovebox MB200B from MBraun with our home-made organic evaporator in 2012.

In the following paragraphs, the facilities distributed between CRnE and DEE used for the characterisation of films and devices are exposed.

CRnE facilities

Purification System

High material purity is one critical aspect to the functioning of organic electronic devices. It is possible to aim for purities > 99.9%, typically even >> 99.99% independently of the initial purity of the raw material. A purification organic semiconductor leads to higher power efficiency and longer lifetime of the devices. The optimised process can get a material yield of about 20%. The Tube-based Vacuum Sublimation System (CreaPhys GmbH) provides the means to purify organic volatile compounds by gradient thermal sublimation in vacuum. The DSU-05 has a nominal capacity of 5 g, which are, however, strongly dependent on the material properties like density, sublimation and melting behaviour. The system features a three zone gradient oven. Figure 4.10 shows the result of sublimation CuPc. Initially, the aim of DSU-05 system was to purify organic compounds provided by chemist laboratories specialized in synthesis. Nevertheless, the system has not been used very often due to the low yielding.

Figure 4.10 - Purification of CuPc molecules.

Focused Ion Beam

The Zeiss Neon 40 combines the imaging and analytical capabilities of a high resolution Scanning Electron Microscope (SEM) with a Focused Ion Beam (FIB) column (Figure 4.11). In addition, this cross-beam system has a multi-channel gas injection system (GIS) for deposition of metal and insulating layers, and can also perform enhanced and selective etching. This cross-beam workstation is used for sample observation, selective milling and deposition, 3D

tomography, Transmission Electron Microscopy (TEM) lamella preparation, microfabrication and elemental analysis.

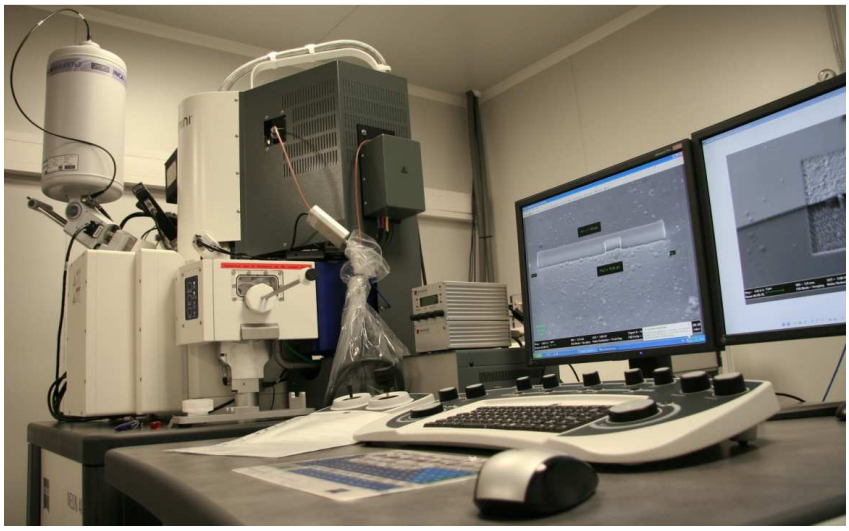

Figure 4.11 - Cross-beam workstation Zeiss Neon 40

Atomic Force Microscope

In this thesis, the Atomic Force Microscopy (AFM) has been used to measure the topography of the organic thin-films in tapping mode. In fact, the basic technique of AFM, which is contact AFM, is not well adapted to examine such surfaces due to problems of friction and adhesion. Therefore, the tapping mode of operation was developed to overcome drawbacks of contact mode [22]. This mode uses oscillation of the cantilever tip at or near its natural resonant frequency while allowing the cantilever tip to impact the target sample for a minimal amount of time. This intermittent contact lessens the damage done to the soft surface and to the tip, compared to the amount done in contact. Hence the dragging forces during scanning are greatly reduced [23]. Moreover, during oscillation, the tip goes through both the attractive and the repulsive regions of the tip-sample force field.

The Dimension 3100 Nanoman AFM from Veeco (Figure 4.12) provides a variety of high resolution surface imaging techniques, such as: atomic force microscopy, in tapping and contact mode or Kelvin probe or surface potential microscopy (KPM) among others.

Figure 4.12 - Atomic Force Microscope Dimension 3100 Nanoman from Veeco

Spectrophotometer

This equipment allows complete characterisation of the optical properties of thin-film layers; in particular allows the measure of optical density. UV-visible-NIR Spectrophotometer (Shimadzu 3600) has UV-probe software for photometric analysis of solid and liquid materials in the 185 to 3300 nm range (Figure 4.13). It is equipped with ISR 3100 integrating sphere and transmission liquid sample holder.

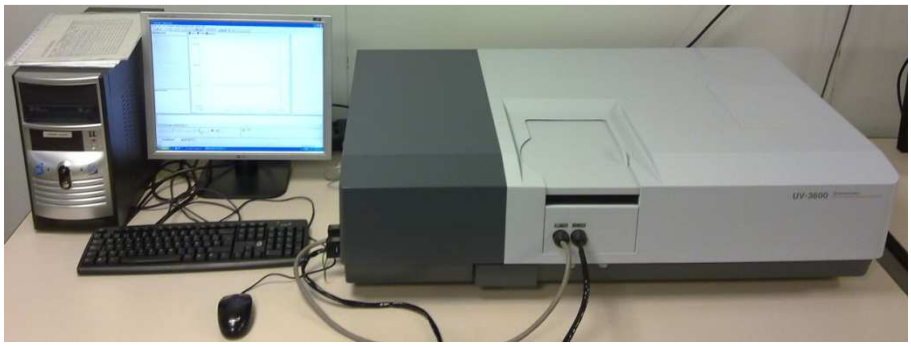

Figure 4.13 - UV-visible-NIR Spectrometer. Shimadzu 3600.

Profilometer

Thicknesses of thin film layers were determined ex-situ by Veeco DEKTAK 150 profilometer (Figure 4.14). The profilometer measures the vertical depth of a material across a specified horizontal length. The profile is displayed on a graphical interface. Uses for this equipment include measuring etch depth, deposited film thickness, and surface roughness. The resolution of a step to determine the film thickness is about tens of nanometres.

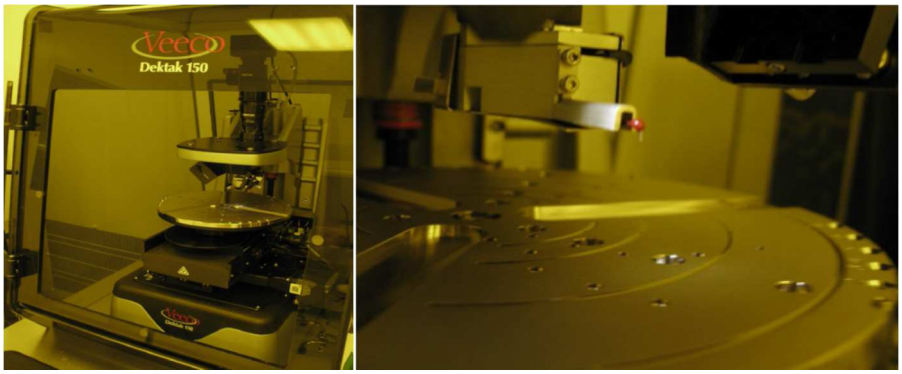

Figure 4.14 - Veeco DEKTAK 150 (right) with DEKTAT Stylus (left)

4.2.1 Fabrication process for Organic Solar Cells

Organic solar cells fabricated in MNT-UPC are processed by thermal evaporation in high vacuum conditions, which is the most generally used method for depositing low weight organic compounds [24]. The use of this technique has some advantages over solution – processable thin films in the application of organic optoelectronic devices. Higher control of the structure and morphology of the films is possible because solvents are not required, leading to a high reproducibility of device fabrication. The flexibility in device design (i.e. layer thicknesses, multilayer structure, materials selection) is an intrinsic attribute of dry processing techniques such as thermal evaporation. In this work, the structure of the fabricated organic solar cells consist of a glass substrate with a transparent electrode acting as the anode, the organic films and the top metal contact acting as the cathode.

Vacuum deposition Systems

Vacuum deposition is a family of processes used to deposit layers of material atom-by-atom or molecule-by-molecule on a solid surface. The deposited layers can range from a thickness of one atom up to millimetres. When the vapour source is a liquid or solid the process is called physical vapour deposition (PVD), on the other hand if the source is a chemical vapour precursor the process is called chemical vapour deposition (CVD). The vacuum environment in thermal evaporation reduce the particle density, hence the mean free path for collision is long and reducing the particle density of undesirable molecules or atoms (contaminants).

Three types of flow are mostly encountered in vacuum technology: viscous or continuous flow, molecular flow and Knudsen flow at the transition between these two. A backing pump, working in viscous flow, is needed in a high vacuum system to start turbomolecular pump, since turbomolecular pumps usually work in the pressure region below 10^{-3} mbar. In this thesis, the

high vacuum systems used to evacuate the evaporator chambers are comprised by a turbomolecular pump and an oil-sealed rotary pump.

Thermal evaporation process consists on the sublimation of a compound from a resistively heated crucible or boat (source) in vacuum from 10^{-6} mbar to 10^{-10} mbar onto a substrate [25]. Hence, a molecular beam is created from the boat to the substrate. This molecular beam is defined by the elongated shape of the boat. The mean free path of the molecules evaporated in the vacuum chamber is usually longer than the size of the chamber. Consequently, the molecules can travel from the source to the substrate without collide with other molecules in the chamber.

The limitation in the deposition rate is fixed by the escape rate of the molecules from the solid or melt phase into vacuum, since molecular transport through vacuum is almost immediate. The deposition rate is controlled by the source temperature. Using shutters for substrate and sources, which can interrupt the molecular beam, allow nanometre control of film thickness.

The quartz crystal microbalance (QCM) coating thickness gauge (thin film controller) utilizes the piezoelectric sensitivity of a quartz oscillator (monitor crystal) to measure the supplied mass on the gauge. This property is utilised to monitor the deposition rate and film thickness during vacuum coating. A very sharp electromechanical resonance occurs at different discrete frequencies of the voltage applied. Resonance frequency is reduced when a quantity of mass is added to the surface of the quartz crystal oscillating in resonance. This frequency shift is very reproducible.

Fabrication process

Preparation of the substrates is very important in order to obtain reproducible results. All the solar cells presented in this thesis are fabricated on glass coated with the transparent conductor indium tin oxide (In_2O_3:SnO_2, ITO) (Luminescence Technology Corporation). Glass substrates with pre-patterned ITO have a sheet resistance of 12Ω/sq and a thickness of 120 nm (Figure 4.15).

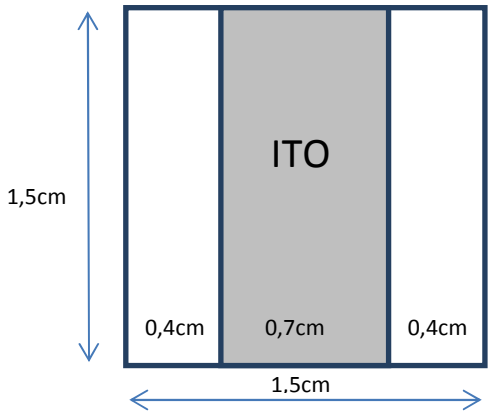

Figure 4.15 - Geometry of ITO patterned substrate.

The ITO surface is cleaned in an ultrasonic bath with acetone (15 min) and isopropyl alcohol (15 min) and dried with nitrogen flux. Finally, the substrates are treated in ultraviolet/ozone for 30 min. This treatment increases the work function [26] and removes any remaining carbon residues.

Once substrates are cleaned, they are transferred into the vacuum system for film deposition. Organic layers were deposited by thermal evaporation under a base pressure of approximately 10^{-7} mbar at a rate in the range of 0.1–0.2 Å/s. The substrate temperature is a crucial parameter for the morphology of the film. For that reason, substrate temperature was controlled during the organic deposition molecules. In Chapter 5, a detailed work about the influence of the deposition substrate temperature on the optoelectronic properties of the donor material is presented.

The crucible or boat, holding the evaporation material, is at the core of the evaporation process. A conical alumina (Al_2O_3) boat is used in this work (Figure 4.16). The alumina boat can achieve high temperatures, above 500ºC. The maximum temperature reached in this thesis was 350ºC, to evaporate fullerene C_{70}.

Figure 4.16 - Alumina boat (left). Alumina boat inside the heater system equipped with shutter (right).

Glove box MBraun200B has integrated the vacuum deposition system MB-EcoVap which allows evaporating metals (Figure 4.17). The equipment includes several recipes programmable

PLC control to evaporate different metals. There are two evaporation sources controlled independently. This double source setup allows the evaporation and co-evaporation of different metal layers without break the vacuum with nitrogen. A structure to hold the mask with 9 solar cells substrates were designed and adapted in MB-EcoVap system. Moreover, there is an automatic mechanism with electro-pneumatic valves to lift the chamber.

Figure 4.17 - MB-EcoVap (left); inside view with holder for mask (right).

The metal used as the cathode in the organic solar cells was aluminium. Aluminium was presented in form of pellet. The metal was deposited by thermal evaporation on organic layers through metallic shadow mask to give an active are of 0.075 cm^2 (Figure 4.18). Deposit rate was below than 0.2 Å/s during first 20nm and 1 Å/s up to required thickness. Since the evaporated material reaches the substrate mostly from a single direction, during the evaporation process the samples rotated at 30 rpm to obtain a uniform layer.

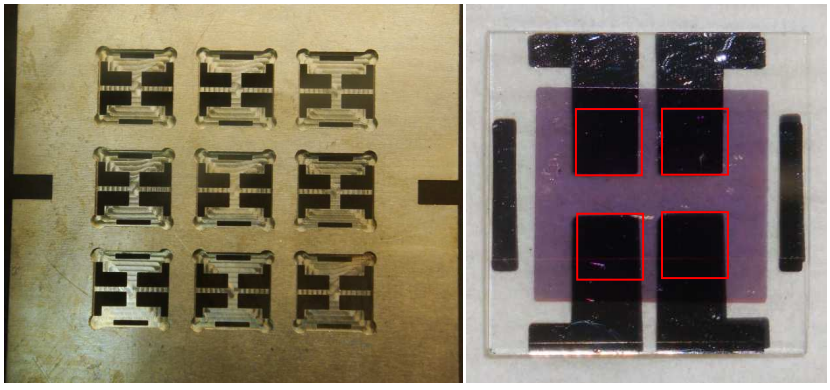

Figure 4.18 - Shadow metal mask for evaporation (left); substrate with four organic solar cells, its active area is 0.075 cm^2 (right).

Metal deposition is an extremely critical point in organic small-molecules solar cells. Metal atoms may diffuse though organic layers; this effect can short the device.

Figure 4.19 shows a typical SEM image of the cross-section of an organic solar cell based on CuPc and C_{60}. In this case, the structure of the solar cell was glass/ITO/CuPc/C60/Ag. The cross-section was obtained by using a FIB process. The observed layer thicknesses are in agreement with profilometry measurements. In addition, the layers are uniform and no shortcircuits are visible.

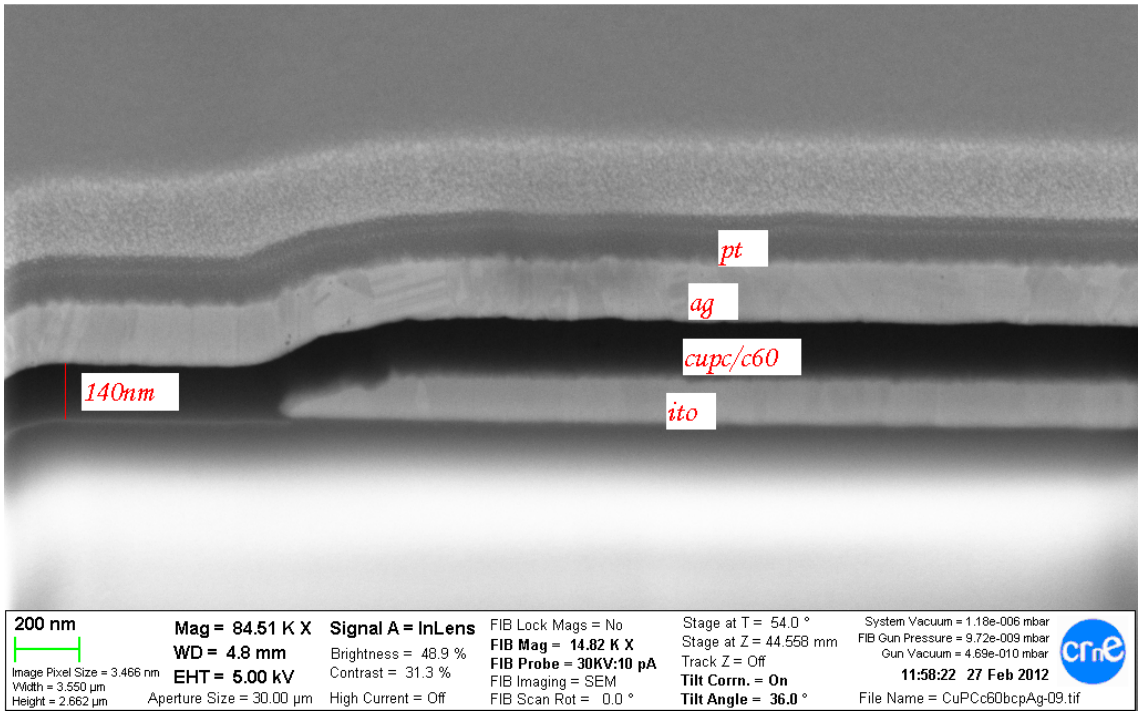

Figure 4.19 - Cross-section of organic solar cell.

4.2.2 Characterisation of Organic Solar Cells

Electrical characterisations of all devices were carried out in nitrogen ambient using a plastic prototype (Figure 4.20), specifically designed to minimise oxygen and humidity degradation. This prototype allows the measurement of 4 different substrates with 4 cells in each substrate in nitrogen atmosphere. Metallic tips contact all anodes and cathodes of solar cells. There are two selectors that allow selecting one solar cell from a specific substrate. The prototype has been fabricated by the company microLIQUID.

Figure 4.20 - Prototype to measure organic solar cells in nitrogen atmosphere.

Current – Voltage Measurement

The most important characterisation is the measurement of the current-voltage characteristics (I-V curve), delivering the power conversion efficiency. The basic parameters of I-V characteristics are discussed in Chapter 3. Devices were measured at room temperature in the dark and under AM 1.5G conditions using a solar simulator (Newport Oriel Instruments Model: 94061A Class ABB (Figure 4.21).

Figure 4.21 - Solar simulator Newport Oriel Model 94061A Class ABB.

Illumination source uses a Xenon lamp and a proprietary filter to meet Class A performance parameters without compromising the one sun output power in 6 x 6 inch area (Figure 4.22). The overall illumination intensity is calibrated with a pyranometer prior to each measurement run.

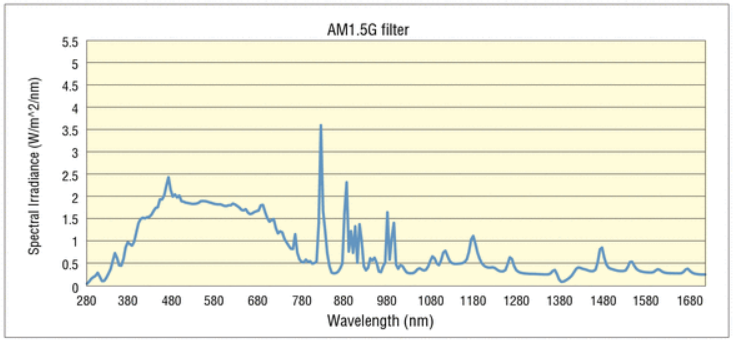

Figure 4.22 - Spectral output of Solar Simulator with standard AM1.5G filter (Newport).

The measurements were carried out applying bias and recording the current using a HP 4142B DC Source measurement unit. A Matlab interface was used to control the source meter and record the I-V curves.

External Quantum Efficiency Measurement

The External Quantum Efficiency (*EQE*) of a solar cell is given by the extracted electron hole pairs per incident photons. *EQE* measurements of photovoltaic cells were performed with a quantum efficiency integrated system, model QEX10 (PV Measurements, Inc.), under standard measurement conditions using a 150 W xenon lamp coupled with a slit monochromator (Figure 4.23). The intensity of incident monochromatic light was calibrated with a Si photodiode. The QEX10 spectral response system uses an adjustable mechanical chopper to modulate the light at rates between 4 Hz and 200 Hz, chopping frequency was fixed at 66 Hz to avoid any perturbation from light ambient. The measurements were carried out in the wavelength range of 300 nm to 800 nm at resolution of 5 nm.

Figure 4.23 - Quantum efficiency integrated system, model QEX10 (PV Measurements, Inc.).

Variable Intensity Measurement

The solar cell performance is dependent on light intensity. Measuring the *J–V* curve over a wide range of illumination levels, rather than at a fixed illumination level of 100 mW/cm^2, can be obtained additional information about the device performance. We call this method the Variable Illumination Measurement (VIM) method. From the *J–V* measurements at different illumination levels, a model of an organic solar cell can be obtained. In this thesis, a study about the recombination of organic solar cells is detailed in Chapter 6.

The VIM measurements were carried out in Departament de Física Aplicada i Òptica of the Universitat de Barcelona (UB) (Figure 4.24). The illumination level can vary from 10 mW/cm^2 (0.1 suns) to 200 mW/cm^2 (2 suns) by means of neutral grey filters to preserve the spectral distribution of the incident light (Figure 4.25).

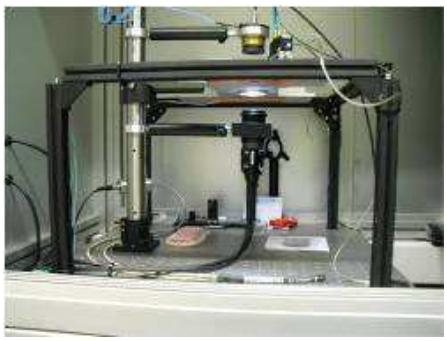

Figure 4.24 - Image of characterisation setup for Variable Intensity Measurements.

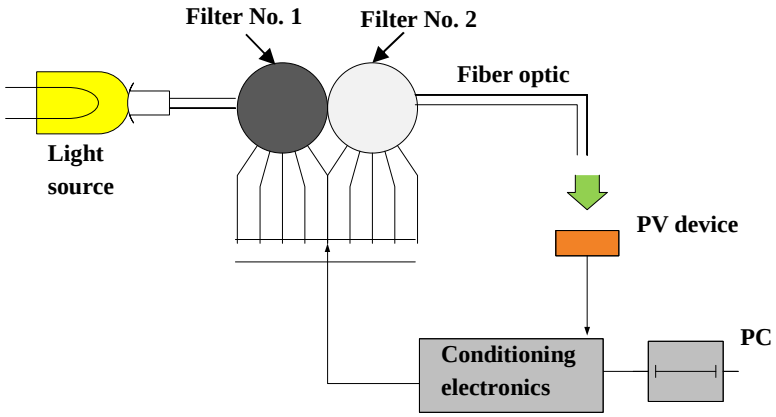

Figure 4.25 - Scheme of Variable Intensity Measurement.

References

[1] D. Fujishima, H. Kanno, T. Kinoshita, E. Maruyama, M. Tanaka, M. Shirakawa, K. Shibata, "Organic thin-film solar cell employing a novel electron-donor material", *Sol. Energy Mater. Sol. Cells*, 93 (**2009**) 1029.

[2] M. Hirade, C. Adachi, "Small molecular organic photovoltaic cells with exciton blocking layer at anode interface for improved device performance", *Appl. Phys. Lett.* 99 (**2011**) 153302.

[3] D. Yokoyama, Z. Qiang Wang, Y.-J. Pu, K. Kobayashi, J. Kido, Z. Hong, "High-efficiency simple planar heterojunction organic thin-film photovoltaics with horizontally oriented amorphous donors". *Sol. Energy Mater. Sol. Cells* 98 (**2012**) 472.

[4] Y. Zheng, W. J. Potscavage, T. Komino, M. Hirade, J. Adachi, C. Adachi, "Highly efficient bulk heterojunction photovoltaic cells based on C70 and tetraphenyldibenzoperiflanthene", *Appl. Phys. Lett.* 102 (**2013**) 143304.

[5] X. Xiao, J. D. Zimmerman, B. E. Lassiter, K. J. Bergemann, S. R. Forrest, "A hybrid planar-mixed tetraphenyldibenzoperiflanthene/C_{70} photovoltaic cell", *Appl. Phys. Lett.* 102 (**2013**) 073302.

[6] Z. Wang, D. Yokoyama, X. Wang, "Highly efficient organic p-i-n photovoltaic cells based on tetraphenyldibenzoperiflanthene and fullerene C_{70}", *Energy Environ. Sci.* 6 (**2013**) 249.

[7] B. Rand, D. Burk, S. Forrest, "Offset energies at organic semiconductor heterojunctions and their influence on the open-circuit voltage of thin-film solar cells", *Phys. Rev. B* 75 (**2007**) 115327.

[8] H.W. Kroto, J. R. Heath, S. C. O'Brien, R. F. Curl, R. E. Smalley, "C_{60}: buckminsterfullerene", *Nature* 318 (**1985**) 162.

[9] K. Thirunavukkuarasu, V. C. Long, J. L. Musfeldt, F. Borondics, G. Klupp, K. Kamarás, C. A. Kuntscher, "Rotational dynamics in C_{70}: temperature- and pressure-dependent infrared studies". *J. Phys. Chem. C* 115 (**2011**) 3646.

[10] H. You , Y. F. Dai , Z. Q. Zhang , D. G. Ma, "Improved performances of organic light-emitting diodes with metal oxide as anode buffer" *J. Appl. Phys.* 101 (**2007**) 026105.

[11] C. W. Chu, S. H. Li, C. W. Chen, V. Shrotriya, Y. Yang, "High-performance organic thin-film transistors with metal oxide/metal bilayer electrode", *Appl. Phys. Lett.* 87 (**2005**) 193508.

[12] M. Kröger, Sami Hamwi, Jens Meyer, T. Riedl, W. Kowalsky, A. Kahn, "P-type doping of organic wide band gap materials by transition metal oxides: A case-study on Molybdenum trioxide", *Org. Electron.* 10 (**2009**) 932.

[13] J. Meyer, K. Zilberberg, T. Riedl, A. Kahn, "Electronic structure of Vanadium pentoxide: An efficient hole injector for organic electronic materials", *J. Appl. Phys.*, 110 (**2011**) 033710.

[14] D. Y. Kim, J. Subbiah, G. Sarasqueta, F. So, H. Ding, Irfan, Y. Gao, "The effect of molybdenum oxide interlayer on organic photovoltaic cells", *Appl. Phys. Lett.*, 95 (**2009**) 093304.

[15] M. T. Greiner, M. G. Helander, W.-M. Tang, Z.-B. Wang, J. Qiu, Z.-H. Lu, "Universal energy-level alignment of molecules on metal oxides", *Nat. Mater.*, 11 (**2012**) 76.

[16] M. T Greiner, Z-H. Lu, "Thin-film metal oxides in organic semiconductor devices: their electronic structures, work functions and interfaces", *NPG Asia Mater.* 5 (**2013**) e55.

[17] F. Wang, X. Qiao, T. Xiong, D. Ma, "The role of molybdenum oxide as anode interfacial modification in the improvement of efficiency and stability in organic light-emitting diodes", *Org. Electron.* 9 (**2008**) 985.

[18] Y. Masumoto, T. Mori, "Application of organic bathocuproine-based alloy film to organic light-emitting diodes", *Thin Solid Films* 516 (**2008**) 3350.

[19] P. Peumans, S. Uchida, S. R. Forrest, "Efficient bulk heterojunction photovoltaic cells using small-molecular-weight organic thin films", *Nature* 425 (**2003**) 158.

[20] M. Vogel, S. Doka, Ch. Breyer, M. Ch. Lux-Steiner, K. Fostiropoulos, "On the function of a bathocuproine buffer layer in organic photovoltaic cells", *Appl. Phys. Lett.* 89 (**2006**) 163501.

[21] J. Huang, J. Yu, H. Lin, Y. Jiang, "Detailed analysis of bathocuproine layer for organic solar cells based on copper phthalocyanine and C_{60}", *J. Appl. Phys.* 105 (**2009**) 073105.

[22] G. Binnig, C.F. Quate, C. Gerber, "Atomic Force Microscope", *Phys. Rev. Lett.* 56 (**1986**) 930.

[23] J. Tamayo, R. Garcia, "Deformation, contact time, and phase-contrast in tapping mode scanning force microscopy", *Langmuir*, 2 (**1996**) 4430.

[24] S.R. Forrest, "Ultrathin organic films grown by organic molecular beam deposition and related techniques", *Chem. Rev.* 97 (**1997**) 1793.

[25] M. Knudsen, "The law of the molecular flow and viscosity of gases moving through tubes", *Ann. Phys* 28 (**1909**) 75.

[26] J. Xue, S. R. Forrest, "Carrier transport in multilayer organic photodetectors: II. Effects of anode preparation", *J. Appl. Phys.* 95 (**2004**) 1869.

5. Organic Solar Cells based on DBP and fullerene C_{70}

The main results obtained on the characterisation of organic solar cells based on small-molecules tetraphenyldibenzoperiflanthene (DBP) and fullerene C_{70} are presented and discussed in this chapter.

In the first section, the electrical performance of bilayer solar cells is analysed. In particular we will focus on the influence of the deposition substrate temperature of the donor material on the performance of the solar cells.

In the second section, the influence of the density of localised states in the band gap of the donor layer on the open circuit voltage (V_{OC}) of the solar cells will be discussed.

Finally, using the optimised deposition parameters solar cells with p-i-n structure will be fabricated, where the intrinsic layer is obtained by the coevaporation of donor and acceptor. The influence of the thickness of the intrinsic layer of p-i-n solar cell will be studied.

5.1 Bilayer Solar Cells based on DBP and C_{70}

5.1.1 Introduction

Solar cells based on bilayer structure (donor/acceptor) were presented in Chapter 3, section 3.3. This structure allows higher control of the film morphology of the donor and the acceptor material during the deposition process. As we also mentioned, the optimum geometry for high efficiency organic solar cells would be the p-i-n structure, where the intrinsic layer is composed of donor and acceptor material (bulk heterojunction approach). Contrary to the situation of solution processed bulk heterojunction solar cells, this approach is not easy to optimise when cells are based on thermal evaporated small-molecule. The coevaporation of two compounds in a controlled manner is not easy. Since the sublimation temperatures usually are different for each compound, the deposition rates should be stabilized separately, making the fabrication of the solar cell a complex process. Moreover, deposition rates depend on the amount of material

present in the crucible, adding more uncertainty on the control de deposition rates when both compounds are sublimated simultaneously.

For all these reasons, our approach started with the optimisation of the optoelectronic properties of a solar cell with bilayer structure. The fabrication of organic solar cells involves the optimisation of different layers, each of them with very low thickness (tens of nm). In the case of a multilayer structure composed of individual single compounds allows us to optimise separately each of the layers of the solar cell having a good control of the thicknesses (usually in the range of tens nanometres) of each layer. Moreover, this approach allows us to be more confident with the measured experimental data and extract conclusive conclusions.

Our experimental deposition set-up allows the deposition of thin-film layers with good thickness control over an area of around diameter of 5 inches (variation of 5% between the maximum (central part) and minimum thickness (external part)). Considering this, our holder 10 cm x 10 cm allows to deposit simultaneously over 9 substrates (1 cm x 1 cm). As mentioned before (Chapter 4) each substrate allocates 4 solar cells. This allows us to fabricate 36 organic solar cells in a single run process. The reproducibility of the optoelectronic performance of the fabricated solar cells is not very high, including solar cells measured on the same substrate. Therefore, obtaining conclusive results is based on the trend observed on the evolution of the solar cell performance with its structure/geometry and the deposition parameters used when processing.

The basic structure of our solar cell consists on a bilayer structure of the donor and acceptor materials sandwiched between a Hole Transport Layer (HTL) in contact with the anode electrode and an Electron Transport Layer (ETL) in contact with the cathode electrode. In our case, we have used molybdenum trioxide (MoO_3) as HTL and BCP as ETL. The structure of the solar cells studied in this Chapter is glass/ITO/MoO_3/DBP(10nm)/C_{70}(40nm)/BCP(8nm)/Al(150nm). Glass substrates with prepatterned ITO were supplied by Luminiscence Technology Corporation (Lumtec Taiwan). ITO thickness was 1200~1600Å, with a sheet resistance of 9~15 Ω/sq and a maximum of optical transmission of 84% at 550nm. The DBP, C_{70}, MoO_3 and BCP compounds were purchased from Sigma Aldrich. The absorbing part of the solar cell is formed by DBP acting as a donor and C_{70} as an acceptor.

The substrate temperature is one of the deposition parameters that have strong influence on the performance of thin-film solar cells. Previous works have reported the influence of substrate temperature on the morphology of amorphous silicon thin films and its influence on the

optoelectronic properties [1–3]. In this section, we study the variation in performance of bilayer organic solar cells where the donor material was deposited at different substrate temperatures.

Fullerenes and its derivatives are the most common used electron acceptor materials to fabricate organic solar cells due to its excellent electronic properties. Although different electron acceptor materials have been used in solar cell technology, like perylene derivatives, its performance was clearly lower when compared with fullerenes derivatives. Main advantages of fullerene derivatives are its deep-lying LUMO energy level (~3.8–4.2 eV) for effective charge separation at D/A interface and its high electron mobility.

Contrary, there are a vast number of electron donor materials. Among them, DBP has recently emerged as a promising donor material for photovoltaic applications [4–9]. The most important advantages of DBP in application to solar cells are its high optical light absorption and its deep HOMO level position. High optical absorption values allow a reduction in the thickness of the layer, which is a favourable condition for the exciton to reach the donor – acceptor (D/A) interface. The HOMO energy level of DBP is estimated to be 5.5eV [4], which makes it appropriate to combine with fullerene acceptors. The relatively deep HOMO level of DBP can help to obtain a high V_{OC}. It has been reported that V_{OC} is related to the difference between the HOMO level of the donor and the LUMO level of the acceptor [10].

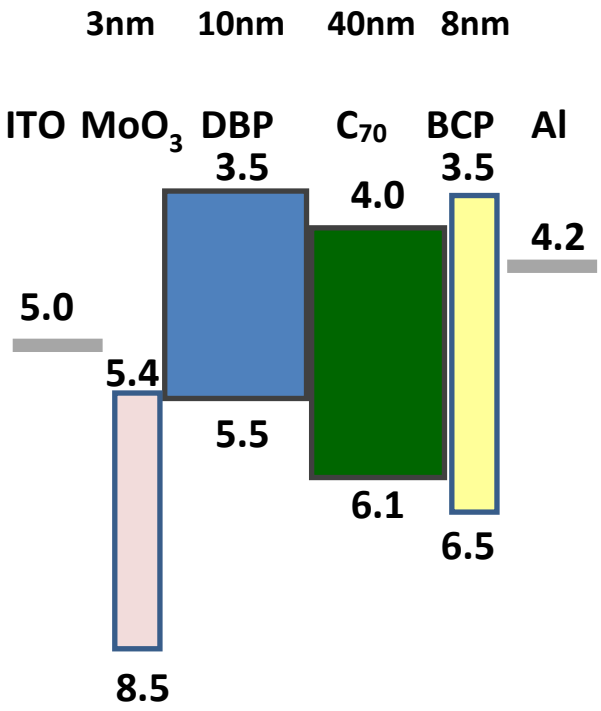

Figure 5.1 - Energy levels (eV) of the different layers comprising the bilayer solar cell.

The electrical properties of MoO_3 have been presented in Chapter 4. This material is an n-type semiconductor exhibiting very deep lying electronic states [11–14]. Recent investigations have led to a reinterpretation of the electronic structure of MoO_3/semiconductor interfaces. The hole injection mechanism is considered via electron extraction from the HOMO through the MoO_3 conduction band [15].

5.1.2 Electrical Characterisation

The photovoltaic performances of bilayer solar cells where the DBP was deposited at different substrate temperatures are presented in this section. First, the main photovoltaic parameters from *J–V* characteristic are exposed. Following, spectral analyses of bilayer solar cells are discussed.

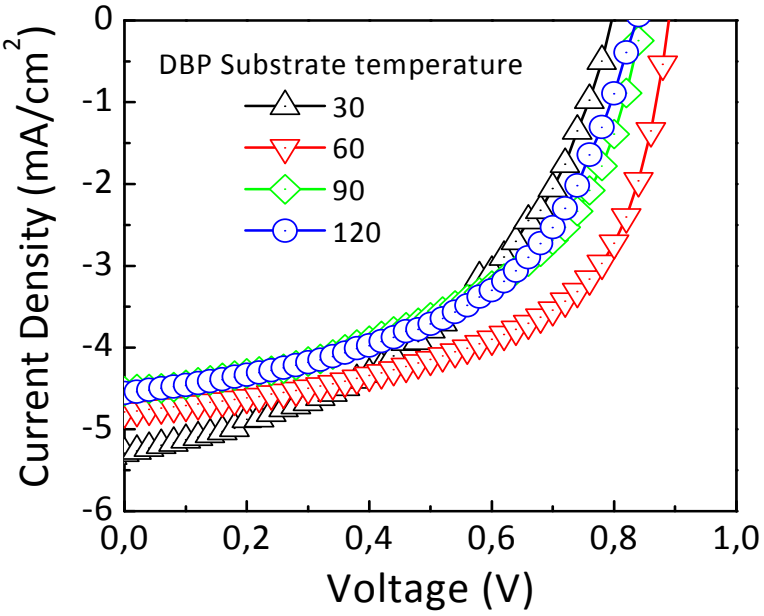

Figure 5.2 - Current – Voltage measurements of bilayer cells under one sun illumination with DBP layer deposited at different temperatures.

The *J–V* characteristics of bilayer solar cells are shown in Figure 5.2. From *J–V* characteristics have been estimated the main photovoltaic parameters as a function of the DBP deposition temperature. Results are summarised in Figure 5.3. The device with a DBP layer deposited at a substrate temperature of 30 ºC showed a J_{SC} = 5.29 mA/cm^2, V_{OC} = 0.79 V and *FF* = 46% for a *PCE* = 1.9%. The best V_{OC} and *FF* values were obtained for a substrate temperature of 60 ºC during DBP deposition, leading to a maximum *PCE* of 2.5%. Particularly, this device achieved a V_{OC} = 0.89 V, *FF* = 58% and only the J_{SC} = 4.79 mA/cm^2 was slightly reduced with respect to the reference device fabricated at 30 ºC. Substrate temperatures higher than 60 ºC resulted in lower solar cell performance, basically due to the reduction of J_{SC}.

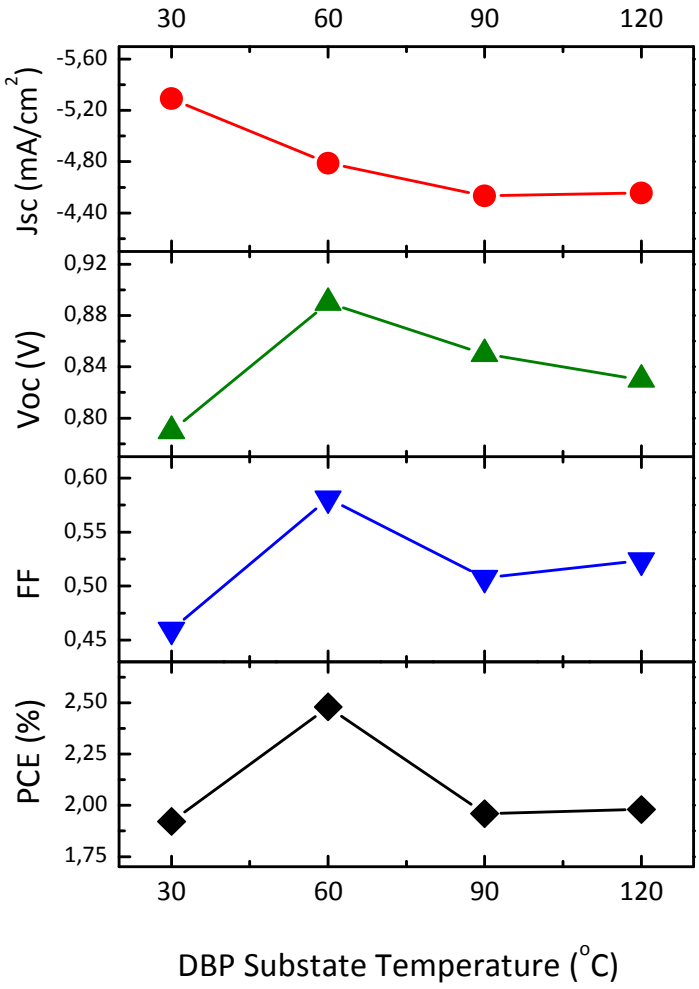

Figure 5.3 - Photovoltaic parameters of organic solar cells versus DBP substrate temperature.

The Optical Density (OD) of the photoactive materials DBP and C_{70} single layers and in a bilayer structure are shown in Figure 5.4. Thicknesses of the DBP and C_{70} were 10 nm and 40 nm respectively. The donor DBP presents different absorption bands in the visible region around

330, 550 and 600 nm. The acceptor C_{70} shows a strong absorption band at 350 nm and a broader band in the region of 450 nm. The OD of the DBP/C_{70} bilayer structure is significant from 300 nm to 700 nm. The higher OD of the device with DBP deposited at 30 ºC agrees with the highest J_{SC} value obtained for this device. As the deposition temperature increases, the actual thickness of the DBP layers could be slightly reduced because of a lower sticking coefficient of the organic molecule on the substrate. This effect could explain the reduction in the OD at higher substrate temperatures and the decrease of the J_{SC} values observed in Figure 5.3.

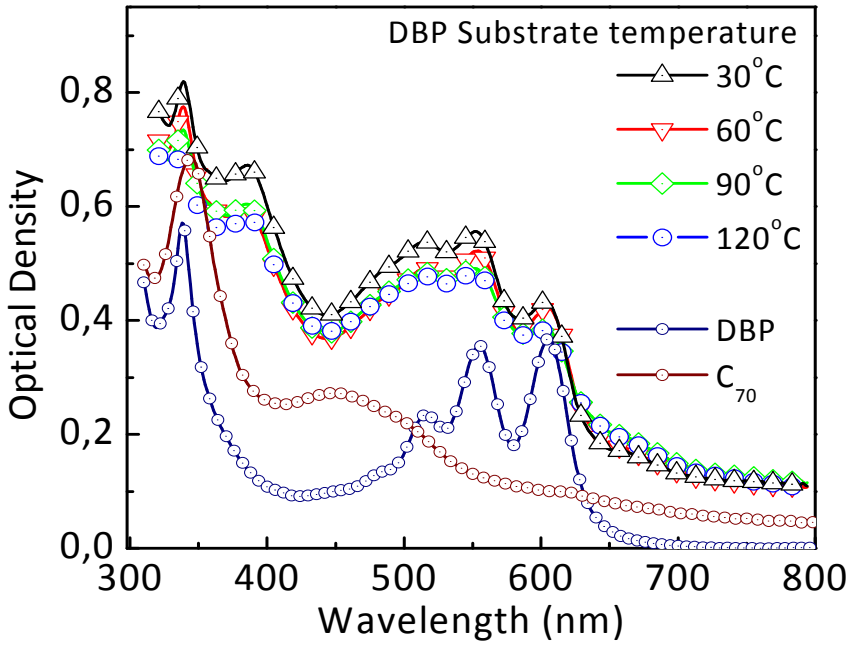

Figure 5.4 - Optical density of the active layers used for the fabrication of bilayer solar cells.

The spectral dependence of photocurrent generation and collection was analysed by measuring the *EQE* curves (Figure 5.5). The *EQE* curves were quite similar for all the solar cells with a slight reduction on devices incorporating DBP deposited at higher temperatures. This behaviour reproduces the trend observed in the measurements of the OD (Figure 5.4). The *EQE* curves also evidence a good correlation with the J_{SC} values measured for these devices.

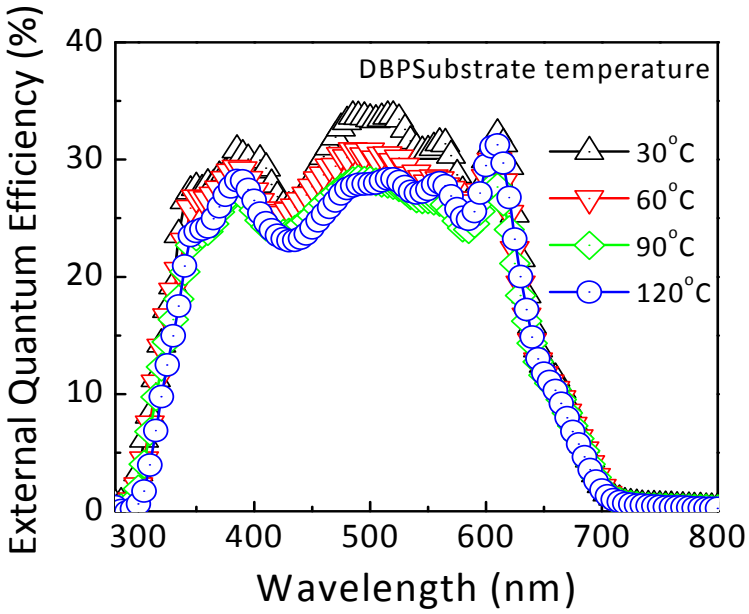

Figure 5.5 - *EQE* of bilayer solar cells in which the DBP layer was deposited at different substrate temperature.

5.1.3 Morphology analysis

The effect of the substrate temperature on the topography of the DBP films was studied by Atomic Force Microscopy (AFM). For that purpose, a series of DBP films with a thickness of 20 nm were deposited on crystalline silicon substrates. Figure 5.6 shows the top view AFM images (1 x 1 μm^2 scanning square) for four samples deposited at the different substrate temperatures. It can be observed that pillar-like grain structures were created as the substrate temperature increase. The density and size of these pillars also seem to increase with the substrate temperature during the deposition of the DBP.

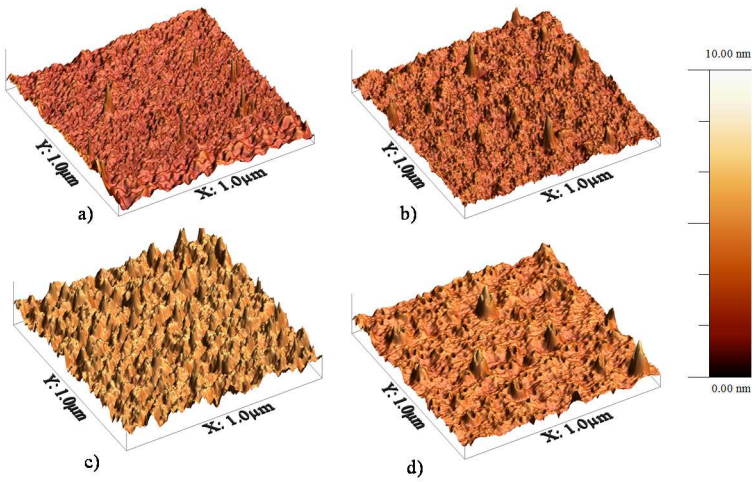

Figure 5.6 - AFM images of DBP thin films deposited at different substrate temperatures:

a) 30 ºC b) 60 ºC c) 90 ºC d) 120 ºC

The roughness values were estimated by using software techniques and its dependence with substrate temperature is shown in Figure 5.7. The surface of the films prepared at 30 ºC and 60 ºC was relatively smooth with roughness values around 0.35 nm. A sharp increase of the surface roughness is observed for the films deposited at 90 ºC and 120 ºC. This modification of the surface morphology with substrate temperature is rather similar to that reported by other groups (Zhou et al. [16]).

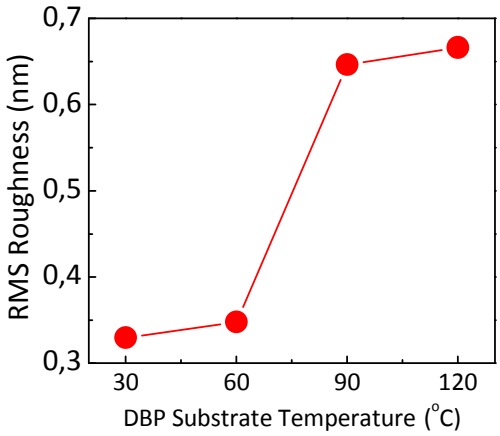

Figure 5.7 - Root-mean-square roughness of DBP thin films as function of the substrate temperature.

The nanostructure of the 20nm DBP layers on SiO_2 substrates were also analysed by X-Ray Diffraction (XRD) spectroscopy. The absence of diffraction peaks indicates the amorphous nature of the samples (Figure 5.8). Therefore, we could expect that transport properties, and particularly carrier mobility, are rather isotropic in these films.

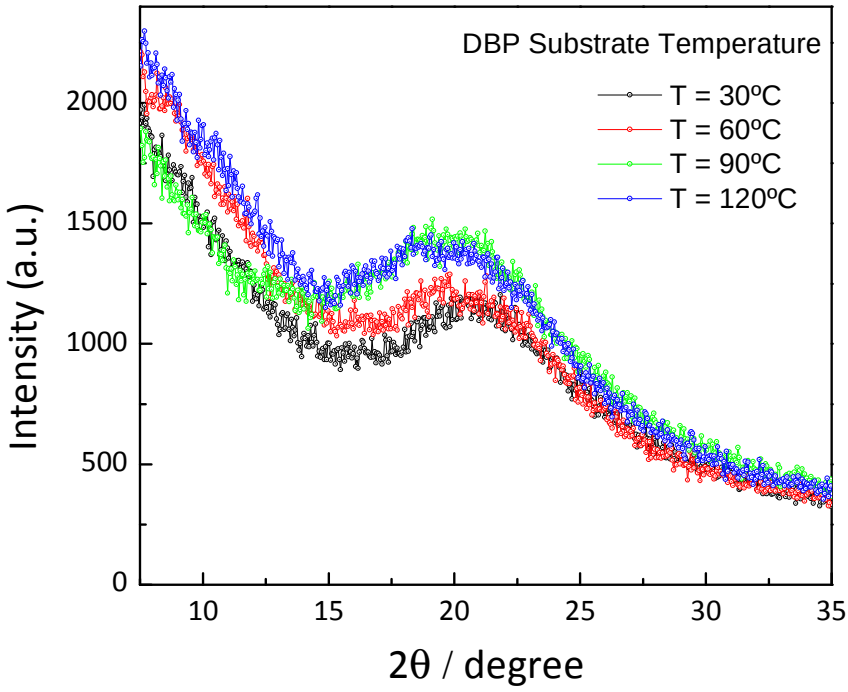

Figure 5.8 - XRD of DBP thin films deposited at different substrate temperature.

5.2 Influence of the Density of States in the open circuit voltage

5.2.1 Introduction

The optoelectronic properties of thin-film devices based on disordered semiconductors depend largely on the distribution of localised states in the band gap of the semiconductor. This is especially true in the case of organic solar cells in which thicknesses of the different layers composing the device are very thin, a few tenths of nm. It is rational to assume that by lowering the Density-of-States (DOS) in the band-gap of the semiconductor would improve the device performance, since defect states act as traps and recombination centres in the active layer. In particular open-circuit voltages are strongly dependent on the DOS of the active semiconductor material. Open circuit voltages are proportional to the difference between the quasi-Femi level of electrons and holes. Therefore, separation between quasi-Fermi levels will be lower for semiconductors with high level of localised states, i.e. recombination centres. Experimental information on the distribution of defects cannot be obtained in a straightforward manner. Different techniques have been proposed to obtain information about the energy distribution of the DOS in thin-film semiconductors. These include: ultraviolet photoelectron spectroscopy, Kelvin probe force microscopy, electron spin resonance spectroscopy, space-charge-limited-

current spectroscopy, deep-level transient spectroscopy, photoconductivity measurements and impedance spectroscopy [17–23]. Alternatively, field-effect structures such as thin-film transistors (TFTs) can be also used to obtain information regarding the energy distribution of trapped charges. Thin film transistors (TFTs) have been extensively used to determine the density of localised states in the band gap of inorganic semiconductors, such as polycrystalline silicon or hydrogenated amorphous silicon [24], and more recently in the study of organic semiconductors [25].

The presence of carrier traps in organic semiconductors necessarily affects the performance of electronic devices, and particularly solar cells. A higher DOS distribution causes more charge trapping and a reduced carrier mobility, which has a detrimental effect in the charge carrier collection that degrades the J_{SC} and *FF* values [26]. On the other hand, the influence of the DOS distribution on the V_{OC} has been also widely discussed in relation to the disorder of organic semiconductors [27]. Under some assumptions analytical expressions have been proposed to quantify the loss in V_{OC} depending on the particular DOS distribution [28–29]. These models are based on the calculation of the V_{OC} values from the separation of the electron and hole under illumination. Then, a higher density of localised states reduces the separation of the quasi-Fermi levels of electrons and holes and results in lower V_{OC} values.

The effect of the carrier mobility in relation to the V_{OC} value is more complex, since in open-circuit conditions there is no direct current extraction. The carrier mobility can have influence in the recombination mechanism, which in open-circuit and steady-state conditions must equal the generation rate. This recombination is typically assumed to be dominated by bimolecular mechanisms around open-circuit conditions [28], where for instance the Langevin model considers a mobility-dependent prefactor [29]. However, many reported studies using a variety of different techniques have found bimolecular recombination rates far below the Langevin formulation [30–34]. Hence, the influence that carrier mobility has in the V_{OC} is still unclear and needs further investigation as there can be different mobility-dependent recombination mechanisms [33–34]. Nonetheless, in many practical cases disorder induces a broader DOS distribution that causes a decrease of carrier mobility owing to charge trapping. Then, the V_{OC} drops because of a higher DOS along with the J_{SC} and *FF* values due to the decreased carrier mobility. In this section, the performance of DBP/C_{70} organic solar cells is correlated with the DOS distribution of the donor material.

5.2.2 Mobility and density of states of donor DBP

To study the influence of substrate temperature on the electronic properties of DBP, a series of OTFTs were fabricated at different substrate temperature. As mentioned before, OTFTs are a good tool to get information about the electrical properties of the charge carrier. In particular, field-effect mobility can be easily estimated from the analysis of the transistor electrical characteristics. However, as shown in Appendix I, detailed analysis of the electrical characteristics of TFT measured at different temperature allows to get more basic information of the electronic structure of thin-film semiconductors. In particular, from the transfer electrical characteristics measured at differed temperature and estimation of the density of localised states within the band gap of the semiconductor can be obtained. A detailed description of the methodology used to determine the mobility and the density of localised states can be found in Appendix I.

Figure 5.9 shows the output characteristics of OTFT based on DBP (20 nm thick) deposited at substrate temperature of 60 ºC. The thickness of the SiO_2 dielectric was 100 nm. The transistor exhibits the expected behaviour for a p-channel field effect transistor. A linear dependence between I_{DS} and V_{DS} is observed for low V_{DS} voltages. At higher V_{DS} voltages I_{DS} saturates.

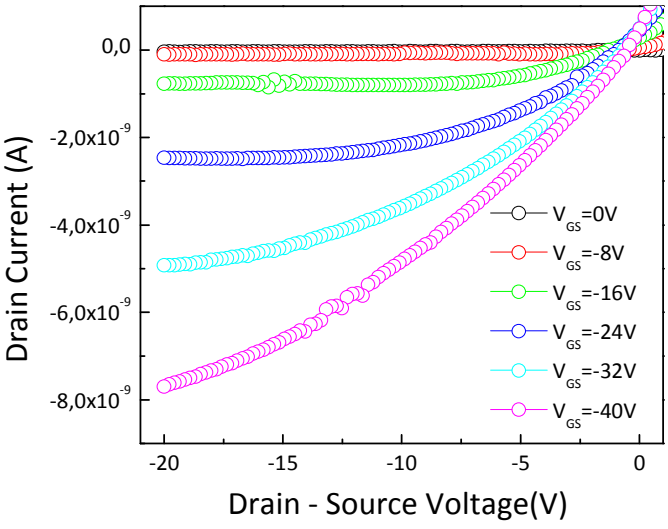

Figure 5.9 - Output characteristics of a DBP based OTFT with a SiO_2 gate dielectric.

Figure 5.10 shows the hole mobility as a function of the substrate temperature for two series of DBP transistors with different active layer thicknesses (20 and 50 nm). The field-effect mobility values are of the order of 10^{-5} $cm^2/V \cdot s$ and show a similar dependence with the substrate temperature. The highest field-effect mobility values were obtained for devices deposited at 60

ºC, which agrees with similar experiments reported in [5]. The highest V_{OC} and *FF* values were routinely obtained when substrate temperature was fixed at 60 ºC during the deposition of the DBPlayer (Figure 5.3). This correlation between the solar cell performance (in particular V_{OC} and *FF* values) with the field-effect mobility has already been reported for thermally evaporated small-molecule organic solar cells [35].

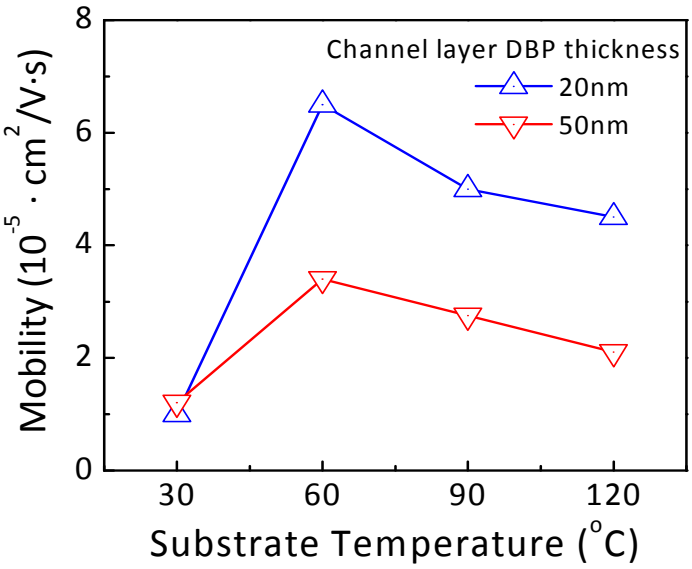

Figure 5.10 - Hole mobility of DBP as a function of the substrate temperature.

In order to determine the DOS, transfer characteristics were measured under vacuum conditions at different temperatures. Detailed information about the procedure to determine DOS can be found in Appendix I. Figure 5.11 shows an example of the transfer curves measured in the temperature range from 300 to 360 K in steps of 10 K. In this example, DBP active layer was 20 nm thick and deposited at substrate temperature of 30ºC. We observe that for negative V_{GS} (ON region), I_{DS} increase with temperature. Whereas for positive V_{GS} (OFF region), I_{DS} shows no dependence with the temperature.

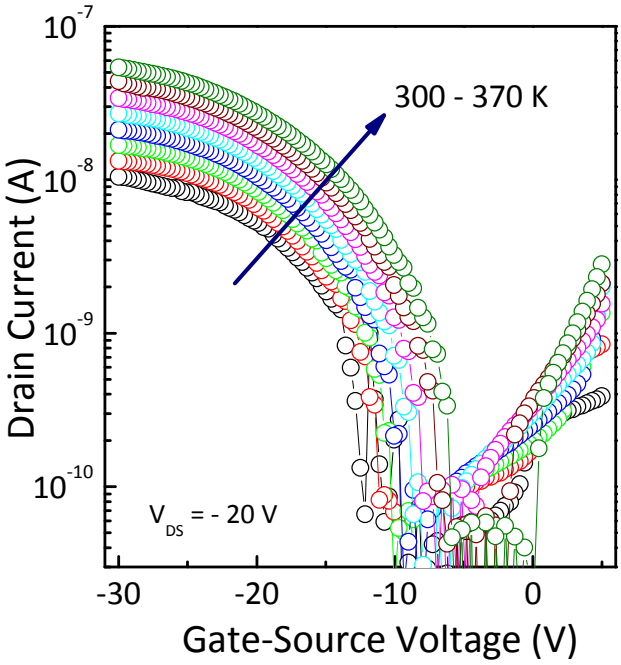

Figure 5.11 - Transfer characteristics of a DBP based OTFT measured at various temperatures (for a fixed V_{DS} = - 20V). DBP thickness was 20 nm and was deposited at substrate temperature of 30ºC.

Figure 5.12 shows the DOS of localised states as a function of Fermi level position for DBP transistors, 20 nm-thick, deposited at different substrate temperatures (30, 60, 90, 120 ºC).

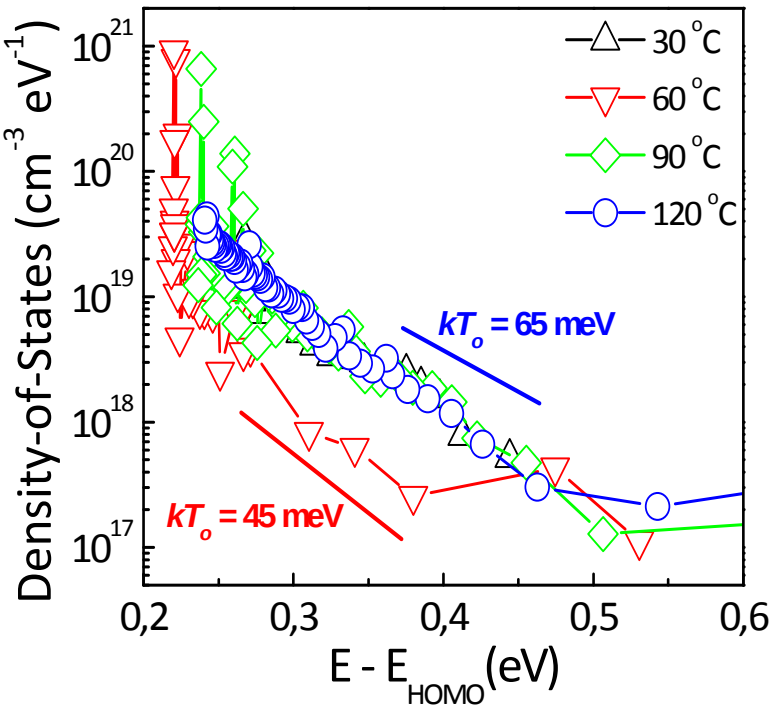

Figure 5.12 - Density of states of DBP as function of the substrate temperature.

Charge transport properties in thin-film small-molecule organic semiconductors can be described by an effective transport level and a distribution of trap states below this transport level [36–37]. This description is similar to the mobility edge picture developed for amorphous inorganic semiconductors, especially hydrogenated amorphous silicon, in which the mobility edge separates extended states from the localised ones. The distribution of traps below the transport level is believed to be exponentially shaped [38]. In analogy to inorganic semiconductors, this exponential region of the DOS can be assumed to be a band tail of localised states induced by structural disorder (Eq. 5.1).

$$N_t(E) = N_0 e^{\left(-\frac{E-E_v}{kT_0}\right)} \quad (5.1)$$

where N_0 is a prefactor that defines the concentration of tail states per unit volume and energy interval ($cm^{-3}eV^{-1}$) at the valence band edge. The slope of the tail given by kT_o measures the extent of the distribution of localised states; in other words, it is an indirect measure of the disorder in the semiconductor. Figure 5.12 shows that in all the samples the DOS increases exponentially up to 10^{20} cm^{-3} close to the valence band edge (E-E_{HOMO}< 0.2 eV). However, the tail of localised states is clearly reduced for the sample deposited at 60 ºC compared to the other

substrate temperatures. The presence of these trap states in the band gap of the semiconductor could act as traps and recombination centres and therefore could affect the position of the quasi Fermi level position for holes in illumination [39]. The origin of these electronic trap states is diverse and is still the subject of many investigations and discussions [36], [40], [41]. Some traps (extrinsic) are related to contaminants and chemical defects with composition different than the organic semiconductor and are associated with chemical impurities in the source material. Another source of defects is related to the chemical instability inherent in many organic compounds. It is well reported that organic molecules are reactive with oxygen and water [42]. Finally, some defects are associated with structural disorder (intrinsic traps) and are primary introduced by the growing conditions [41], [43].

As has been mentioned before, in organic solar cells, it has been shown that the maximum achievable value of V_{OC} is determined by the energy offset between the LUMO of the acceptor and the HOMO of the donor [44]. Experimentally, it has been found for a wide range of materials the relationship $qV_{OC} = HOMO_{DONOR} - LUMO_{ACCEPTOR} - \Delta$ [45]. The loss term (Δ) has been related to the exciton binding energy of radiative or non-radiative recombination of polaron pairs [47–48]. Despite the physical mechanisms contributing to the loss term Δ are still under discussion, there is also a consensus that the distribution of localised states plays an important role when determining V_{OC} values [48]. The presence of tail states (broader DOS) causes a lower effective energy gap and therefore a reduction of the V_{OC}. In the particular case of a DBP donor, photogenerated holes will prefer to occupy tail states rather than energy states in the HOMO level, leading to a higher hole quasi-Fermi level position and, as a consequence, bringing the average energy of electrons and holes closer together.

This phenomenon has already been studied in organic solar cells, both from the viewpoint of numerical device simulation and experimental measurements. Blakesley et al. studied the influence of energetic disorder on the V_{OC} using numerical simulation [49]. They found that a large increase of energetic disorder, or in other words broader DOS, causes a significant reduction in V_{OC}. Meanwhile, both J_{SC} and FF also drop along with V_{OC}.

5.3 p-i-n Organic Solar Cells based on DBP:C_{70}

The p-i-n organic solar cell structure is presented in Chapter 3, section 3.3. In this section, the results obtained from the characterisation of p-i-n solar cells are presented. The intrinsic layer (i-layer) is composed by the coevaporation of donor and acceptor (at ratio 1:1). The i-layer

thickness in p-i-n solar cells has strong influence in the performance. Increasing the thickness of intrinsic layer can increase the efficiency caused by higher absorption; however, excess of thickness reduce the efficiency due to recombination losses of free charge carriers. The optimisation of active layer thickness taking into account the trade-off between absorption and recombination is the objective of this section. Figure 5.13 shows the structure of the solar cells.

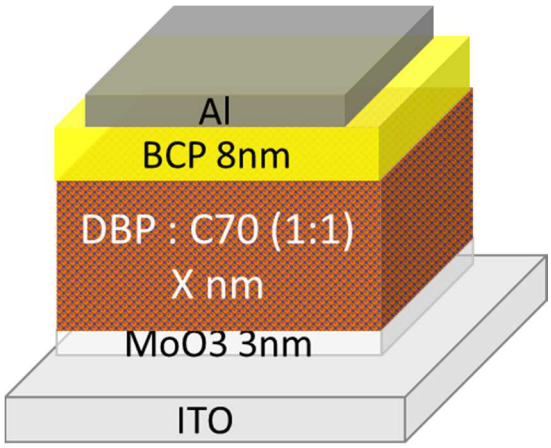

Figure 5.13 - Structure of p-i-n solar cell where i-layer is coevaporated at ratio donor – acceptor (1:1).

As previous section, the donor is DBP and the acceptor C_{70}. In order to facilitate holes and electrons collection, MoO_3 has been used as hole transport layer and BCP as electron transport layer inserted between the active layers and electrodes. The detailed configuration was ITO/MoO_3(3nm)/DBP:C_{70}(1:1)(x nm)/BCP(8nm)/Al(150nm). The thickness of i-layer (x) varies from 30 nm up to 70 nm. Figure 5.14 shows *J-V* curves of p-i-n cells with different i-layer thickness. The substrate temperature during coevaporation of donor and acceptor were fixed at 60 ºC due to it is the optimum temperature for lower tail of DOS of DBP as demonstrated in section 5.2.

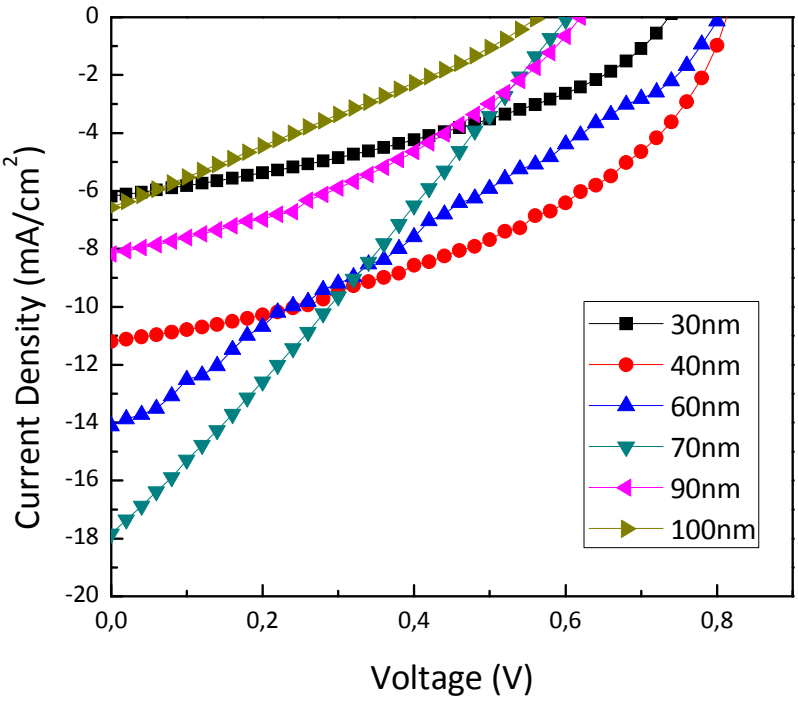

Figure 5.14 - *J–V* Curves of p-i-n cells for different i-layer thickness.

The main photovoltaic parameters as a function of i-layer thickness are summarized in Table 5.1 and shown in Figure 5.15. Following, the influence of i-layer thickness in each parameter is discussed.

Table 5.1 – Measurement results of the devices with various DBP:C_{70} thicknesses

Thickness (nm)	PCE (%)	*FF* (%)	J_{SC} (mA/cm^2)	V_{OC} (V)
30	1.76	39	-6.2	0.73
40	2.82	36	-11.2	0.71
60	3.12	33	-14.1	0.65
70	2.90	27	-17.8	0.61
90	1.90	37	-8.4	0.61
100	1.01	27	-6.6	0.57

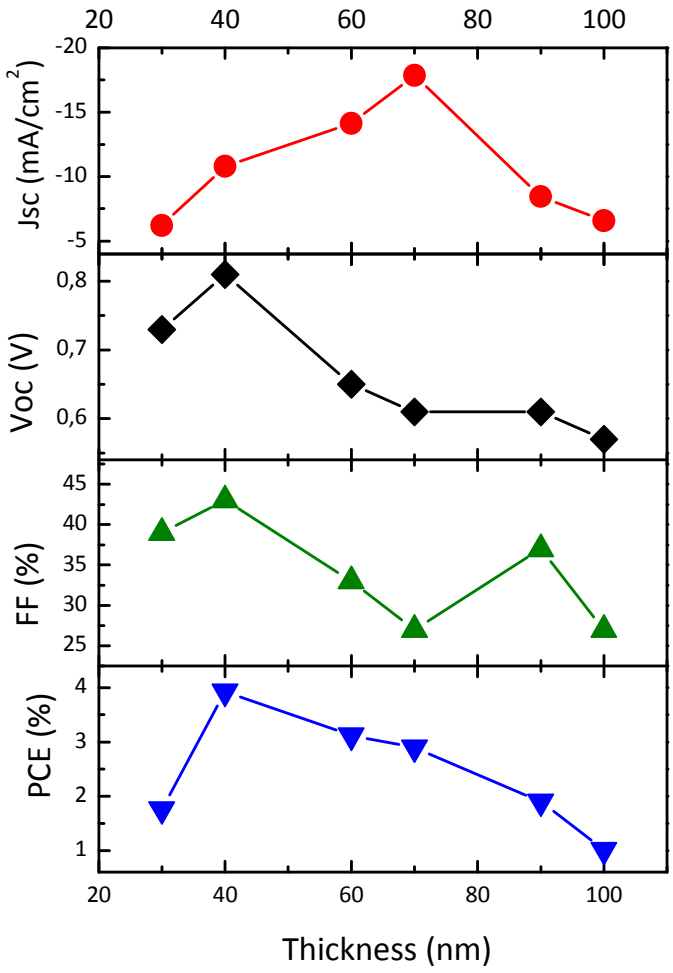

Figure 5.15 - Photovoltaic parameters of p-i-n organic solar cells versus i-layer thickness.

Short Circuit Current (J_{SC})

It was found that the J_{SC} of p-i-n solar cells was increasing while the thickness of i-layer is increasing up to 70 nm, indicating an efficient charge generation for this thickness. The enhancing of J_{SC} could be explained due to the increment of the absorption and the higher donor-acceptor interface. On the other hand, the J_{SC} starts to decrease when the thickness is higher than 70 nm. The J_{SC} reduction could be attributed to geminate recombination of the excitions due to the short exciton diffusion length. As a result, J_{SC} has the highest value at 70 nm (17.84 mA/cm^2) and the lowest value was reached with thickness about 30 nm (6.19 mA/cm^2).

Open Circuit Voltage (V_{OC})

The V_{OC} value is falling whereas i-layer thickness is higher than 40nm, when V_{OC} reaches the highest value. As explained above, V_{OC} value is related to the separation of the electron and hole

quasi-Fermi levels under illumination. The recombination in open-circuit is typically assumed to be dominated by bimolecular recombination. The higher i-layer thickness also implies higher bimolecular recombination since the free charge carriers (electrons and holes) must to travel longer distances up to the electrodes. Consequently, V_{OC} decrease because of the higher bimolecular recombination.

Fill Factor (FF)

The *FF* of p-i-n cells seems to decrease when i-layer thickness increase. However, no clear trend is observed. This phenomena could be explained because of *FF* is affected by both recombination mechanisms of organic solar cells. The maximum *FF* value is 39%, achieved by i-layer thickness of 30 nm, and the lowest *FF* value is 27%, reached by i-layer thickness of 70 nm.

Power Conversion Efficiency (PCE)

The PCE of solar cells is influenced by *FF*, V_{OC} and J_{SC}. The optimum p-i-n solar cell based on DBP:C_{70} (1:1) has been obtained for i-layer thickness. For higher values of i-layer thickness the PCE decreases, mainly leaded by the diminution of V_{OC}. The performance of p-i-n solar cell with i-layer thickness of 40 nm is J_{SC} = 11.20 mA/cm^2, V_{OC} = 0.81 V, *FF* = 0.43 and PCE of 3.93%.The PCE could be improved by optimising the volume ratio between the donor and acceptor, most likely with higher a concentration of the acceptor C_{70}, since the exciton lifetime in fullerene domains is higher than in DBP domains [8].

External Quantum Efficiency (EQE)

The spectral analysis of p-i-n cells from wavelength of 300 to 850 nm was examined by measuring the *EQE* curves (Figure 5.16). The *EQE* curves keep a good correspondence with the J_{SC} values measured (Figure 5.15). The highest area of *EQE* belongs to p-i-n cell with i-layer thickness of 70 nm, which has also the highest J_{SC}. Conversely, the lowest area belongs to p-i-n cells with 30 nm and 100 nm of i-layer thickness. The J_{SC} of both cells are similar which are about 6.19 mA/cm^2 and 6.57 mA/cm^2.

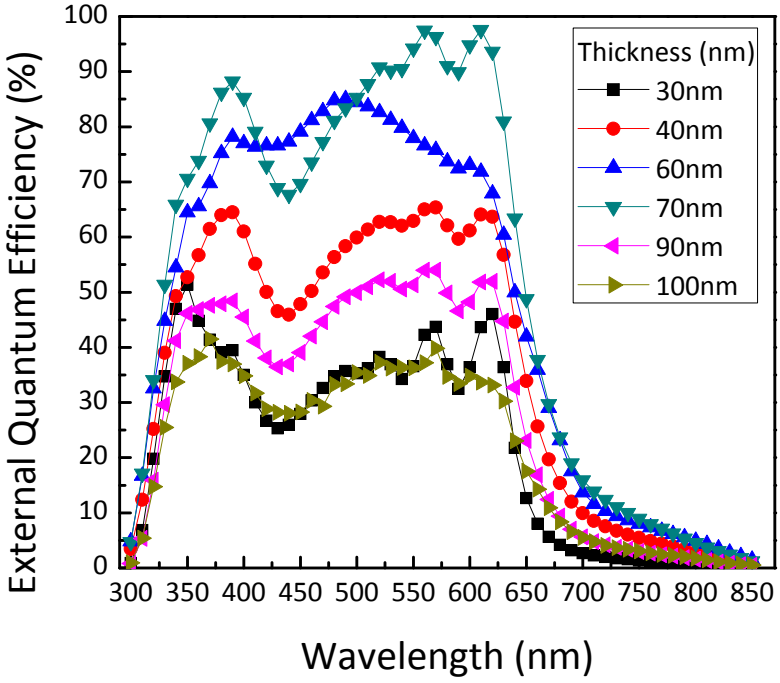

Figure 5.16 - *EQE* curves of p-i-n solar cells with different i-layer thicknesses.

Furthermore, the peak around 350–400 nm can be related to the C_{70} absorption; on the other hand, the peaks around 550–650 nm belong to DBP absorption. The curve of p-i-n cell with 60 nm of i-layer thickness has tendency almost flat comparing with other cells.

References

[1] W. M. Wang, H. D. Yang, J. S. Zhang, S. Li, X. R. Luo, S. L. Feng, "Influence of Substrate Temperature on Properties of Transition Materials from Amorphous to Microcrystalline Silicon Prepared by VHF-PECVD", *Adv. Mat. Res.* 750 (**2013**) 1906.

[2] A. de Calheiros Velozo, G. Lavareda, C. Nunes de Carvalho, A. Amaral, "Thermal dehydrogenation of amorphous silicon deposited on c-Si: Effect of the substrate temperature during deposition", *Phys. Status Solidi C* 9 (**2012**) 2198.

[3] J. Shirafuji, M. Kuwagaki, T. Sato, Y. Inuishi, "Effect of Substrate Temperature on Properties of Glow-Discharged Hydrogenated Amorphous Silicon" *Jpn. J. Appl. Phys.* 23 (**1984**) 1278.

[4] D. Fujishima, H. Kanno, T. Kinoshita, E. Maruyama, M. Tanaka, M. Shirakawa, K. Shibata, "Organic thin-film solar cell employing a novel electron-donor material" *Sol. Energ. Mat. Sol.* 93 (**2009**) 1029.

[5] M. Hirade, C. Adachi, "Small molecular organic photovoltaic cells with exciton blocking layer at anode interface for improved device performance", *Appl. Phys. Lett.* 99 (**2011**) 153302.

[6] D. Yokoyama, Z. Qiang Wang, Y.-J. Pu, K. Kobayashi, J. Kido, Z. Hong, "High-efficiency simple planar heterojunction organic thin-film photovoltaics with horizontally oriented amorphous donors", *Sol. Energy Mater. Sol. Cells*, 98 (**2012**) 472.

[7] Y. Zheng, W. J. Potscavage, T. Komino, M. Hirade, J. Adachi, C. Adachi, "Highly efficient bulk heterojunction photovoltaic cells based on C_{70} and tetraphenyldibenzoperiflanthene", *Appl. Phys. Lett.* 102 (**2013**) 143304.

[8] X. Xiao, J. D. Zimmerman, B. E. Lassiter, K. J. Bergemann, S. R. Forrest, "A hybrid planar-mixed tetraphenyldibenzoperiflanthene/C_{70} photovoltaic cell", *Appl. Phys. Lett.* 102 (**2013**) 073302.

[9] Z. Wang, D. Yokoyama, X. Wang, "Highly efficient organic p-i-n photovoltaic cells based on tetraphenyldibenzoperiflanthene and fullerene C_{70}", *Energy Environ. Sci.* 6 (**2013**) 249.

[10] B. Rand, D. Burk, S. Forrest, "Offset energies at organic semiconductor heterojunctions and their influence on the open-circuit voltage of thin-film solar cells", *Phys. Rev. B*, 75 (**2007**) 115327.

[11] M. Kröger, S. Hamwi, J. Meyer, T. Riedl, W. Kowalsky, A. Kahn, "P-type doping of organic wide band gap materials by transition metal oxides: A case-study on Molybdenum trioxide", *Org. Electron.* 10 (**2009**) 932.

[12] J. Meyer, K. Zilberberg, T. Riedl, A. Kahn, "Electronic structure of Vanadium pentoxide: An efficient hole injector for organic electronic materials", *J. Appl. Phys.* 110 (**2011**) 033710.

[13] D. Y. Kim, J. Subbiah, G. Sarasqueta, F. So, H. Ding, Irfan, Y. Gao, "The effect of molybdenum oxide interlayer on organic photovoltaic cells", *Appl. Phys. Lett.* 95 (**2009**) 093304.

[14] M. T. Greiner, M. G. Helander, W.-M. Tang, Z.-B. Wang, J. Qiu, Z.-H. Lu, "Universal energy-level alignment of molecules on metal oxides", *Nat. Mater.*, 11 (**2012**) 76.

[15] M. Kroger, S. Hamwi, J. Meyer, T. Riedl, W. Kowalsky, A. Kahn, "Role of the deep-lying electronic states of MoO_3 in the enhancement of hole-injection in organic thin films", *Appl. Phys. Lett.* 95 (**2009**) 123301.

[16] Y. Zhou, T. Taima, Y. Shibata, T. Miyadera, T. Yamanari, Y. Yoshida, "Controlled growth of dibenzotetraphenylperiflanthene thin films by varying substrate temperature for photovoltaic applications", *Sol. Energy Mater. Sol. Cells* 95 (**2011**) 2861.

[17] T. Sueyoshi, H. Fukagawa, M. Ono, S. Kera, N. Ueno, "Low-density band-gap states in pentacene thin films probed with ultrahigh-sensitivity ultraviolet photoelectron spectroscopy", *Appl. Phys. Lett.* 95 (**2009**) 183303.

[18] O. Tal, Y. Rosenwaks, Y. Preezant, N. Tessler, C. Chan, A. Kahn, "Direct determination of the hole density of states in undoped and doped amorphous organic films with high lateral resolution", *Phys. Rev. Lett.* 95 (**2005**) 256405.

[19] H. Matsui, A. S. Mishchenko, T. Hasegawa, "Distribution of localized states from fine analysis of electron spin resonance spectra in organic transistors", *Phys. Rev. Lett.*, 104 (**2010**) 056602.

[20] C. Krellner, S. Haas, C. Goldmann, K. P. Pernstich, D. J. Gundlach, B. Batlogg, "Density of bulk trap states in organic semiconductor crystals: Discrete levels induced by oxygen in rubrene", *Phys. Rev. B*, 75 (**2007**) 245115.

[21] V. Nádaždy, R. Durný, J. Puigdollers, C. Voz, S. Cheylan, K. Gmucová, "Experimental observation of oxygen-related defect state in pentacene thin films", *Appl. Phys. Lett.* 90 (**2007**) 092112.

[22] D. V. Lang, X. Chi, T. Siegrist, A. M. Sergent, A. P. Ramirez, "Amorphouslike density of gap states in single-crystal pentacene", *Phys. Rev. Lett.* 93 (**2004**) 086802.

[23] G. Garcia-Belmonte, P. P. Boix, J. Bisquert, M. Lenes, H. J. Bolink, A. La Rosa, S. Filippone, N. Martín, "Influence of the intermediate density-of-states occupancy on open-circuit voltage of bulk heterojunction solar cells with different fullerene acceptors", *J. Phys. Chem. Lett.*, 1 (**2010**) 2566.

[24] T. Globus, H. C. Slade, M. Shur, M. Hack, "Density of deep bandgap states in amorphous silicon from the temperature dependence of thin film transistor current", *MRS Proceedings* 336 (**1994**) 823.

[25] J. Puigdollers, A. Marsal, S. Cheylan, C. Voz, R. Alcubilla, "Density-of-states in pentacene from the electrical characteristics of thin-film transistors", *Org. Electron.* 11 (**2010**) 1333.

[26] J. C. Blakesley, D. Neher, "Relationship between energetic disorder and open-circuit voltage in bulk heterojunction organic solar cells", *Phys. Rev. B* 84 (**2011**) 075210.

[27] G. Garcia-Belmonte, "Temperature dependence of open-circuit voltage in organic solar cells from generation–recombination kinetic balance", *Sol. Energy Mater. Sol. Cells*, 94 (**2010**) 2166.

[28] S. R. Cowan, A. Roy, A. J. Heeger, "Recombination in polymer-fullerene bulk heterojunction solar cells", *Phys. Rev. B*, 82 (**2010**) 245207.

[29] M. Pope, C. E. Swenberg, "Electronic Processes in Organic Crystals and Polymers", Oxford University Press. 1999.

[30] C. Deibel, A. Wagenpfahl, V. Dyakonov, "Origin of reduced polaron recombination in organic semiconductor devices", *Phys. Rev. B*, 80 (**2009**) 075203.

[31] C. Shuttle, B. O'Regan, A. Ballantyne, J. Nelson, D. Bradley, J. Durrant, "Bimolecular recombination losses in polythiophene: Fullerene solar cells", *Phys. Rev. B* 78 (**2008**) 113201.

[32] G. Juška, G. Sliaužys, K. Genevičius, K. Arlauskas, A. Pivrikas, M. Scharber, G. Dennler, N. Sariciftci, R. Österbacka, "Charge-carrier transport and recombination in thin insulating films studied via extraction of injected plasma", *Phys. Rev. B*, 74 (**2006**) 115314.

[33] J.-T. Shieh, C.-H. Liu, H.-F. Meng, S.-R. Tseng, Y.-C. Chao, S.-F. Horng, "The effect of carrier mobility in organic solar cells", *J. Appl. Phys.* 107 (**2010**) 084503.

[34] W. Tress, K. Leo, M. Riede, "Optimum mobility, contact properties, and open-circuit voltage of organic solar cells: A drift-diffusion simulation study", *Phys. Rev. B* 85 (**2012**) 155201.

[35] Y. Terao, H. Sasabe, C. Adachi, "Correlation of hole mobility, exciton diffusion length, and solar cell characteristics in phthalocyanine/fullerene organic solar cells", *Appl. Phys. Lett.* 90 (**2007**) 103515.

[36] W. L. Kalb, S. Haas, C. Krellner, T. Mathis, B. Batlogg, "Trap density of states in small-molecule organic semiconductors: A quantitative comparison of thin-film transistors with single crystals", *Phys. Rev. B* 81 (**2010**) 155315.

[37] V. I. Arkhipov, P. Heremans, E. V. Emelianova, G. J. Adriaenssens, H. Bässler, "Charge carrier mobility in doped semiconducting polymers", *Appl. Phys. Lett.* 82 (**2003**) 3245.

[38] K. Celebi, P. J. Jadhav, K. M. Milaninia, M. Bora, M. A. Baldo, "The density of states in thin film copper phthalocyanine measured by Kelvin probe force microscopy", *Appl. Phys. Lett.* 93 (**2008**) 083308.

[39] G. Horowitz, R. Hajlaoui, P. Delannoy, "Temperature dependence of the field-effect mobility of sexithiophene. Determination of the density of traps", *Journal de Physique* III, 5 (**1995**) 355.

[40] J. A. Carr, S. Chaudhary, "The identification, characterization and mitigation of defect states in organic photovoltaic devices: a review and outlook", *Energy Environ. Sci*. 6 (**2013**) 3414.

[41] L. G. Kaake, P. F. Barbara, X.-Y. Zhu, "Intrinsic charge trapping in organic and polymeric semiconductors: a physical chemistry perspective", *J. Phys. Chem. Lett.* 1 (**2010**) 628.

[42] D. Knipp, J. E. Northrup, "Electric-Field-Induced Gap States in Pentacene", *Adv. Mater*. 21 (**2009**) 2511.

[43] T. S. Ripolles, A. Guerrero, G. Garcia-Belmonte, "Polymer defect states modulate open-circuit voltage in bulk-heterojunction solar cells", *Appl. Phys. Lett*., 103 (**2013**) 243306.

[44] C. J. Brabec, A. Cravino, D. Meissner, N. S. Sariciftci, T. Fromherz, M. T. Rispens, L. Sanchez, J. C. Hummelen, "Origin of the open circuit voltage of plastic solar cells", *Adv. Funct. Mater*. 11 (**2001**) 374.

[45] M. C. Scharber, D. Mühlbacher, M. Koppe, P. Denk, C. Waldauf, A. J. Heeger, C. J. Brabec, "Design rules for donors in bulk-heterojunction solar cells-towards 10% energy-conversion efficiency", *Adv. Mater*. 18 (**2006**) 789.

[46] K. Vandewal, K. Tvingstedt, A. Gadisa, O. Inganäs, J. V. Manca, "Relating the open-circuit voltage to interface molecular properties of donor: acceptor bulk heterojunction solar cells", *Phys. Rev. B* 81 (**2010**) 125204.

[47] N. C. Giebink, B. E. Lassiter, G. P. Wiederrecht, M. R. Wasielewski, S. R. Forrest, "Ideal diode equation for organic heterojunctions. II. The role of polaron pair recombination", *Phys. Rev. B,* 82 (**2010**) 155306.

[48] G. Garcia-Belmonte, "Carrier recombination flux in bulk heterojunction polymer: fullerene solar cells: Effect of energy disorder on ideality factor", *Solid. State. Electron.*, 79 (**2013**) 201.

[49] J. C. Blakesley, N. C. Greenham, "Charge transfer at polymer-electrode interfaces: The effect of energetic disorder and thermal injection on band bending and open-circuit voltage", *J. Appl. Phys*. 106 (**2009**) 034507.

6. Model for charge carrier collection efficiency in Organic Solar Cells

In this Chapter, an equivalent circuit for organic solar cells is presented. It is based on the classic combination of a diode with an exponential current–voltage characteristic, parasitic series and parallel resistances, a photogenerated current source, plus a new term representing recombination losses in the active layer of the device. The model clearly separates technological issues (series and parallel resistance) from effects related to the physics of the device (recombination losses). It also allows an effective $\mu\tau$ product in the active layer of the device to be determined, characterising its state of degradation.

6.1 Model for Organic Solar Cell

The use of equivalent circuits is a convenient way to describe the electrical behaviour of electronic devices. Therefore, an equivalent circuit model is helpful in the understanding and optimisation of solar cells by providing a quantitative estimate for losses in the device. The conventional circuit model developed in the context of photovoltaic solar cells is presented in Chapter 3 and shown in Figure 6.1[1]. According to this equivalent circuit, the *J–V* characteristic can be expressed by an implicit equation (Eq. 6.1). This model essentially consists of a current source shunted by a diode. These two elements correspond to generation and loss of photocurrent in the device. The resistances R_S and R_P can be considered to be "parasitic" circuit elements, introduced to describe the behaviour of real solar cells with their technological limitations. This model has been used to interpret results obtained with organic solar cells as well [2–4]. In view of the fact that photovoltaic response in organic solar cells is considerably different from that in inorganic solar cells, the modification of conventional solar cell circuit model is discussed in this Chapter.

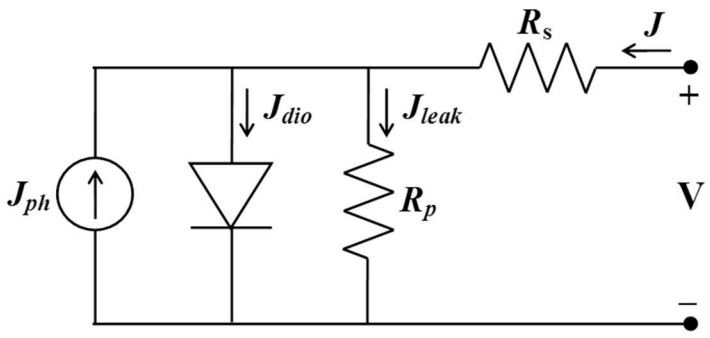

Figure 6.1 - Equivalent circuit for standard solar cell.

$$J = -J_{ph} + J_o\left[\exp\left(\frac{V - R_s J}{nV_T}\right) - 1\right] + \frac{V - R_s J}{R_p} \tag{6.1}$$

6.2 Introduction to the Variable Illumination Measurement method

The standard equivalent circuit superposes a photocurrent source on the electrical characteristic of the dark diode. Nonetheless, it is important to note that the photogeneration of electrons and holes within the solar cell will change the carrier concentration at every point. Thus, in principle, a new solution for the drift-diffusion differential equations throughout the whole device would be required. However, such a simple superposition of a dark diode and a photocurrent source is indeed valid and can be theoretically justified for crystalline solar cells, consisting of pn-diodes. The theoretical justification [5] is based on the linear form of the drift-diffusion differential equations for minority carriers, within the p- or n-type bulk regions of the pn-diode.

However, it is well known that the main part of the photovoltaic generation in solar cells with a p-i-n structure occurs in the active i-layer, as in the case of amorphous silicon solar cells. As a striking example, the curves for different illumination levels usually all meet at a single point in the first quadrant [6], which has been called collection voltage (V_C). This fact can only be reconciled with the simple equivalent circuit of Fig. 6.2 by including an additional loss term, which increases strongly with the forward voltage. Such a loss term takes into account the recombination losses in the active layer of the device. Then, this term has to be considered in the implicit equation (Eq. 6.2). In this section, we propose a method to gain valuable information about the device operation and, in particular, the recombination term. The basic idea is to measure the *J(V)* curve over a wide range of illumination levels, rather than at a fixed level of

one sun. For that reason, we have called it the Variable Illumination Measurement (VIM) method.

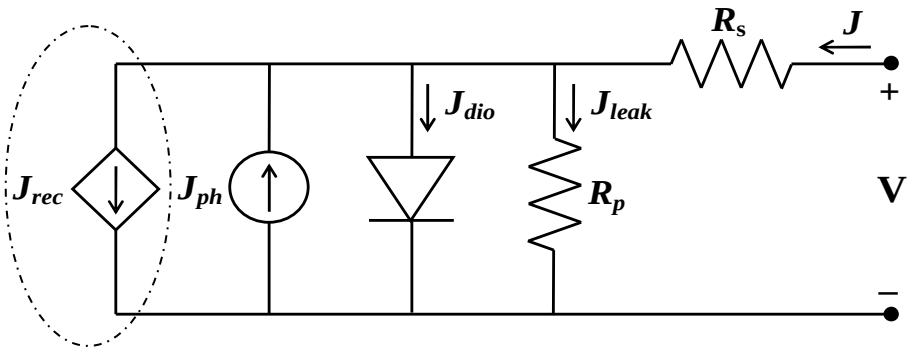

Figure 6.2 - Equivalent circuit for solar cell with recombination term.

$$J = -J_{ph} + J_o\left[\exp\left(\frac{V - R_s J}{nV_T}\right) - 1\right] + \frac{V - R_s J}{R_p} + J_{rec} \tag{6.2}$$

6.2.1 Parameters of the model

We have used the standard characterisation procedure for solar cells that consists of measuring the curve at a given illumination level as it shown in Figure 6.3. The resulting data may be condensed into the six characteristic parameters which are:

1) the short circuit current I_{SC};
2) the open circuit voltage V_{OC};
3) the fill factor FF;
4) the efficiency η;
5) the "open circuit resistance" R_{OC}, which at a high illumination level may be related to the series resistance ;
6) and the "short circuit resistance" R_{SC}, which at a low illumination level may be related to the parallel resistance

The latter two parameters are key parameters for the present treatment; they are defined as the reciprocal slopes of the J-V curve.

Dynamic resistances:

- Open circuit resistance $$R_{OC} = \left.\frac{\partial V}{\partial J}\right|_{J=0}$$ (6.3)

- Short circuit resistance $$R_{SC} = \left.\frac{\partial V}{\partial J}\right|_{V=0}$$ (6.4)

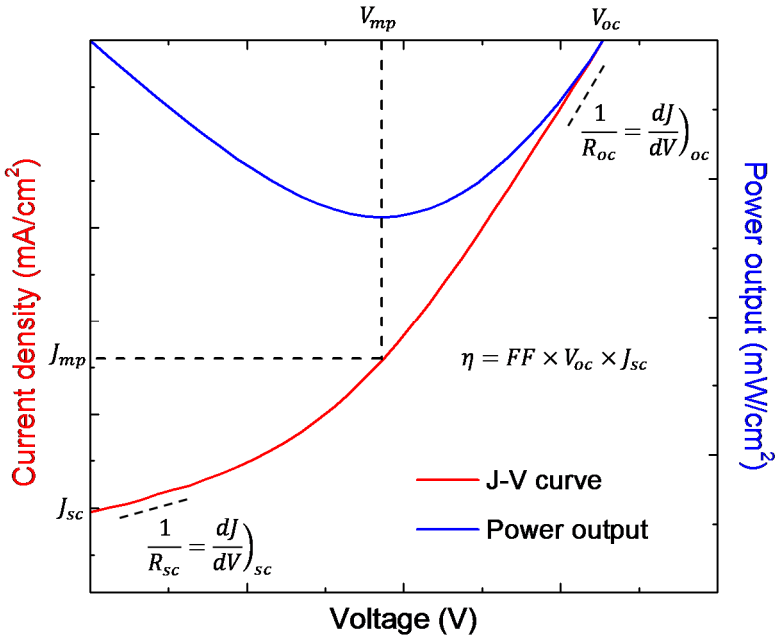

Figure 6.3 - *J–V* curve of a p-i-n solar cell. Apart from the standard photovoltaic parameters (J_{SC}, V_{OC} and *FF*), we also consider the dynamic resistance of the device evaluated at short-circuit and open-circuit conditions (R_{SC} and R_{OC}).

The logarithmic variation on the illumination intensity can be classified in five distinct levels, each one of them with a characteristic *J(V)* curve (Figure 6.3):

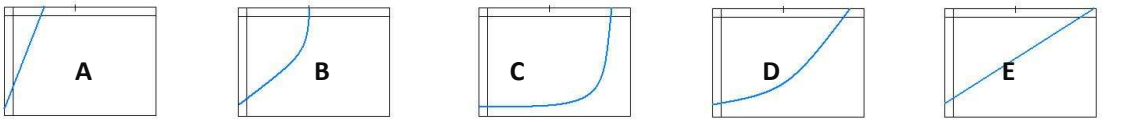

$R_{SC} = R_{OC} = R_P$ $R_{SC} = R_P$ $J(V) \neq f(R_{SC}, R_{OC})$ $R_{OC} = R_S$ $R_{OC} = R_{SC} = R_S$

Figure 6.4 - Five illumination levels used in the VIM method, where Level C ≈1 sun. Figure adapted from [7].

Level A) At very low illumination levels, the *J(V)* curve is completely shaped by the parallel resistance R_P, which determines the values of both R_{SC} and R_{OC}. The value of R_P limits the V_{OC} the FF is equal to a minimum 0.25.

Level B) By increasing the illumination, the R_P still determines the R_{SC} value, which shapes the short circuit region of the measurement. The *J(V)* curve at forward voltage is

already shaped by the physics of the device. Both the V_{OC} and the *FF* progressively increase.

Level C) In this regime, the *J(V)* curve is not affected by neither R_S nor R_P but by the physics of the device. The *FF* reaches a maximum and the device is at its optimum operating point (≈1 sun).

Level D) Further increasing the illumination level, the R_{OC} vale equals the series resistance R_S, which begins to shape the open circuit region of the *J(V)* curve, while the rest remains shaped by the physics of the device. While the V_{OC} still increases, the *FF* starts to decrease.

Level E) At very high illumination levels the *J(V)* is completely shaped by the R_S value, which determines both R_{SC} and R_{OC}. At this level, V_{OC} reaches a maximum while the *FF* is again at a minimum 0.25.

6.2.2 Assumptions for the model

A few assumptions and modelling simplifications were done, many of them based upon the experience in amorphous silicon solar cells, but also extendable to organic solar cells with p-i-n structure:

a) Charge collection in p-i-n solar cells is mainly a drift-driven process, while diffusion plays a minor role [8]. This assumption is particularly true around the short circuit condition, as it has been justified in the literature [9–10].

b) Several works also support that the *J–V* curve is affected by a first-order recombination process from the short-circuit condition to around the maximum power point [11–12]. Recently, this behaviour has been explained considering a monomolecular recombination process through localised states near the interface between donor and acceptor domains [13–14].

c) The electric field *E* is constant through the intrinsic layer. This approximation has been widely used to describe the behaviour of inorganic thin film solar cells based on amorphous silicon due to the low fixed charge density in their intrinsic active layers [8, 15–16]. Although the relevance of fixed charge densities in organic semiconductors is still subject of discussion [17–18], a constant electric field approximation is often assumed in the literature considering the rather thin active layer of these devices (<100

nm) [9, 19]. The electrostatic potential on the active layer is given by the difference between the built-in voltage across the electrodes (V_{bi}) and the applied voltage V. Thus, the intensity of the electric field within the active layer of thickness L can be calculated as:

$$E = \frac{V_{bi} - V}{L} \tag{6.5}$$

6.2.3 Effective mobility-lifetime product ($\mu\tau_{eff}$) of charge carriers

Under the previous assumptions (drift-driven collection, monomolecular recombination and constant electric field), a compact analytical expression for the current density near the short-circuit condition can be used [8] (Eq. 6.6):

$$J = qGl_c\left[1 - exp\left(-\frac{L}{l_c}\right)\right] \tag{6.6}$$

where q is the elementary charge and G the effective generation rate of charge carriers per unit volume, which considers only those excitons which are effectively dissociated. A constant generation rate is a good approximation for the typically thin active layers of p-i-n solar cells illuminated under the AM1.5 spectra. The collection length l_c in Eq. 6.6 is defined as the sum of the corresponding drift lengths for electrons ($l_n = \mu_n\tau_n E$) and holes ($l_p = \mu_p\tau_p E$), that is, $l_c = l_e + l_h$. The collection length is interpreted as the maximum distance these charges separate apart driven by the electric field before recombining.

Then, by introducing an effective $\mu\tau_{eff}$ product and taking into account Eq. (6.5), the collection length l_c can be written as:

$$l_c = (\mu_e\tau_e + \mu_h\tau_h)E = \mu\tau_{eff}\frac{V_{bi} - V}{L} \tag{6.7}$$

where $\mu\tau_{eff} = \mu_n\tau_n + \mu_p\tau_p$.

The validity of Eq. 6.6 is limited to small applied voltages, since it does not consider charge carrier injection by the electrodes. This means that the contribution of the diode term and shunt resistance to the current density must be much lower than the total photogenerated current density reduced by the recombination term:

$$J \approx J_{ph} - J_{rec} \tag{6.8}$$

Anyhow, Eq. 6.6 indeed describes the *J*–*V* curve under illumination at moderate applied voltages. For long collection lengths compared to the active layer thickness, it can be approximated by:

$$J \approx qGL\left(1 - \frac{L/2}{l_c}\right) \tag{6.9}$$

where we can identify the photogenerated current density $J_{ph} = qGL$, that we would obtain if all the charge carriers were collected in the external circuit. Eq. 6.9 can be particularised at the short-circuit condition to obtain an expression for J_{SC}:

$$J_{SC} = J_{ph}\left(1 - \frac{L/2}{l_{c_o}}\right) \tag{6.10}$$

where we have introduced the short-circuit collection length $lc_o = \mu\tau_{eff}\ V_{bi} / L$, that is the collection length given by Eq. 6.7 evaluated at zero applied voltage. According to Eq. 6.9, the collection efficiency at moderate applied voltages can be calculated as:

$$\eta_c = 1 - \frac{L/2}{l_c} \tag{6.11}$$

Eq. 6.11 states that the fraction of the photogenerated current that recombines into the active layer is given by the ratio of $L/2$ to l_c. This result can be physically interpreted considering that the mean distance that charge carriers have to move in order to reach its corresponding electrode is actually half of the thickness of the active layer. Then, we finally obtain an analytical expression for the recombination term valid for moderate applied voltages:

$$J_{rec} = J_{ph}\left(\frac{L/2}{l_c}\right) = J_{ph}\frac{L^2/2}{\mu\tau_{eff}(V_{bi} - V)} \tag{6.12}$$

Finally, according to definition of R_{SC}, by evaluating the derivative $\partial J_{rec}/\partial V|_{sc}$ we obtain the following expression for R_{SC}:

$$R_{sc} = \left(\frac{2\mu\tau_{eff}V_{bi}}{L^2} - 1\right)\frac{V_{bi}}{J_{sc}} = \frac{V_C}{J_{sc}} \tag{6.13}$$

This last equation gives a direct relation between the collection voltage V_C and the physical mechanisms governing charge carrier collection [20]:

$$V_C = \left(\frac{l_{c_o}}{L/2} - 1 \right) V_{bi} \tag{6.14}$$

6.3 Results for p-i-n small-molecule solar cells based on DBP/C_{70}

The VIM method has been used to study the quality of the intrinsic layer of organic solar cells with pin structure. The solar cells used in this study have the following structure: glass/ITO/MoO_3/DBP:C_{70}(X nm)/BCP(8 nm)/Al(150 nm). The i-layer (DBP:C_{70}) thickness was 30nm and 40 nm for two different devices.

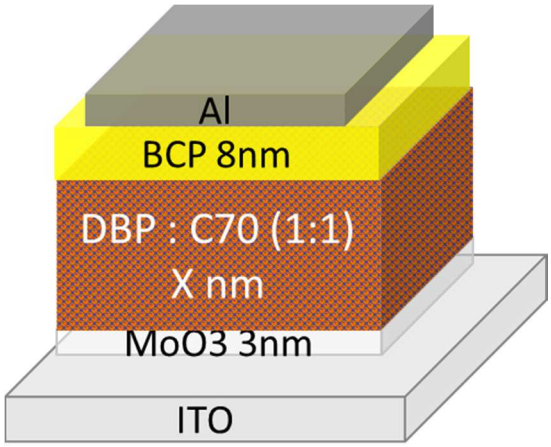

Figure 6.5 - Structure of p-i-n solar cell used for VIM analysis.

A simple graphical interpretation for the collection voltage is obtained when analysing the *J(V)* curves for the different illumination levels applied to the solar cells under study (Figure 6.6). The V_C value can then be obtained as that single point where all $1/R_{SC}$ slopes meet when extrapolated into the *x* axis. This fact also implies that, under reverse bias conditions, the short-circuit current approaches the total photogenerated current ($J_{SC} \lesssim J_{ph}$) [21].

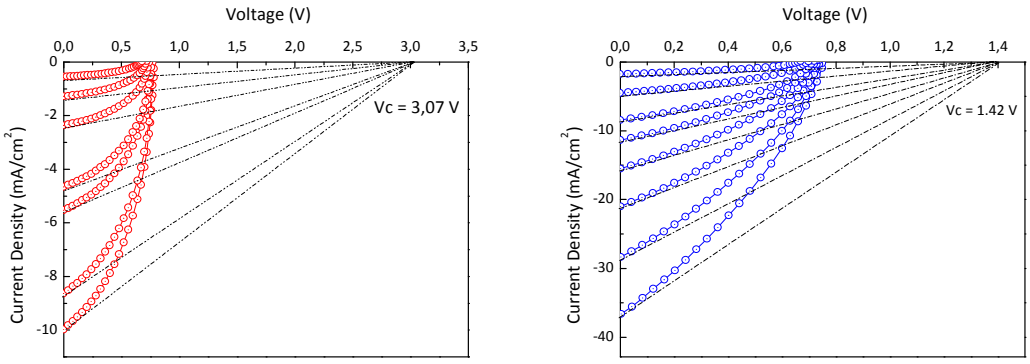

Figure 6.6 - *J -V* curves for the p-i-n organic solar cells measured with VIM method. The collection voltage V_C is obtained by the x-axis intersection of the $1/R_{SC}$ slopes. i-layer thickness of 40nm (left) and 30nm (right)

After extracting the V_C value from experimental VIM data (Figure 6.6) and considering that $V_{bi} \approx W_{\text{anode}} - W_{\text{cathode}} = 0.7$ V, the $\mu\tau_{eff}$ of each solar cell can be calculated (Table 6.1). These values are comparable to those reported in the literature for similar devices [13][22–23].

Table 6.1 Values for the carrier collection process obtained from the VIM analysis.

i-layer thickness (nm)	V_C (V)	$\mu\tau_{eff}$ (cm^2/V)	l_C (nm)	η_C	J_{rec} (mA/cm^2)
40	3.07	3.07×10^{-10}	173.5	88%	1.46
30	1.42	3.56×10^{-11}	50.6	70%	2.60

These results give us an insight on the carrier transport process in the active layer, which can be related to its quality. For the device with a 40 nm thick i-layer, the higher $\mu\tau_{eff}$ value indicates lower recombination losses and a better current extraction into the electrodes. Namely, the collection length (at short circuit conditions) is almost 4 times larger than the active layer. This leads to a carrier collection efficiency of 88%, meaning that only 12% of the photogenerated current is lost because of recombination (J_{rec}). On the other hand, for the 30 nm thick i-layer, the lower $\mu\tau_{eff}$ value indicates a poorer carrier transport quality of the device. Consequently, the collection efficiency is limited to a value of 70% because of the higher recombination term. Note that the collection efficiency depends on the active layer quality but also on its thickness, which influences the strength of the electric field. By contrast, the $\mu\tau_{eff}$ value is only characteristic of the active layer quality. The differences observed between these two devices, fabricated under very similar deposition conditions, could be related to the fast degradation of non- encapsulated devices in ambient.

6.4 Degradation of p-i-n Organic Solar Cells

One of the main drawbacks of organic solar cells is that they are prone to degradation in the presence of oxygen and humidity, making necessary the encapsulation under transparent polymer membranes or glass to maintain their electronic properties.

An insight on the causes of solar cell degradation can be obtained by applying the VIM method for a long time after the fabrication. Since R_S, R_P and $\mu\tau_{eff}$ are related to specific quality aspects of the cell, a distinction can be made between degradation of the i-layer and other parts of the cell, such as the metal contacts.

For an organic p-i-n solar cell with the following structure: glass/ITO/MoO_3/DBP:C_{70}(30nm)/BCP(8nm)/Al(150nm), VIM measurements were done after cell fabrication and every 5 hours. The cell remained under nitrogen atmosphere, in a fixed position and under dark conditions between these measurements. Table 6.2 shows the performance parameters for one measure of the VIM data.

Table 6.2 Main performance parameters of p-i-n organic solar cell based on DBP:C_{70}(1:1) with i-layer thickness of 30 nm at t=0 h and t=30 h.

Time	***PCE*** (%)	***FF*** (%)	P_{MAX} (mW/cm^2)	J_{SC} (mA/cm^2)	V_{OC} (V)	***Diode n***
0 h	1.60	38	2.1	7.77	0.71	1.41
30 h	0.66	35	0.86	3.60	0.68	1.40

Even though the cell was kept under N_2 atmosphere and it was only illuminated every 5 hours during data acquisition, the decrease in the conversion efficiency is substantial (59%). The largest degradation comes from a J_{SC} drop of 54%, while *FF* drops only by 7% and there is also a very slight decrease in the V_{OC}. This is consistent with experimental results reported by [24], where similar losses in J_{SC} and *PCE* occurred when measuring the cell under ambient conditions. Almost no change was observed in the ideality factor *n*, although reported degradation tests have signalled an increase as a possible reason for loss of efficiency [25].

Analysis of the series resistance R_S shows an important increment, somewhat explaining the decrease in *FF* (Figure 6.7). This is attributed to degradation outside i-layer, such as corrosion or

delamination of the contacts, leading to a drop in conductivity and a change in the work function. This effect has also been reported in previous studies [26].

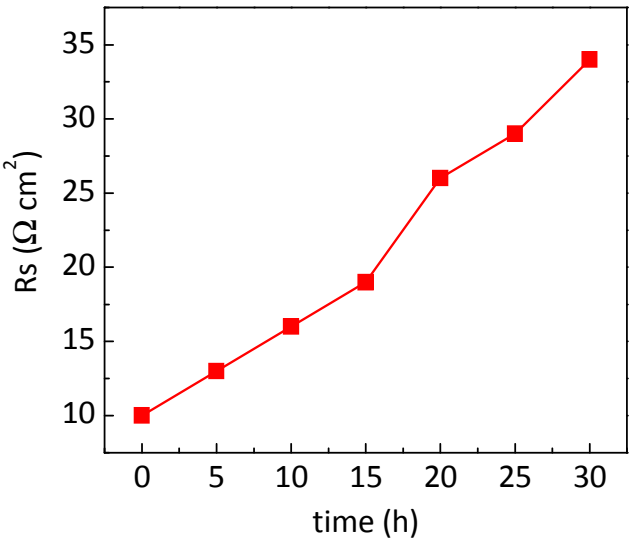

Figure 6.7 - Evolution of series resistance of p-i-n solar cells based on DBP:C_{70} (1:1)

Figure 6.8 shows how $\mu\tau_{eff}$ also decreases with time, clearly representative of a loss in carrier mobility and/or lifetime. Following the same explanation as in [13], the larger than expected drop in J_{SC} and FF cannot attribute to the decrease of $\mu\tau_{eff}$ (Figure 6.8), indicating that some other factor (different from η_C) contributes to the drop of the power conversion efficiency. This major degradation could be due to a loss of optical absorbance in the active layer (η_A), a loss in the exciton diffusion capability (η_{ED}), or a loss in the exciton transfer into carriers (η_{CT}).

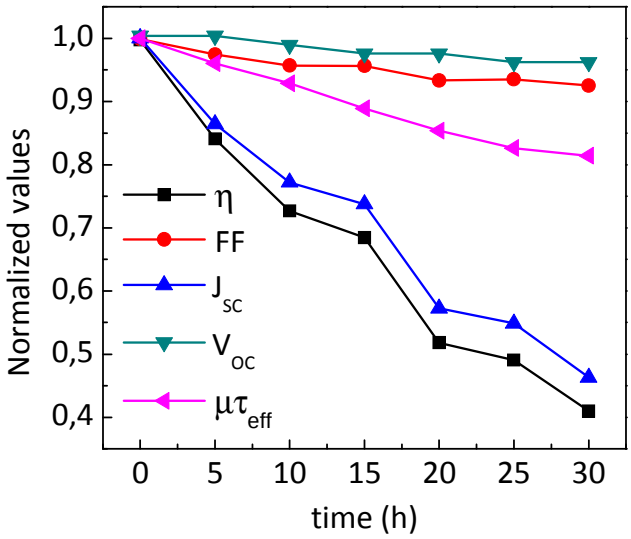

Figure 6.8 - p-i-n solar cells based on DBP:C_{70} (1:1) performance parameters across 30 h (normalized to initial values). Solar cells were under N_2 atmosphere.

This last possibility seems probable, and it has been explained by [24] as the formation of a space-charge region within the active layer due to p-doping by oxygen. This effect shields the electric field inside the active layer and inhibits charge carrier extraction, which leads to a drop in J_{SC}.

It is worth noting that a fraction of the degradation suffered by the organic materials has been reported to be of reversible nature, with J_{SC} partially recovering after a short annealing period at 140 °C [24].

References

[1] S. M. Sze, "Physics of Semiconductor Devices", second ed., Wiley, New York.

[2] H. Hoppe, N. S. Sariciftci "Organic solar cells: An overview", *J. Mater. Res.* 19 (**2004**) 1924.

[3] S. Yoo, B. Domercq, B. Kippelen, "Efficient thin-film organic solar cells based on pentacene/C_{60} heterojunctions", *Appl. Phys. Lett.* 85 (**2004**) 5427.

[4] J. M. Nunzi, "Organic photovoltaic materials and devices", *C. R. Physique* 3 (**2002**) 523.

[5] H. G. Wagemann, H. Estrich, Grundlagen der photovoltaischen Energiewandlung. Stuttgart, Germany: Teubner, (**1994**).

[6] W. Kusian, H. Pfleiderer, W. Jürgens, "Buffer layer and light degradation of a-Si pin solar cells," *Proc. 9th E.C. Photovoltaic Solar Energy Conf.* (**1989**) 52.

[7] J. Merten, C. Voz, A. Muñoz, J. Asensi, J. Andreu, "The role of the buffer layer in the light of a new equivalent circuit for amorphous silicon solar cells", *Sol. Energy Mater. Sol. Cells* 57 (**1999**) 153.

[8] R. Crandall, "Modeling of thin film solar cells: Uniform field approximation", *J. Appl. Phys.* 54 (**1983**) 7176.

[9] P. Schilinsky, C. Waldauf, J. Hauch, C.J. Brabec, "Simulation of light intensity dependent current characteristics of polymer solar cells", *J. Appl. Phys.* 95 (**2004**) 2816.

[10] S. R. Cowan, R. A. Street, S. Cho, A. J. Heeger, "Transient photoconductivity in polymer bulk heterojunction solar cells: Competition between sweep-out and recombination", *Phys. Rev. B* 83 (**2011**) 035205.

[11] L. Liu, G. Li, "Investigation of Recombination Loss in Organic Solar Cells by Simulating Intensity-Dependent Current-Voltage Measurements", *Sol. Energy Mater. Sol. Cells* 95 (**2011**) 2557.

[12] S. R. Cowan, A. Roy, A. J. Heeger, "Recombination in polymer-fullerene bulk heterojunction solar cells", *Phys. Rev. B* 82 (**2010**) 245207.

[13] R. A. Street, M. Schoendorf, A. Roy, J. H. Lee, "Interface state recombination in organic solar cells", *Phys. Rev. B* 81 (**2010**) 205307.

[14] R. A. Street, A. Krakaris, S.R. Cowan, "Recombination Through Different Types of Localized States in Organic Solar Cells", *Adv. Funct. Mater.* 22 (**2012**) 4608.

[15] J. Hubin, A. V. Shah, "Effect of the recombination function on the collection in a p-i-n solar cell" *Philos. Mag. Part B* 72 (**1995**) 589.

[16] J. Merten, J. M. Asensi, C. Voz, A. V. Shah, R. Platz, J. Andreu, "Improved Equivalent Circuit and Analytical Model for Amorphous Silicon Solar Cells and Modules", *IEEE Trans. Electron. Devices* 45 (**1998**) 423.

[17] J. Bisquert, G. Garcia-Belmonte, "On Voltage, Photovoltage, and Photocurrent in Bulk Heterojunction Organic Solar Cells", *J. Phys. Chem. Lett.* 2 (**2011**) 1950.

[18] Z. Liang, B. A. Gregg, "Compensating poly(3-hexylthiophene) reveals its doping density and its strong exciton quenching by free carriers", *Adv. Mater.* 24 (**2012**) 3258.

[19] P. Kumar, S. C. Jain, V. Kumar, S. Chand, R. P. Tandon, "A model for the current–voltage characteristics of organic bulk heterojunction solar cells", *J. Phys. D Appl. Phys.* 42 (**2009**) 055102.

[20] C. Voz, J. Puigdollers, J. Asensi, S. Galindo, S. Cheylan, R. Pacios, P. Ortega, R. Alcubilla, "Analysis of the dynamic short-circuit resistance in organic bulk-heterojunction solar cells: relation to the charge carrier collection efficiency", *Org. Electron.* 14 (**2013**)1643.

[21] C. Hof, N. Wyrsch, A. Shah, "Influence of electric Field distortion and i-layer quality on the collection function of drift-driven a-Si:H solar cells", *J. Non-Cryst. Solids* 266 (**2000**) 1114.

[22] C. Deibel, "Charge carrier dissociation and recombination in polymer solar cells", *Phys. Status Solidi A* 206 (**2009**) 2731.

[23] A. Pivrikas, N. Sariciftci, G. Juska, R. Osterbacka, "A Review of Charge Transport and Recombination in Polymer/Fullerene Organic Solar Cells" *Prog. Photovolt: Res. Appl*, 15 (**2007**) 677.

[24] A. Seemann, T. Sauermann, C. Lungenschmied, O. Armbruster, H. Egelhaaf, J. Hauch, "Reversible and irreversible degradation of organic solar cell performance by oxygen", *Sol. Energy* 85 (**2011**) 1238.

[25] P. Schilinsky, "Loss Analysis of the Power Conversion Efficiency of Organic Bulk Heterojunction Solar Cells", PhD Thesis, Oldenburg University, 2005.

[26] R. A. Street, P. P. Khlyabich, B. C. Thompson, "Electrical characterization of organic solar cell contact degradation resulting from ambient exposure", *Org. Electron.*, 14 (**2013**) 2932.

7. Conclusions and Outlook

Organic solar cells have gathered much attention last decades, mainly since 2005 when its record efficiencies have increased exponentially. However, their interest seems to have diminished since 2012, when was reported the highest power conversion efficiency of OSC with 12%. It is worth to mention that most of the research labs working on dye and organic solar cells have shifted its activities to perovskites solar cells.

This thesis deals with the research on organic solar cells based on small-molecules semiconductors. Organic solar cells were fabricated by thermal evaporation on glass substrates. All the fabrication process were done in inert conditions. The materials used in this thesis were tetraphenyldibenzoperiflanthene as donor material and fullerene C_{70} as acceptor material.

In the first results of this thesis, we focus on the influence of the density of states of the donor layer on the characteristic parameters of organic solar cells. For that reason, a study of the variation in performance of solar cells where the donor material was deposited at different substrate temperatures were done. This work demonstrated that the optimum substrate temperature for this kind of solar cells was 60 ºC, since the tail of localised states is clearly reduced for the sample deposited at 60 ºC compared to the other substrate temperatures. This effect leads to an enhancement of the open circuit voltage in the solar cell. Further, organic solar cells with p-i-n structure, where the intrinsic layer is obtained by coevaporation of donor and acceptor, were analysed. This work demonstrated that the optimum thickness of the intrinsic layer of the p-i-n solar cell based on DBP and fullerene C_{70} is 40 nm.

In the second part, an equivalent circuit for organic solar cells with a new term representing recombination losses in the active layer of the organic solar cell is considered. The model allows obtaining of an effective mobility-lifetime product in the active layer of the device to be determined, characterising its state of degradation. The degradation of p-i-n organic solar cells based on DBP and C_{70} were analysed. The main factor of the degradation of solar cells was not its intrinsic layer, indicating that some other factor contributes strongly to the decrease of the

power conversion efficiency. Due to the increment of series resistance, the degradation of this kind of solar cells could be attributed to the contacts.

APPENDIX I: Electrical Characterisation of Organic Semiconductors from OTFT

In this appendix detailed information about fabrication and characterisation of organic Thin-Film Transistors (OTFTs) can be found. In the framework of this thesis, OTFTs have been used to characterise the electrical properties of the organic semiconductors used in the fabrication of the organic solar cells. In particular, we focused on the determination of the field-effect mobility and on the estimation of the density of states (DOS) of localised states in the band-gap of the semiconductor.

A_I.1 Introduction

First OTFTs were based on polymers like polyacetylene [1–2] and polythiophene [3], these transistors had very low mobilities, below than 10^{-5}cm^2/Vs. First OTFT based on polymers with high mobility (μ = 0.2 cm^2/Vs) was reported by Fuchigami et al. in 1993 [4], but with low ON-OFF current ratio. On the other hand, the first small-molecule OTFT based on sexithiophene was reported in 1989 and had a mobility in order of 10^{-3}–10^{-2} cm^2/Vs [5]. Further improvement in performance was achieved in 1997 with first vacuum sublimed pentacene molecule OTFT, with mobility of 0.7 cm^2/Vs [6]. Alternatively, the first OTFT based on solution-processed conjugated polymer (P3HT) was reported in 1998, having with high mobility (0.1 cm^2/Vs) and high ON-OFF current ratio [7].

Tuning of molecular structure it is possible to optimise a determinate function and achieve a performance enhancement. In addition, OTFTs are based on naturally abundant and sustainable elements. On the other hand, the fabrication process by solution-processing is compatible with large area and flexible devices. These advantages of OTFTs lead an increasing interest to use it for applications such as smart cards, identification (ID) tags and flexible displays [8]. However, the goal of use OTFT in this thesis is to characterise electrically organic semiconductor molecules for its use in small-molecule solar cells. Following, the fabrication process and characterisation details are exposed.

A_I.2 Fabrication of OTFT

OTFTs were fabricated using the same experimental set-up used to fabricate the solar cells. Since we want to correlate the properties of TFTs with OSC, the parameters to deposit organic semiconductor were the same than the used for solar cells fabrication. Electrical properties obtained when measuring TFT corresponds to longitudinal (planar) conductivity between two electrodes (drain and source). Of course, this is not the ideal situation to compare with solar cells, in which conductivity of the carriers between electrodes (anode and cathode) is essentially transversal.

The structure of the fabricated TFT is shown in Figure A 1. An inverted-staggered (top contact, bottom gate) geometry was choose. Crystalline silicon was used as a substrate. Thermally-grown silicon dioxide (SiO_2) 100-nm thick was used as a dielectric.

Top contact geometry is preferred to the bottom contact geometry, due to the easiness when contact electrodes. Moreover, it has been reported that in top contact geometry devices perform better due to lower contact resistance between electrodes and conductance channel.

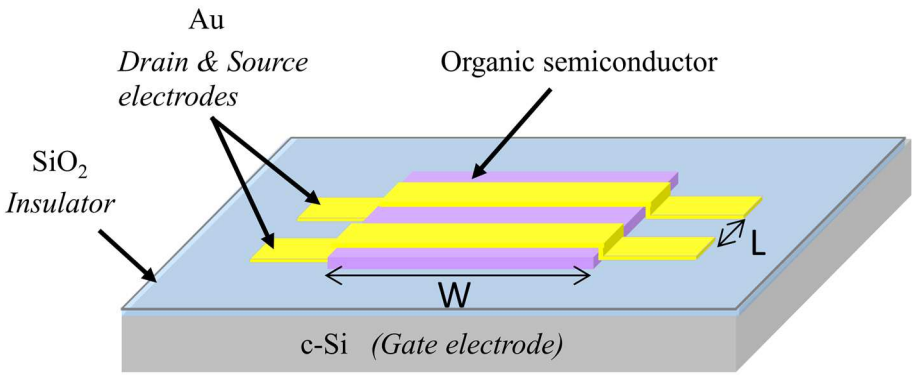

Figure A 1 - Inverted-staggered (top contact) OTFT

Crystalline silicon is commonly used as a substrate and a gate electrode for OTFTs and leads the great advantage of easily growth of silicon oxide (SiO_2) as insulator (Figure A 2), which has well known dielectric properties in the field of microelectronics and its flat surface ideal to deposit organic layers. The thermal oxidation of silicon consists in a chemical reaction of surface of the silicon wafer and an oxidant. The oxidant could be oxygen (dry oxidation) or water vapour (wet oxidation). To facilitate the reaction should work with furnaces at high temperatures in the order of 800–1100ºC, depending on the speed and thickness desired. Thermal oxidation was carried out in clean room facilities of Universitat Politècnica de Catalunya inside a furnace at 1000ºC with oxygen as the oxidant.

Figure A 2 - Silicon wafer with SiO_2 100-nm thick used as dielectric.

Organic semiconductor and gold electrodes (Drain and Source) were deposited in different vacuum chambers in order to avoid cross contamination. Magnetic shadow masks were used to define the area in both cases (Figure A 3 - Magnetic shadow mask for OTFT.Figure A 3). The use of magnetic shadow masks provides better adhesion to the surface, thus increasing edge definition of the electrodes. Shadow masks consisting of electrodeposited nickel on lithographic pre-patterned copper surfaces were fabricated on glass substrates (acting as sacrificial substrate). Nickel layer (50 microns thick) provides the magnetic properties and desired mechanical properties, like flexibility. This process has a resolution up to ±10 μm and it also carried out in the clean room facilities of Universitat Politècnica de Catalunya. The drain and source gold electrodes used in this thesis defines geometry of channel length (L) and width (W) of 80 μm and 2 mm, respectively.

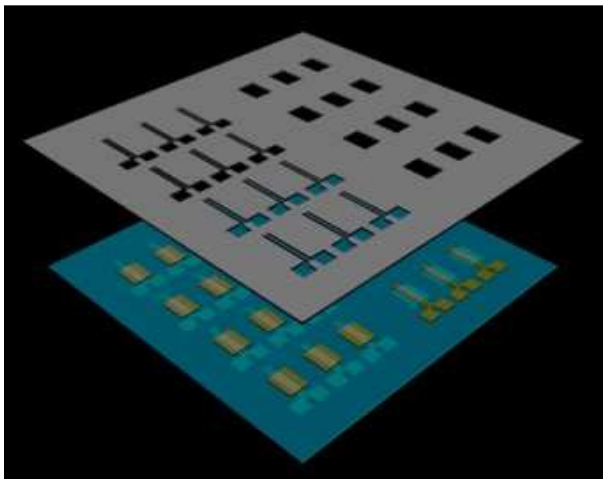

Figure A 3 - Magnetic shadow mask for OTFT.

A_I.3 Characterisation of OTFT

The fabricated OTFTs were characterised in the dark and under moderate vacuum conditions (10^{-1} mbar) to minimise oxidation effects during the electrical characterisation process. The electrical characteristics were measured using an Agilent 4156C parameter analyser. The device temperature was varied from 300 to 390 K by means of an MMR Technologies controller (model K–20).

A_I.3.1 Determination of Mobility μ

A brief review of different methods to determine the charge carrier mobility of organic semiconductors can be found in Chapter 2, section 2.4. Here, it is detailed the methodology followed in order to determine the mobility from electrical characterisation of OTFT.

The current between source and drain I_{SD} depends on the mobility of the charge carriers μ, geometry of device: channel length L and width W, capacitance of the oxide per unit area C_{ox}, gate voltage V_G, source-drain voltage V_{SD}, and the threshold voltage V_{TH} which is required to create the channel.

The following Eq. A.1 defines the drain-source current in the linear region for a Thin-Film Transistor:

$$I_{DS} = \frac{\mu W C_{ox}}{L}\left(V_{GS} - V_{TH} - \frac{V_{DS}}{2}\right) V_{DS} \tag{A.1}$$

In saturation regime ($V_{GS} - V_{TH} < V_{DS}$), the induced charge carriers limit the current between source and drain, therefore I_{DS} is constant independently of the increasing voltage between the electrodes. The current flow depends only on V_G and the parameters of the transistor. Applying the condition ($V_{GS} - V_{TH} = V_{DS}$) to Eq. A1, the I_{SD} for this regime can be expressed as Eq. A2, which depends quadratically on the gate voltage:

$$I_{DS} = \frac{1}{2}\mu \frac{W}{L} C_{ox} (V_{GS} - V_{TH})^2 \tag{A.2}$$

The mobility can be determined from equation Eq. A2 by plotting the square root of I_{SD} versus V_G. Fitting a straight line to the square root of the measured drain current yields the field-effect charge carrier mobility μ and the threshold voltage V_T. Eq. A3 shows the steps to determine the equation for the linear fit.

$$\sqrt{I_{DS}} = \sqrt{\frac{1}{2}\mu\frac{W}{L}C_{ox}(V_{GS}-V_{TH})^2} = \sqrt{\frac{\mu W C_{ox}}{2L}}V_{GS} - \sqrt{\frac{\mu W C_{ox}}{2L}}V_{TH} \quad \text{(A.3)}$$

Using the expression of linear fit ($y = Ax - B$) (Eq. A4):

$$A = \sqrt{\frac{\mu W C_{ox}}{2L}} \qquad B = \sqrt{\frac{\mu W C_{ox}}{2L}}V_{TH} \qquad x = V_{GS} \quad \text{(A.4)}$$

Finally, the expressions to determinate the μ and V_T are:

$$\mu = \frac{A^2}{\frac{W C_{ox}}{2L}} \qquad V_{TH} = \frac{B}{A} \quad \text{(A.5)}$$

It is important to note that, as mentioned above, the mobility is not a constant parameter as it depends on the V_{GS}. Hence, the Eq. A5 is estimation and the obtained values must be treated as such.

If V_{GS} is equal to V_{DS} we ensure that the device is in saturation regime. To carry out the saturation characteristic, I_{SD} is measured by a sweep of voltages (V_{GS} = V_{DS}) from very low conduction to high conduction ($|V_{GS}| >> |V_{TH}|$). This measurement shows an exponential characteristic as depicted in Figure A4.

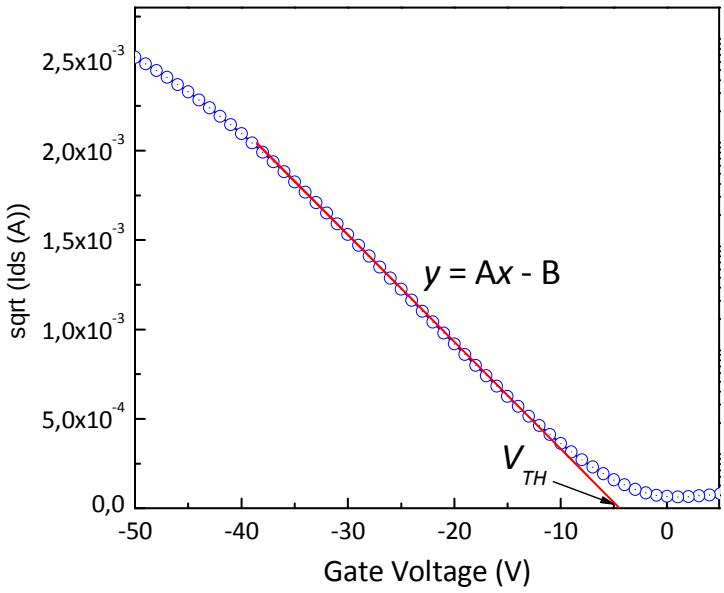

Figure A 4 - Linear fit in saturation measurement for p-type OTFT.

A_I.3.2 Determination of Density of States (DOS)

The optoelectronic properties of the devices depend largely on the density of states (DOS) in the band gap of the active semiconductor layers. DOS distribution in semiconductors determines the electrical transport, photosensitivity, doping efficiency and, at the end, impairs the device performance (traps and recombination centres). Figure A5 illustrates how the energy spectrum of amorphous semiconductors differs from that of crystal semiconductors in the presence of density "tails" of electronic states that penetrate the energy gap.

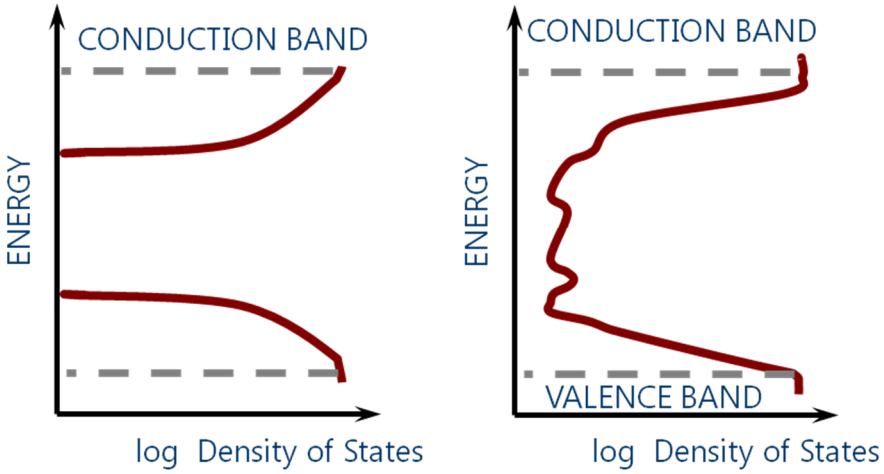

Figure A 5 - (left) Ideal semiconductor (Crystalline materials (silicon). Well defined valence & conduction bands. No states in the middle of the gap. (right) Amorphous and polycrystalline semiconductors. States inside the gap.

Experimental information on the distribution of defects cannot be obtained in a straightforward way. Different techniques for extracting information about the energy distribution of the DOS in thin-film semiconductors: ultraviolet photoelectron spectroscopy, Kelvin probe force microscopy, electron spin resonance spectroscopy, space-charge-limited-current spectroscopy, deep-level spectroscopy, photoconductivity measurements [9–14].

In this thesis, we estimate the DOS distribution in organic semiconductor thin-films from electrical measurements performed at different temperatures on OTFTs. This measurements will provide information about the thermal emission energy distribution of trapped charges.

The multiple trapping and thermal release model (MTR) should describe charge transport in disordered small-molecule organic semiconductors [15]. The trapping and release mechanisms determines the overall mobility and the thermally activated behaviour. The trap distribution DOS within the gap is believed to be exponentially shaped. Therefore, a crucial feature for the MTR model is the determination of the DOS in the gap of the semiconductor.

The position of the Fermi level provides extensive information about the electrical characteristics of the semiconductor material, such as the density of trap states in the bandgap or the distribution of states in the band tails.

It has been observed that the behaviour conductivity (σ) in thin-film organic semiconductors is thermally activated, following the Arrhenius model (Eq A6):

$$\sigma = \sigma_0 \, e^{\left(\frac{-E_a}{k_B T}\right)} \tag{A. 6}$$

where E_a is the activation energy, k_B the Boltzmann constant, T the temperature in K and σ_0 a constant of the material. E_a can be considered a measure of the distance from the Fermi level (E_F) position to the transport band edge. In consequence, E_a is $E_a = E_c - E_F$ for n-type semiconductors and $E_a = E_F - E_v$ for p-type.

On the other hand, from the experimental data obtained from the characterisation of OTFTs, the conductivity can also be calculated from the I_{DS}-V_{DS} curve, as expressed in the following expression (Eq A7):

$$\sigma = \frac{W \, d}{L \, \rho} \frac{I_{DS}}{V_{DS}} \tag{A. 7}$$

Applying Eq A6 in Eq A7 can be obtained (Eq. A8):

$$I_{DS} = \frac{L \, \rho}{W \, d} V_{DS} \sigma_0 \, e^{\left(\frac{-E_a}{k_B T}\right)} = I_0 \, e^{\left(\frac{-E_a}{k_B T}\right)} \tag{A. 8}$$

Thus, if I_{SD} is measured at two different temperatures with a fixed $V_{GS} = V_{DS}$, we obtain (Eq. A9):

$$\ln\left(I_{DS_2}\right) - \ln\left(I_{DS_1}\right) = \left(\frac{-E_a}{k_B \, T_2}\right) - \left(\frac{-E_a}{k_B \, T_1}\right) = \frac{-E_a}{k_B}\left(\frac{1}{T_2} - \frac{1}{T_1}\right) \tag{A. 9}$$

From Eq A9, it can be easily extracted the value of E_a of the conductivity.

On the other hand, Fermi level position in the semiconductor can be varied with the V_{GS} voltage. When applying a V_{GS} voltage, more charge is accumulated in the conductive channel of the Thin-Film Transistor. For a n-type semiconductor applying a positive voltage in the gate will induce more negative charge (electrons) to be accumulated in the channel, whereas the application of positive V_{GS} will empty the channel from electrons. Since the amount of charge accumulated in the channel depends on the position of the Fermi level, changing V_{GS} shifts the Fermi level position inside the band-gap of the semiconductor. In the case of n-type semiconductor, a

positive V_{GS} will shift the E_F to the LUMO level (conduction band in the case of inorganic semiconductors), whereas a negative E_F will shift E_F towards the middle of the gap (in an n-type semiconductor E_F lies close to LUMO level). A similar description can be made in the case of p-type semiconductor. In this case, E_F lies close to the HOMO level, and the application of a V_{GS} voltage will shift E_F to the HOMO level for a negative V_{GS} and to the middle of the band-gap for a positive V_{GS}.

The transfer characteristic of the device is necessary to be measured at different temperatures to achieve E_a.

The transfer curve was measured several times by applying heating and cooling cycles until the results were stable. Since the transfer characteristics are measured at a fixed V_{DS} voltage, the drain current is proportional to the channel conductance for each V_{GS} voltage. An Arrhenius plot of the channel conductance gives evidence of a thermally activated behaviour.

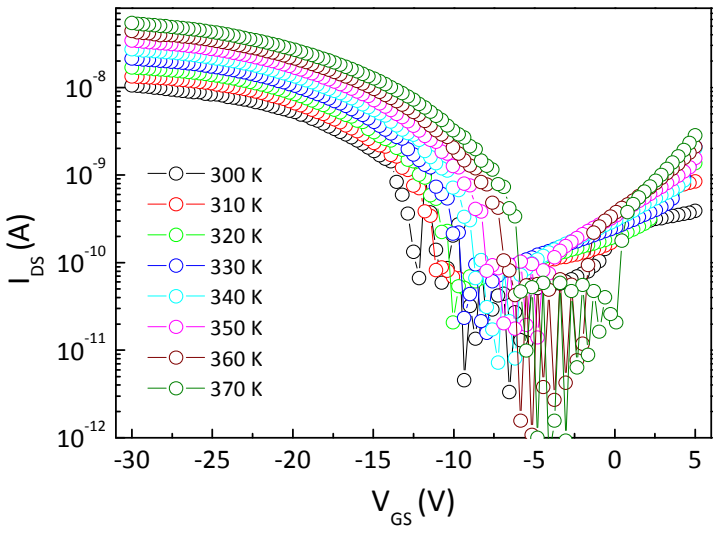

Figure A 6 - Transfer characteristic of TFT measured from 300 K to 370 K with step of 10 K.

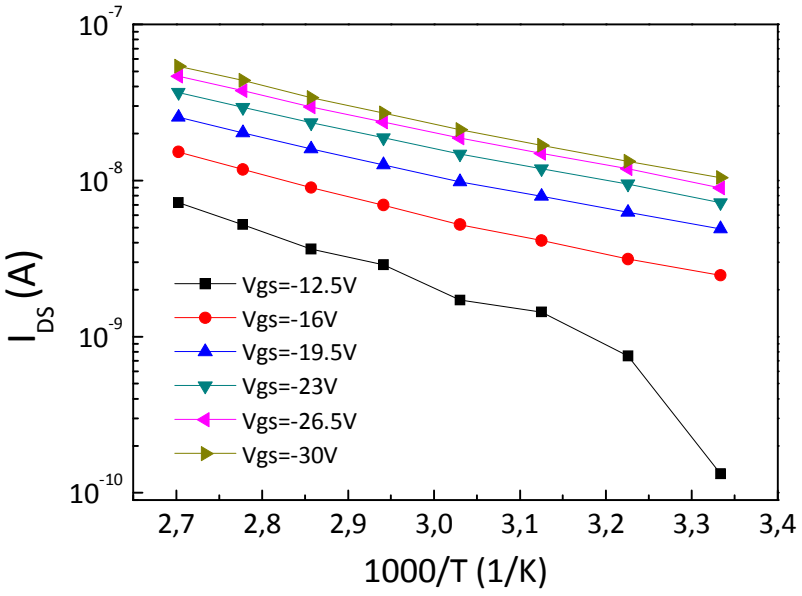

Figure A 7 - Arrhenius plot of drain-source current in function of temperature.

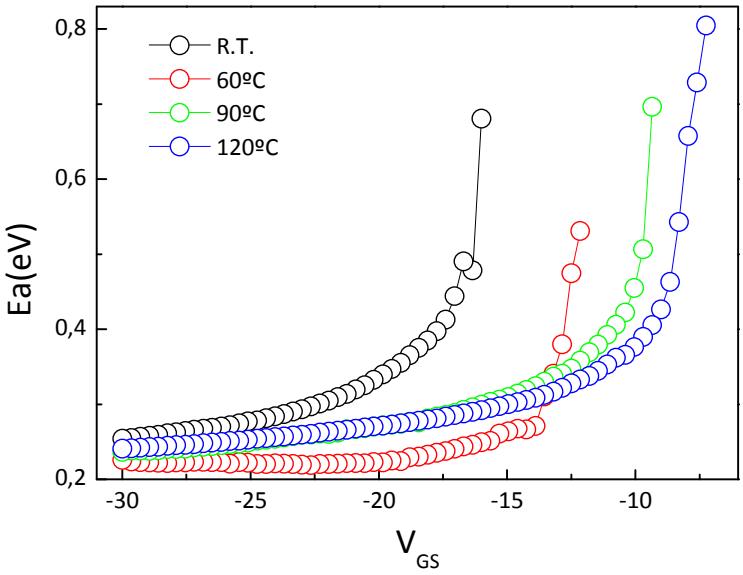

Figure A 8 - Activation energy of TFTs, where the semiconductor layer were deposited at different substrate temperature, in function of gate-source voltage.

The rate at which E_a varies with V_{GS} indicates how easily the Fermi level can shift through the DOS distribution in the gap of the organic semiconductor. A fast variation of E_a with V_{GS} takes place if a low density of localised states has to be filled by trapped carriers. In contrast, a high DOS in the gap results in slower variations of E_a with V_{GS}.

This method to extract the density-of-states inside the band-gap in thin-film semiconductors has been applied to hydrogenated amorphous silicon (a-Si:H). Globus et al. [16] using the transfer characteristics measured at different temperatures of a-Si:H TFTs derived an estimation of the distribution of localised states. Recently, the method has been also successfully used to extract the DOS of organic semiconductors, such as pentacene and PTCDI-C_8 [17–19].

Following this method the DOS in the gap of the semiconductor can be estimated from the derivative of E_a with respect to V_{GS}:

$$DOS(E) = \frac{C_i}{q}\frac{1}{t\,\frac{dE_a}{dV_{GS}}} \tag{A. 10}$$

where E_a is the energy measured from the valence band edge, C_i is the capacity of the dielectric per unit area, q is the elementary charge and t is the thickness of the accumulation channel. It has been reported that the accumulation channel of OTFTs is formed within the first monolayers near the dielectric interface [20–22]. Therefore, in the calculations we have considered an accumulation channel of thickness t=10 nm. Using Eq. A10, we can estimate the distribution of localised states in the region from the valence band edge to approximately the middle of the gap (Figure A 9).

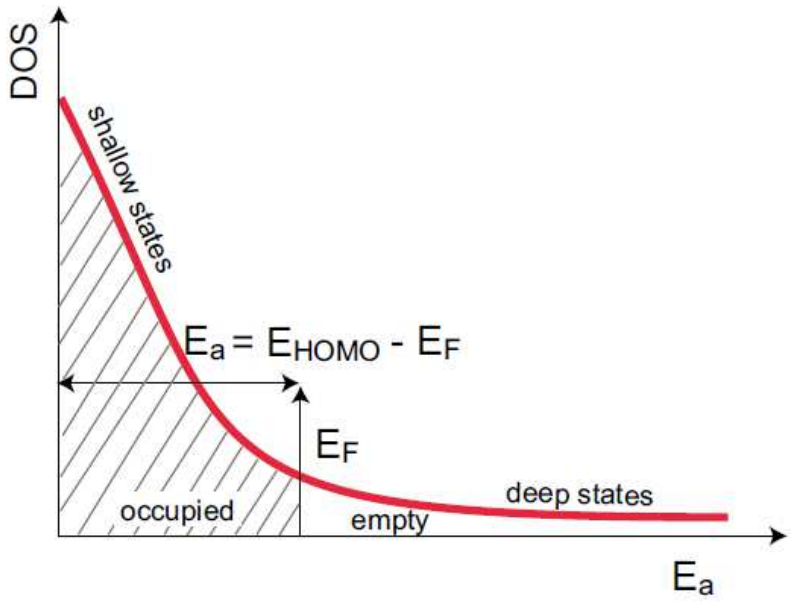

Figure A 9- Schematic diagram of DOS as a function of E_a for a p-type semiconductor. Applying a negative V_{GS} the E_F shifts closer to the HOMO level. Deep states located in the forbidden band gap and shallow states located closer to the HOMO are indicated.

References

[1] F. Ebisawa, T. Kurokawa, S. Nara, "Electrical properties of polyacetylene/polysiloxane interface", *J. Appl. Phys.* 54 (**1983**) 3255.

[2] J. H. Burroughes, C. A. Jones, R. H. Friend, "New semiconductor device physics in polymer diodes and transistors", *Nature* 335 (**1988**) 137.

[3] A. Tsumura, H. Fuchigami, H. Koezuka, "Field-effect transistor with a conducting polymer film" *Synth. Met.* 18 (**1987**) 699.

[4] H. Fuchigami, A. Tsumura, H. Koezuka, "Polythienylenevinylene thin-film transistor with high carrier mobility" *Appl. Phys. Lett.* 63 (**1993**) 1372.

[5] G. Horowitz, D. Fichou, X. Peng, Z. Xu, F. Garnier, "A field-effect transistor based on conjugated alpha-sexithienyl" *Solid State Commun.*72 (**1989**) 381.

[6] Y -Y. Lin, D. I. Gundlach, S. F. Nelson, T. N. Jackson, "Pentacene-based organic thin-film transistors" *IEEE Trans. Electron Dev*. 444 (**1997**) 1325.

[7] H. Sirringhaus, N. Tessler, R. H. Friend, "Integrated Optoelectronic Devices Based on Conjugated Polymers" *Science* 280 (**1998**) 1741.

[8] C.D. Dimitrakopoulos, P.R.L. Malenfantols "Organic thin film transistors for large area electronics", *Adv. Mater.*, 14 (**2002**) 99.

[9] T. Sueyoshi, H. Fukagawa, M. Ono, S. Kera, N. Ueno, "Low-density band-gap states in pentacene thin films probed with ultrahigh-sensitivity ultraviolet photoelectron spectroscopy" *Appl. Phys. Lett*. 95 (**2009**)183303.

[10] O. Tal, Y. Rosenwaks, Y. Preezant, N. Tessler, C. K. Chan, A. Kahn, "Direct Determination of the Hole Density of States in Undoped and Doped Amorphous Organic Films with High Lateral Resolution", *Phys. Rev. Lett.* 95 (**2005**) 256405.

[11] H. Matsui, A. S. Mishchenko, T. Hasegawa, "Distribution of Localized States from Fine Analysis of Electron Spin Resonance Spectra in Organic Transistors", *Phys. Rev. Lett.* 104 (**2010**) 056602.

[12] C. Krellner, S. Haas, C. Goldmann, K. P. Pernstich, D. J. Gundlach, B. Batlogg, "Density of bulk trap states in organic semiconductor crystals: Discrete levels induced by oxygen in rubrene", *Phys. Rev. B* 75 (**2007**) 245115.

[13] V. Nádaždy, R. Durný, J. Puigdollers, C. Voz, S. Cheylan, K. Gmucová, "Experimental observation of oxygen-related defect state in pentacene thin films", *App. Phys. Lett.* 90 (**2007**) 092112.

[14] D. V. Lang, X. Chi, T. Siegrist, A. M. Sergent, A. P. Ramirez, "Amorphouslike Density of Gap States in Single-Crystal Pentacene", *Phys. Rev. Lett*. 93 (**2004**) 086802.

[15] G. Horowitz, M. E. Hajlaoui, R. Hajlaoui, "Temperature and gate voltage dependence of hole mobility in polycrystalline oligothiophene thin film transistors", *J. Appl. Phys.* 87 (**2000**) 4456.

[16] T. Globus, H. C. Slade, M. Shur, M. Hack, "Density of deep bandgap states in amorphous silicon from the temperature dependence of thin film transistor current", *MRS Proceedings* 336 (**1994**) 823.

[17] S. Scheinert, K. P. Pernstich, B. Batlogg, G. Paasch, "Determination of trap distributions from current characteristics of pentacene field-effect transistors with surface modified gate oxide", *J. Appl. Phys.* 102 (**2007**) 104503.

[18] J. Puigdollers, A. Marsal, S. Cheylan, C. Voz, R. Alcubilla, "Density-of-states in pentacene from the electrical characteristics of thin-film transistors", *Org. Electron.*, 11 (**2010**) 1333.

[19] M. R. Shijeesh, L. S. Vikas, M. K. Jayaraj, J. Puigdollers, "Degradation study and calculation of density-of-states in PTCDI–C_8 channel layer from the electrical characteristics of thin-film transistors", *J. Appl. Phys.*, 116 (**2014**) 024507.

[20] A. R. Völkel, R. A. Street, D. Knipp, "Carrier transport and density of state distributions in pentacene transistors", *Phys. Rev. B*, 66 (**2002**) 195336.

[21] A. Dodabalapur, L. Torsi, H. E. Katz, "Organic transistors: two-dimensional transport and improved electrical characteristics" *Science* 268 (**1995**) 270.

[22] G. Horowitz, "Organic thin film transistors: from theory to real devices" *J. Mater. Res.* 19 (**2004**) 1946.